DEVELOPMENT OF ESTER OIL BASED NANOFLUID AS LIQUID INSULATION FOR POWER TRANSFORMERS

A THESIS

submitted in fulfilment of requirements for the award of the degree of

Doctor of Philosophy

In Engineering

Submitted by

Zaid bin Siddique

(Registration No.: 901804009)

Under the supervision of

Dr. Prasenjit Basak

Associate Professor
Electrical and Instrumentation Engineering Department
Thapar Institute of Engineering and Technology
Patiala

Dr. Soumen Basu

Professor
School of Chemistry and Biochemistry
Thapar Institute of Engineering and Technology
Patiala

Department of Electrical and Instrumentation Engineering

THAPAR INSTITUTE OF ENGINEERING & TECHNOLOGY
(Deemed-to-be-University)

P.O. Box 32, Bhadson Road, Patiala, Punjab, India – 147004, India

www.thapar.edu

September, 2022

In The Name of God, The Most Gracious, The Most Merciful.

Dedicated to:

My parents ***Mr. Mohd. Siddique Zargar*** *and* ***Mrs. Nasreen Zargar*** *who together have been a continuous support for me since the day I was born: my mother, under whose feet lies the Paradise for me, and my father, whom I consider as a path to that Paradise.*

My sister ***Mrs. Bushra Nasreen*** *who has stood by my side in every situation no matter how rough.*

CERTIFICATE

This is to certify that the thesis entitled **'Development of Ester Oil Based Nanofluid as Liquid Insulation for Power Transformers'** being submitted by **Mr. Zaid bin Siddique** to the **Department of Electrical and Instrumentation Engineering, Thapar Institute of Engineering and Technology** (Deemed to-be University) Patiala, Punjab, India for the award of the degree of **Doctor of Philosophy,** is a record of bona-fide research work carried out by him under our guidance and supervision, and has fulfilled the requirements for the submission of this thesis, which to our knowledge has reached the requisite standard.

The results embodied in this thesis have not been submitted in part or full to any other Institute or University for the award of any diploma or degree.

Dr. Prasenjit Basak
Associate Professor
Department of Electrical and Instrumentation Engineering,
Thapar Institute of Engineering and Technology,
(Deemed to-be University)
Patiala, Punjab, India (147001)

Dr. Soumen Basu
Professor
School of Chemistry and Bio-chemistry,
Thapar Institute of Engineering and Technology,
(Deemed to-be University)
Patiala, Punjab, India (147001)

ACKNOWLEDGMENTS

All praise be to **God, The Almighty,** and His peace and blessings be upon His final **Prophet**. I would like to start by thanking **God** for showering His blessings and granting me the inner strength without which it would have been impossible to successfully complete this research.

My family has always been providing the main impetus for commuting me into the person I am today. Their continuous motivation has resulted in an unconditional amelioration within me. Regardless of whether I was around them or far from them during this research tenure, their pearls of enlightenment and counselling were always felt in furtherance of this research. I would like to thank my parents **Mr. Mohd. Siddique Zargar** and **Mrs. Nasreen Zargar** as well as my sister, **Mrs. Bushra Nasreen**, for every bit of their effort to transform me into a better person and eventually into a better researcher. Thank you for lending your shoulder whenever needed. You made it much easier for me.

"Research means that you don't know, but are willing to find out" quoth Charles F. Kettering (the engineer who invented electric starter). As someone who wished to enter the field of High Voltage Engineering for his Ph.D. research, I handed myself over as an absolute layman to the best supervisors one can ever think of. My research supervisors casted me into a whole different person through their incessant efforts; a person with a goal-oriented vision who knew no dithering in starting things from the scratch. I would like to extend my heartfelt gratitude and unpayable indebtedness to both of my research supervisors, **Dr. Prasenjit Basak**, Associate Professor, Electrical and Instrumentation Engineering Department and **Dr. Soumen Basu**, Professor, School of Chemistry and Bio-chemistry, Thapar Institute of Engineering and Technology (Deemed to be University) Patiala, India, for their continuous support, skillful guidance and proficient supervision throughout my academic endeavor. I feel it as an obligation upon me to thank my supervisors for their availability whenever it was required even during the odd hours of their jobs. I am grateful to **Dr. Ashish Paramane** for his timely guidance.

I am highly grateful to **Dr. Mukesh Singh,** Professor and **Dr. Surya Prakash**, Associate Professor, Electrical and Instrumentation Department, TIET, Patiala and **Dr. O. P. Pandey**, Senior Professor and Head, School of Physics and Material Science, TIET, Patiala, for being the esteemed

members of Doctoral Committee and for providing their valuable comments along with the constructive criticism while reviewing this work.

I extend my gratitude to **Dr. Prakash Gopalan**, Honorable Director and **Dr. Rafat Siddique**, Senior Professor and Dean, Research and Sponsored Projects, TIET, Patiala, for providing all the necessary facilities to carry out this research on steady course. I owe sincere gratitude to **Savita Chemicals,** India and **Mubasa Electrical Pvt. Ltd.,** India for providing the necessary insulation materials required for this research.

I would like to thank **Mr. Ravail Singh**, High Voltage Lab Supervisor, TIET, Patiala for sharing his unmatchable apparatus handling expertise with me and thus, guiding me to conduct experiments with every possible caution. I am grateful to **PSPCL,** Patiala, for letting me carry out some important experiments in their laboratories.

I am extremely thankful to **Tafheem Ashraf** who continuously steered me for getting my doctorate from TIET, Patiala. I can't thank enough to wonderful colleagues that I had during my research period. I am thankful to **Sahil Mehta** who always lent a helping hand whenever needed. Coming from engineering background, dealing with chemical part of the research was a herculean task for me but my ever-enthusiast colleagues in Advanced Nanomaterial Lab helped tirelessly in vanquishing the hurdles. I would like to send my heartfelt gratitude to **Surbhi, Aashna, Anushka, Aanchal, Divya, Neeraj and Ayushi** for all their support.

I owe a deepfelt gratitude to **Yusuf Ali**, **Moeed Nazki** and **Ifrah Saify** whom I met during my earliest days in TIET and the bond between us only grew stronger. Their company turned my stay in Patiala into an amazingly wonderful experience that I would never forget.

My memories with the city of **Patiala** are simply unforgettable ones. From taking a bike ride during the late-night hours to relieve the stress caused by a failed experiment to celebrating the acceptance of the very first publication from this research, I have shown Patiala every side of me. The hospitality of Patiala and its people will surely be missed.

Zaid b. Siddique
(Regn. No. 901804009)

A philosopher once said "It is necessary for the very existence of science that the same conditions always produce the same results". Well, they don't!

Richard Feynman

DEVELOPMENT OF ESTER OIL BASED NANOFLUID AS LIQUID INSULATION FOR POWER TRANSFORMERS

ABSTRACT

The conventional mineral oil is the most widely used insulating oil in transformers. The reason for its wide usage is its easy availability and good insulating and cooling properties. However, with these superior qualities, the usage of mineral oil poses some serious threats like the depletion of its resources, its non bio-degradibilty and high inflammability. Due to these issues, there has been a continuous increase in research for finding suitable alternative insulating fluids which can possess comparable insulating and cooling properties and can also eliminate the risk of threats posed by the usage of mineral oil. Vegetable oils are gaining popularity nowadays as alternatives to conventional mineral oil for transformers. Also known as natural ester oils, the dielectric properties of these oils are very much comparable to the mineral oil and in many cases better than the conventional mineral oil. For example, the dielectric strength of vegetable oils is generally better than the mineral oil. However, in a few qualities like total acidity and oxidation stability, these vegetable oils lack behind the conventional mineral oil. The latest trend in research these days is to further enhance these qualities of vegetable oils by dispersing suitable nanomaterials in them in order to enable the researchers to synthesize 3rd generation insulating fluids for transformers and to increase the transformer voltage ratings.

In the field of nanomaterials, a recent in-trend nanomaterial, i.e., graphene oxide, has created a boom in research. Graphene oxide is constantly emerging as an attractive alternative to various other materials due to its low cost and large-scale production. Graphene oxide is currently becoming a basis for exploring innovative opportunities in the fields of emerging trends of research. While being extensively researched in the fields of medicine, chemistry and physics, the role of graphene oxide in insulation systems still remains unexplored. Moreover, till date, almost all of the research in the field of developing 3rd generation insulating fluids is based on dispersing conducting and /or semi-conducting nanomaterials in either mineral oil or in vegetable oil and to study the dielectric properties of synthesized nanofluids. The 3rd generation transformer oils refer to nanoparticles dispersed insulating fluids which have improved dielectric as well as cooling properties. However, for this research, a natural ester oil based blend having vegetable oil as a primary oil and mineral oil as a secondary oil has been optimized on the basis of its dielectric strength and the optimized blend has been chosen as the base fluid for dispersing the nanomaterials.

The selected oil blend has been dispersed with three different types of nanomaterials on the basis of their conductivity – non-conductive graphene oxide (GO) nanoparticles, semi-conductive titanium di-oxide (TiO_2) nanoparticles and conductive zinc oxide (ZnO) nanoparticles. The main focus is kept on the graphene oxide dispersed nanofluid and its dielectric as well as physio-thermal properties are extensively studied and compared with TiO_2 and ZnO dispersed nanofluids. The effects of these nanofluids on transformer solid insulation before and after subjecting the liquid-solid insulation to extreme thermal stress conditions are also studied. The insulation design of transformers is analyzed when proposed to be filled with the synthesized nanofluids and the proposed changes in transformer design have been formulated.

Results indicate that dispersion of nanomaterials results in an overall enhancement in the dielectric properties of nanofluids. The results have shown that with the addition of GO nanoparticles, the breakdown voltage of nanofluids increases up to 42% as compared to pure mineral oil, 17% as compared to pure ester oil and 15% as compared to the base oil-blend. The breakdown voltage of TiO_2 dispersed nanofluid is reported to be about 30% greater than pure mineral oil, 24% greater than pure ester oil, and 17% greater than the oil-blend. Likewise, the breakdown voltage of ZnO dispersed nanofluid is observed to be around 28% greater than pure mineral oil, 19% greater than pure ester oil, and 16% greater than the oil-blend. The other dielectric properties like relative permittivity as well as the dissipation factor also improve significantly. In terms of physio-thermal properties, the viscosities of GO and TiO_2 dispersed nanofluids show no significant change whereas the viscosity of ZnO dispersed nanofluid keeps on increasing with the increase in concentration level, thus making it a ‘bad’ coolant. Results also show that at peak values, the ac breakdown voltage of nanofluids decreases by just 2.6% after ageing when compared to the base oil for which the ac breakdown voltage decreases by 8.4% after ageing. Similarly, at peak values, the impulse breakdown voltage of nanofluid decreases by just 2.9% after ageing as compared to the base oil for which the impulse breakdown voltage decreases by 7.3%. The dispersion of GO also leads to the possibility of reduction in core size by 14.3% when compared to the base oil. Thus, the developed nanofluids can be used in transformers with successful operation.

TABLE OF CONTENTS

CERTIFICATE I

ACKNOWLEDGEMENTS ii

ABSTRACT vi

TABLE OF CONTENTS viii

LIST OF FIGURES xii

LIST OF TABLES xvii

LIST OF ACRONYMS xviii

CHAPTER 1. INTRODUCTION 1

1.1 Evolution of insulating oils 3

1.2 Theme of the thesis 6

1.3 Organisation of the thesis 7

CHAPTER 2. LITERATURE REVIEW 10

2.1 Increase in demand of electrical energy 10

2.2 Increase in transformer ratings 12

2.3 Usage of mineral oil in transformers 14

2.4 Usage of ester oil in transformers 15

2.4.1 General composition of ester oils 15

2.4.2 Refining of ester oils 17

2.4.3 Ester oil as transformer oil 19

2.5 Usage of nanofluids in transformers 23

2.6 Outcomes of literature survey: Gaps in research 29

2.7 Objectives of the research 30

CHAPTER 3. SYNTHESIS OF MATERIALS 32

3.1 Synthesis of nanomaterials 32

3.1.1 Synthesis of graphene oxide (GO) 32

3.1.2 Synthesis of zinc oxide (ZnO) 33
3.1.3 Availability of titanium di-oxide (TiO_2) 34
3.1.4 Surface modification of nanomaterials 35
3.2 Development of nanofluids 36
3.2.1 Making of base oil-blend 36
3.2.2 Synthesis of nanofluids 39
3.3 Preparation of solid insulation 39
3.4 Characterization of nanomaterials 41
3.4.1 X-Ray Diffraction 41
3.4.2 Fourier Transform Infrared Spectroscopy 42
3.4.3 Field Emission – Scanning Electron Microscopy 44
3.4.4 Brunauer-Emmett-Teller and Barrett-Joyner-Halenda Tests 45
3.4.5 Thermo-gravimetric Analysis 47
3.5 Chapter summary 48

CHAPTER 4. STUDY OF DIELECTRIC PROPERTIES OF SYNTHESIZED NANOFLUIDS FOR TRANSFORMERS 49

4.1 Experimental approach 49
4.2 Insulating properties of synthesized nanofluids 53
4.2.1 Ac breakdown voltage 53
4.2.2 Impulse breakdown voltage 58
4.2.3 Relative permittivity and dissipation factor 62
4.3 Physio-thermal properties of synthesized nanofluids 65
4.3.1 Viscosity 65
4.3.2 Interfacial tension 68
4.3.3 Flash point 69
4.4 Mechanism of improvement 71
4.5 Chapter summary 71

CHAPTER 5. ANALYSIS OF AGEING EFFECTS ON SYNTHESIZED LIQUID INSULATION FOR TRANSFORMERS 73

5.1 Effects of ageing on synthesized nanofluids 73

5.1.1 Dielectric properties of aged nanofluids 73

5.1.2 Physio-thermal properties of aged nanofluids 82

5.2 Chapter summary 87

CHAPTER 6. ANALYSIS OF AGEING EFFECTS ON PREPARED SOLID INSULATION FOR TRANSFORMERS 89

6.1 Experimental approach 89

6.1.1 Dielectric behaviour of solid insulation 89

6.1.2 Mechanical behaviour of solid insulation 90

6.2 Mechanical effects on transformer pressboard 90

6.2.1 XRD analysis 90

6.2.2 Field emission – Scanning electron microscopy 94

6.2.3 Tensile Strength 95

6.3 Dielectric properties of transformer pressboard 97

6.3.1 Ac breakdown voltage 97

6.3.2 Relative permittivity 98

6.3.3 Dissipation factor 99

6.4 Mechanism of Improvement 100

6.5 Chapter summary 101

CHAPTER 7. TRANSFORMER DESIGN CONSIDERATIONS 103

7.1 Constructional design analysis 103

7.2 Material compatibility 112

7.3 Chapter summary 114

CHAPTER 8. CONCLUSIONS AND FUTURE SCOPE 115

8.1 Conclusions 115

8.2 Future scope of Research 118

REFERENCES 119
LIST OF PUBLICATIONS FROM THIS RESEARCH 136

LIST OF FIGURES

Figure No.	Figure Caption	Page No.
Figure 1.1	Evolution timeline of transformer oils.	4
Figure 2.1	Global electric power consumption from 1980 to 2020.	10
Figure 2.2	Region-wise annual electricity consumption in years (a) 2000 and (b) 2020.	11
Figure 2.3	Region-wise share in annual electricity consumption in years (a) 2000 and (b) 2020.	11
Figure 2.4	Increase in voltage and power rating of transformers over the years	14
Figure 2.5	Types of mineral oil for transformer applications.	15
Figure 2.6	Structure of fatty acid in an ester.	16
Figure 2.7	A triglyceride structure	17
Figure 2.8	(a) Structure of glycerol and (b) Formation and basic structure of Propyl ethanoate (an ester).	18
Figure 2.9	Types of nanomaterials and the basis of classification chosen for this research.	29
Figure 3.1	Pictorial representation of synthesis of graphene oxide nanoparticles using modified Hummer's method.	33
Figure 3.2	Pictorial representation of synthesis of zinc oxide nanoparticles using sol-gel method.	34
Figure 3.3	Commercially purchased P25 TiO_2 nanoparticles.	34
Figure 3.4	Pictorial representation of a Two-Step surface modification method used to cap the nanomaterials.	35
Figure 3.5	BDV values of synthesized oil-blends.	38
Figure 3.6	MO, EO as well as optimized blend, OB80	39
Figure 3.7	XRD pattern of (a) synthesized GO, (b) purchased TiO_2 and (c) synthesized ZnO nanomaterials.	42

Figure 3.8	Comparative analysis of FTIR spectra of unmodified and surface modified nanoparticles: (a) GO and OA-GO, (b) TiO_2 and OA-TiO_2, (c) ZnO and OA-ZnO nanoparticles.	43
Figure 3.9	FE-SEM images of (a) GO and (b) OA-GO nanoparticles.	44
Figure 3.10	FE-SEM images of (a) TiO_2 and (b) OA-TiO_2 nanoparticles.	45
Figure 3.11	FE-SEM images of (a) ZnO and (b) OA-ZnO nanoparticles.	45
Figure 3.12	(a) and (b) BET and BJH for OA-GO, (c) and (d) BET and BJH for OA-TiO_2, (e) and (f) BET and BJH for OA-ZnO, respectively.	46
Figure 3.13	TGA of GO, TiO_2 and ZnO nanomaterials.	47
Figure 4.1	BDV test kit with its test cell as well as the dimensions of the electrodes used in the test cell.	50
Figure 4.2	Impulse generator kit used to measure impulse voltages.	51
Figure 4.3	Test kit used to measure the relative permittivity and tan delta of the insulating fluids.	52
Figure 4.4	BDV values of oil blends.	53
Figure 4.5	(a) BDV of GNF samples at 25°C, (b) BDV of GNF samples at 90°C.	54
Figure 4.6	Weibull distribution plots for BDV values of GNF samples at (a) 25°C, (b) 90°C and (c) combined temperature values.	55
Figure 4.7	BDV values of TNF at 25°C and 90°C.	56
Figure 4.8	Weibull distribution plots for BDV values of TNF samples at combined temperature values.	56
Figure 4.9	BDV values of ZNF at 25°C and 90°C.	58
Figure 4.10	Weibull distribution plots for BDV values of ZNF samples at combined temperature values.	58
Figure 4.11	IBDV values of oil blend samples at 25°C.	59
Figure 4.12	(a) IBDV values of GNF samples and (b) Weibull distribution plot for IBDV values of GNF samples.	59
Figure 4.13	(a) IBDV values of TiO_2 and ZnO nanoparticles at 25°C, (b) and (c) Weibull distribution of IBDV values of TiO_2 and ZnO nanoparticles respectively at 50% probability failure.	61

Figure 4.14	(a) Relative Permittivity and (b) Dissipation of oil blend samples at 25°C and 90°C.	63
Figure 4.15	(a) Relative Permittivity and (b) Dissipation of GNF samples at 25°C and 90°C.	63
Figure 4.16	(a) Relative Permittivity and (b) Dissipation of TNF samples at 25°C and 90°C.	64
Figure 4.17	(a) Relative Permittivity and (b) Dissipation of ZNF samples at 25°C and 90°C.	65
Figure 4.18	Viscosity of oil blend samples at 25°C and 90°C.	66
Figure 4.19	Viscosity of GNF samples at 25°C and 90°C.	66
Figure 4.20	Viscosity of TNF samples at 25°C and 90°C.	67
Figure 4.21	Viscosity of ZNF samples at 25°C and 90°C.	67
Figure 4.22	IFT values of GNF samples with respect to OB80.	68
Figure 4.23	IFT values of TNF and ZNF samples with respect to OB80.	69
Figure 4.24	Flash point values of GNF samples with respect to OB80.	70
Figure 4.25	Flash point values of TNF and ZNF samples with respect to OB80.	70
Figure 5.1	BDV values of unaged and aged GNF samples with respect to OB80 at (a) 25°C and (b) 90°C.	74
Figure 5.2	Weibull distribution plots for BDV values of GNF samples (a) at unaged conditions, (b) after 15 days of ageing and (c) after 60 days of ageing.	75
Figure 5.3	BDV values of unaged and aged TNF samples with respect to OB80 at (a) 25°C and (b) 90°C.	75
Figure 5.4	BDV values of unaged and aged ZNF samples with respect to OB80 at (a) 25°C and (b) 90°C.	76
Figure 5.5	BDV values of unaged and aged ZNF samples with respect to OB80 at (a) 25°C and (b) 90°C.	77
Figure 5.6	IBDV values (a) unaged and aged TNF values, (b) unaged and aged ZNF values.	77

Figure 5.7	(a) and (b) Relative permittivity of unaged and aged GNF samples with respect to OB80 (a) at 25°C and (b) at 90°C, and dissipation factor unaged and aged GNF samples with respect to OB80 (c) at 25°C and (d) at 90°C.	79
Figure 5.8	(a) and (b) Relative permittivity of unaged and aged TNF samples with respect to OB80 (a) at 25°C and (b) at 90°C, and dissipation factor unaged and aged TNF samples with respect to OB80 (c) at 25°C and (d) at 90°C.	80
Figure 5.9	(a) and (b) Relative permittivity of unaged and aged ZNF samples with respect to OB80 (a) at 25°C and (b) at 90°C, and dissipation factor unaged and aged ZNF samples with respect to OB80 (c) at 25°C and (d) at 90°C.	81
Figure 5.10	Viscosity of GNF samples with respect to OB80 (a) at 25°C and (b) 90°C.	82
Figure 5.11	Viscosity of TNF samples with respect to OB80 (a) at 25°C and (b) 90°C.	83
Figure 5.12	Viscosity of ZNF samples with respect to OB80 (a) at 25°C and (b) 90°C.	84
Figure 5.13	IFT values of GNF samples with respect to OB80.	84
Figure 5.14	IFT values of (a) TNF and (b) ZNF samples with respect to OB80.	85
Figure 5.15	Flash point values of GNF samples with respect to OB80 samples.	86
Figure 5.16	Flash point values of (a) TNF samples and (b) ZNF samples with respect to OB80 samples.	87
Figure 6.1	(a) BDV test cell with transformer pressboard specimen between the electrodes, (b) dumbbell shapes specimen of pressboard for measuring of tensile strength and (c) tensile strength measuring machine working on the principle of elongation method.	90
Figure 6.2	XRD pattern of (a) OB impregnated pressboard after 15 and 60 days, (b) raw unaged pressboard.	91
Figure 6.3	(a) XRD pattern of GNF impregnated pressboard after 15 days and 60 days of ageing (b) crystallite size of OB and GNF impregnated pressboard samples after 15 days and 60 days of ageing.	92
Figure 6.4	XRD pattern of TNF impregnated pressboard after 15 days and 60 days of ageing.	93
Figure 6.5	Crystallite size of P-TNF and P-GNF samples with respect to P-OB samples after 15 days and 60 days of ageing.	93
Figure 6.6	XRD pattern of ZNF impregnated pressboard after 15 days and 60 days of ageing.	93

Figure 6.7	SEM images of unaged raw pressboard sample as well as OB and NF impregnated pressboard samples after 60 days of ageing.	95
Figure 6.8	Tensile strength of unimpregnated raw pressboard as well as OB and NF impregnated pressboard samples after 15 days and 60 days of ageing.	96
Figure 6.9	BDV of unimpregnated raw pressboard as well as OB and NF impregnated pressboard samples after 15 days and 60 days of ageing.	98
Figure 6.10	Relative permittivity of unimpregnated raw pressboard as well as OB and NF impregnated pressboard samples after 15 days and 60 days of ageing.	99
Figure 6.11	Dissipation factor of unimpregnated raw pressboard as well as OB and NF impregnated pressboard samples after 15 days and 60 days of ageing.	100
Figure 7.1	Basic insulation structure of a transformer.	105
Figure 7.2	Iron stampings of a typical core type transformer.	108

LIST OF TABLES

Table No.	Table Caption	Page No.
Table 1.1	Expected characteristics of a transformer oil with their significances.	2
Table 2.1	Evolution of transformers.	13
Table 2.2	Dielectric properties of various transformer oils.	20
Table 3.1	Comparative analysis of dielectric properties of transformer oils used in this research.	37
Table 3.2	Surface details of modified nanomaterials	46
Table 4.1	Properties studied with their IEC/ASTM Standards.	49
Table 4.2	Minimum and maximum BDV values of GNF samples with their scale and shape parameters at 50% probability failure.	55
Table 4.3	Minimum and maximum BDV values of TNF samples with their scale and shape parameters at 50% probability failure.	57
Table 4.4	Minimum and maximum BDV values of ZNF samples with their scale and shape parameters at 50% probability failure.	58
Table 4.5	Maximum and minimum values of IBDV for GNF samples at 50% probability failure.	60
Table 4.6	Minimum and maximum limits of IBDV values for (a) TNF and (b) ZNF samples at 50% probability failure.	62
Table 6.1	Comparative analysis of the relative crystallinity and crystallite sizes of all the pressboard samples.	94
Table 6.2	Average fibre widths of unaged and 60 days aged pressboard impregnated pressboard samples.	95
Table 7.1	Permittivity ratios of liquid to solid insulation materials	106
Table 7.2	Standards for material compatibility tests	113

LIST OF ACRONYMS

BDV	Breakdown Voltage
BET	Brunauer-Emmett-Teller
BJH	Barrett-Joyner-Halenda
DC	Dielectric Constant
DF	Dissipation Factor
EO	Ester Oil
FE-SEM	Field Emission Scanning Electron Microscopy
FTIR	Fourier Transform Infrared Spectroscopy
GNF	Graphene Oxide Dispersed Nanofluid
GO	Graphene Oxide
IBDV	Impulse Breakdown Voltage
IFT	Inter-Facial Tension
ISO	International Organization for Standards
MO	Mineral Oil
OB	Oil Blend
P-GNF	Pressboard impregnated with Graphene Oxide based Nanofluid
P-TNF	Pressboard impregnated with Titanium Di-oxide based Nanofluid
P-ZNF	Pressboard impregnated with Zinc Oxide based Nanofluid
RP	Relative Permittivity
TGA	Thermo-Gravimetric Analysis
TiO_2	Titanium Di-oxide
TNF	Titanium Di-oxide dispersed Nanofluid
XRD	Pressboard impregnated with Titanium dioxide dispersed Nanofluid

ZnO	Pressboard impregnated with Zinc oxide dispersed Nanofluid
ZNF	International Organization for Standard

CHAPTER 1

INTRODUCTION

TRANSFORMER is considered as one of the most important inventions in the history of the electrical world. It has only been possible with the applications of transformers that we are able to change the input to a particular machine according to the desired values. Transformer has found its usage in almost every electronic as well as electrical equipment. In terms of electrical power consumption, transformers are used at each and every step from generation to transmission and finally to distribution of this power. Power transformers are used at generation and transmission ends whereas the distribution transformers are used at distribution levels in order to maintain a steady flow of electrical power. In other words, it can be said that the continuous and steady flow of power directly depends on the smooth functioning of transformers at every stage. Thus, it becomes of utmost necessity to ensure the protection of these transformers [1-3].

With the onset of global industrialization and ever-increasing population, the demand of electrical power has only been increasing with each passing day. To meet this continuously increasing demand of electrical power, the electrical power providers are forced to use the transformers above their rated capacities in most of the cases. This directly brings the transformer manufacturers and engineers under tremendous pressure to manufacture the transformers with higher ratings. This means higher voltage levels appear on either side of the transformer windings which further means higher dielectric stress is faced by the transformer insulation structure. Studies have shown that in case of transformers used in high voltage applications, 75% of total transformer failures are directly or indirectly caused due to the transformer insulation related issues. Also, the expected average service life span of any typical transformer is about 35-40 years. However, available studies have already shown that the average service life of a transformer which has failed because of any insulation regarding problems is reduced to just only 17.8 years which is even less than half of the life of a healthy transformer [4-8]. Thus, primarily it all melts down to the safety and protection of transformer insulation structure if the higher rated transformers are to be used with more reliability and continuity in their outputs.

A typical transformer's insulation structure necessarily consists of an arrangement of liquid-solid insulating materials. As for liquid insulation, mineral oil is the most commonly used insulating fluid in transformers. Mineral oil has been the conventional insulating fluid for transformers ever since the transformers have been invented [9-12]. Even in power transformers, mineral oil has been used over a century now due to its easy availability, cheap cost and good dielectric as well as cooling properties [12-15]. However, there are some serious issues related to the worldwide usage of mineral oil in transformers. Amongst such issues, the most important one is the depletion of the mineral oil resources. It has already been estimated that at current rate of depletion, almost all the major resources of mineral oil will be exhausted by the end of this century [16]. Another major concern regarding the usage of mineral oil is its non-biodegradability [11,17,18]. Its spillage poses serious environmental threats including the destruction of crops as well as the damage to the aquatic life if spilled in water. Yet another concern is its high inflammability. The fire point of mineral oil is low which makes it easier to catch fire which can lead to explosions in transformers. Due to all these factors, researchers are trying to find suitable alternatives to conventional mineral oil. In general, a transformer oil is expected to have certain characteristics out of which the most important ones are listed in the Table 1.1 along with their significances.

Table 1.1 Expected qualities of a transformer oil with their significances

Expected Characteristics	***Remarks***
High AC Breakdown Voltage	To withstand the high voltage levels without deteriorating the quantity of oil itself.
High Impulse Breakdown Voltage	To withstand the sudden increase in voltage levels due to over-voltage conditions caused by transients and/or lightnings.
High Dielectric Constant	To withstand the non-polarization of the oil in the transformer under high dielectric stress.
Low Dissipation Factor	To generate low overall losses including heat dissipation as well as the leakage current in the oil.

Low viscosity	To enable the easy circulation of oil in the transformer in order to transfer the heat easily.
High Flash Point (Low inflammability)	To reduce the risks of fires and explosions in the transformers.
High Inter-Facial Tension	To ensure the better hydrophobic property of the oil.

1.1 EVOLUTION OF INSULATING OILS

The usage of mineral oil in transformers can be dated back to 1890. It is almost the same era when the first transformer was invented, i.e., in 1885. The first alternative to mineral oil was developed in 1930s in the form polychlorinated biphenyl (PCB) or askerals. PCBs are, in general, a group of synthetic fluids including biphenyls as halogenated carbons attached with fluorine or chlorine. Their application in transformers continued for next 40 years till it was discovered that the chlorinated biphenyls are highly toxic in nature which makes the PCBs environmentally unacceptable – the same problem which was and is still being faced in the case of mineral oil [19]. Meanwhile, the research for another alternative fluids was geared up which led to the development of silicone oils, first used in transformers in 1970s. Silicone oils are silicon based polymers having hydrogen, carbon and oxygen atoms and are obtained by the polymerization of polydimethylsiloxane (PDMS). In 1977, a new class of transformer insulating oil was introduced in the form of synthetic esters. Synthetic esters are obtained as a result of an esterification reaction between tetra-alcohol and monocarboxylic acids thus making them pentaerythritol based tetra-ester oils [19]. Once the synthetic esters started finding their applications in transformer insulation systems, researchers started focusing on natural esters which were found to be almost similar to synthetic esters in dielectric properties but with better bio-degradability. These natural ester oils are bio-based fluids derived from vegetable produce like sunflower seeds, rapeseeds, coconuts, palm, olives, etc. The very first natural ester oil for transformer applications was developed in early 1990s and the first natural ester oil filled transformer prototype was made in 1996. These vegetable based natural ester oils have dielectric properties comparable to those of the other insulating fluids. However, their main advantages are abundant resources, high bio-degradability and non-inflammability thus solving the problems related to the usage of mineral oil. Thus,

vegetable based natural ester oils are being looked at as most suitable alternatives to the conventional mineral oil.

However, in recent years a latest trend has emerged in the field of transformer dielectrics. Researchers are exploring the applications of certain nanomaterials in transformer insulating oils thus giving rise to the term ‘dielectric nanofluids’. The advancements in the field of nanotechnology have made it possible to choose certain nanomaterials and disperse them in transformer oils to enhance their insulating and physio-thermal properties. Several researchers have reported that the use of different nanoparticles in base oils enhances the dielectric, heat transfer and insulation properties. Figure 1.1 shows the timeline of the evolution in transformer oils from the time transformer was invented.

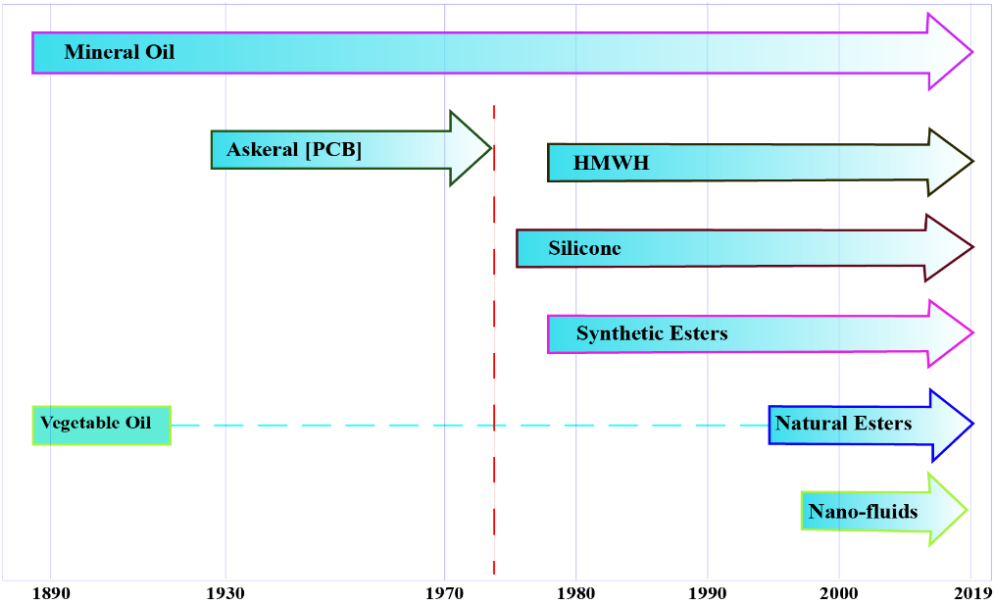

Figure 1.1 Evolution timeline of transformer oils.

In general, the development of nanofluids can be done via two methods:

1. One-step method

2. Two-step method

As per the one-step method, the synthesis as well as the dispersion of particular nanoparticles in the base oil is done simultaneously using physical vapor condensation processes [20]. One of

the advantages of using one-step method is that it results in the uniform dispersion of used nanoparticles in the solvent. Moreover, the avoidance of drying and transportation of nanoparticles can lead to the minimization of the cost involved in the entire process, yet the one-step method can lead to several disadvantages when employed. One such disadvantage of employing the one-step method is the incomplete reaction of the materials involved due to which the stability of the entire process can be lost. This results in the leftover of residual reactants in the base oil which can further lead to the formation of undesired gases in the oil. The solid residue can also cause hindrance to the flow of oil when used in transformer applications [20]. Since, one-step method involves the simultaneous synthesis and dispersion of nanoparticles in the base oil, thus the elimination of impurities from the nanoparticles is not achieved and the effects of dispersion of nanoparticles in the base oil cannot be studied without the intervention of the effects of the impurities. On the other hand, the two-step method generally consists of non-simultaneous synthesis and dispersion of nanoparticles in the base oil. In first step, the required nanoparticles are synthesized using various physical and/or chemical methods in dry powdered form and in second step, these synthesized nanoparticles are dispersed in the base oil with the help of magnetic stirrers as well as ultra-sonicator. This method is economical when employed for large scale production due to the existing high industrial production levels of nanomaterial synthesis techniques. Various nanofluids developed via one-step method as well as two-step method have already been studied for transformer applications. For example, Aberoumand et. al. employed one-step method to develop hybrid WO_3-Ag (tri-tungsten oxide silver) dispersed transformer nanofluid [21]. In another independent research by P. Kopcanský et. al., Fe_3O_4 (iron oxide) dispersed conventional transformer oil i.e., mineral oil at concentration levels up to 0.02 vol% was developed via two-step method [22]. This resulted in an overall increase in the breakdown strength of the base oil. In another separate research by Y. Zhong et. al., TiO_2 (titanium di-oxide) dispersed transformer nanofluids with concentration levels of 0.00625 vol% were developed using two-step method and the results showed significant enhancement in the breakdown strength of the nanofluid [23]. Choi et. al. developed Al_2O_3 (aluminum oxide) dispersed transformer oil with concentration levels up to 4 vol% using two-step method [24] whereas, Alicia et. al. employed two-step method to develop nano-graphene dispersed mineral oil based nanofluids with nanoparticle concentration levels from 0.01 and 0.1 wt.% [25].

1.2 THEME OF THE THESIS

Over a period of 150 years, the transformers – distribution and power transformers have evolved in many aspects such as performance, ratings, lifespan, etc. The insulating oils which are used in various types of transformers have evolved as well. The most common type of oil used for such purpose is mineral oil. Mineral Oil (M.O.) has been worked in transformers since usage of transformers started. While having many advantages like high breakdown strength and excellent cooling material, it has a major drawback of being non-biodegradable. It poses serious environmental threats when leaked or spilled into the water bodies or agricultural land. Also, with the increase in the demand of petroleum and its by-products all over the world, it is estimated that the major oil reserves across the world will start to run dry by the end if thus century. Thus, it becomes necessary to search for other alternatives which can be used in place of mineral oils in transformers with same efficient results.

In recent years, a lot of attention has been given to alternative insulating oils such as natural and synthetic ester oils. Natural ester oils (E.O.) are considered to be the best alternative for mineral oils in coming years. Various dielectric properties of natural ester fluids are comparable to those of mineral oils. The various properties of these oils can be improved further by adding different types of nanoparticles depending upon the qualities to be improved. However, agglomeration of nanoparticles and the thermal conductivity of the ester oils still remains a challenge.

The aforesaid problems are proposed to be solved through the use of ester oil/mineral oil blend based nanofluid. The most important purpose for the preparation of such dielectric nanofluid is to manufacture a transformer insulation oil which on one hand has better dielectric properties like better cooling properties of mineral oil whereas on the other hand is bio-degradable to most of the extent like the ester oil when subjected to the conditions of outer environment. Due to ester's environmentally friendly nature, the leaks and spillages are most likely to be handled in a much easier way than the conventional oils used in transformers whereas the lower viscosity of the mineral oil will enhance the flow of the fluid within the transformer. Furthermore, the addition of various nanoparticles is expected to improve its aforesaid properties. The approach is to use conducting, semi-conducting and insulating nanoparticles in the oil blend and study the effects of these nanoparticles. The methodology used in this research is summarized as follows:

(a) Preparation of EO-MO blend in different volume percentages. (EO as primary oil and MO as secondary oil)
(b) Testing of each sample of the prepared oil blend for its dielectric strength and choosing the most optimum sample for dispersion of the nanoparticles.
(c) Selection and synthesis of nanomaterials on the basis of their conductivity like Graphene Oxide (non-conductive), Titanium di-oxide (semi-conductive) and Zinc Oxide (conductive).
(d) Characterization of the nanomaterials using various techniques like XRD (to check purity), FE-SEM (to check shape and size), BET-BGH (to check surface profile), FTIR (to check various functional groups) and TGA (to check thermal stability).
(e) Mixing of synthesized nanoparticles in the chosen optimum oil blend to prepare various nanoparticle blends (nanofluids) for different concentration of nanoparticles like 0.001, 0.003, 0.005, 0.007 and 0.009 g/L.
(f) Thermal ageing of synthesized nanofluids.
(g) Electrical testing (breakdown strength, relative permittivity, tan delta etc.) of the nanofluid samples before and after ageing according to the IEEE and ASTM standards.
(h) Physio-thermal analysis (viscosity, flash point, inter-facial tension, etc.) of the nanofluid samples before and after ageing according to the IEEE and ASTM standards.
(i) Analyzing the effects of synthesized nanofluids on transformer solid insulation, i.e., transformer pressboard.
(j) Optimizing the process and nanoparticles wt. % to achieve the optimal performance in terms of electrical, chemical and thermal properties.
(k) Analyzing the design considerations and compatibility of various transformer materials with the prepared nanofluids.

1.3 ORGANISATION OF THE THESIS

This thesis has been divided into eight chapters and the brief overview of these chapters is appended below.

Chapter 1. Introduction: This chapter includes the introductory part of the thesis and explains how the transformer oils have evolved over the period of time.

Chapter 2. Literature Review: This chapter includes a detailed comprehensive literature review of transformer dielectric oils. A detailed review of the increase in the global consumption of electrical energy has been presented. A review of the usage of mineral oil, vegetable oil as well as dielectric nanofluids has been presented in order to assist with various explanations of the results obtained in this thesis. The major gaps in research have been identified and the corresponding objectives of this research have been listed.

Chapter 3. Synthesis of Materials: This chapter deals with the various techniques and methods of synthesizing the materials required for this research. Methods of synthesizing the selected nanomaterials as well as their characterizations have been explained in this chapter. The procedure of fabrication of nanofluids as well as the method of preparing the solid insulation samples have also been explained. This chapter fulfils the targets set in Objective-1.

Chapter 4. Study of Dielectric Properties of Synthesized Nanofluids for Transformers: In this chapter, the dielectric properties like ac breakdown voltage, impulse breakdown voltage, permittivity and dissipation factor and the physio-thermal properties like viscosity, flash point and interfacial tension of synthesized liquid insulation samples have been studied using standard IEC and ASTM specifications for transformer oils. The abovesaid properties of synthesized nanofluids have been investigated and compared with the corresponding properties of the base oil. This chapter fulfils the targets set in Objective-2.

Chapter 5. Analysis of Ageing Effects on Synthesized Liquid Insulation for Transformers: This chapter deals with the investigation of dielectric properties as well as physio-thermal properties of synthesized nanofluids after being subjected to thermal stress for periods of 15 days and 60 days. These properties have been studied after ageing and compared to the insulating properties of newly prepared unaged nanofluids. This chapter fulfils the targets set in Objective-2 and sheds some light on Objective-3.

Chapter 6. Analysis of Ageing Effects on Prepared Solid Insulation for Transformers: This chapter investigates the effect of ageing on the solid insulation impregnated with the synthesized

insulating oils. The mechanical properties like the cellulosic degradation and tensile strength and the dielectric properties like breakdown voltage, permittivity and the dissipation factor of solid insulation samples have been studied and compared before and after subjected to thermal ageing conditions. This chapter fulfils the targets set in Objective-3.

Chapter 7. Transformer Design Considerations: In this chapter, the necessity of required changes (if any) in the design of power transformers when filled with the proposed nanofluids has been analyzed in an analytical approach. This chapter fulfils the targets set in Objective-4.

Chapter 8. Conclusions and Future Scope: This section presents the summarized conclusion of this thesis and sheds light on the future scope as well as aspects of this work.

CHAPTER 2

LITERATURE REVIEW

THIS chapter provides an extensive review of continuous increase in the demand of electrical energy worldwide thus leading to the production of transformers with higher ratings. The usage of different insulating oils along with their insulating properties and applications in transformers have been reviewed as well.

2.1 INCREASE IN DEMAND OF ELECTRICAL ENERGY

Over the last century, ever since the first transformer was invented, the demand in electrical energy has been increasing on a daily basis. It is almost impossible to imagine the difference between the consumption of electrical energy during the beginning and the end of the 20th century without having actual statistics. The increasing population as well as the growing industrialization have collectively led to this continuous increase in demand. In 1980, the annual electric energy consumption worldwide was 7.3 trillion kWh, whereas in 2000 this worldwide electric energy consumption increased to 13.2 trillion kWh and further to 23.1 trillion kWh in 2020 [26]. However, the worldwide electric energy consumption has been reported with even a faster increase in the

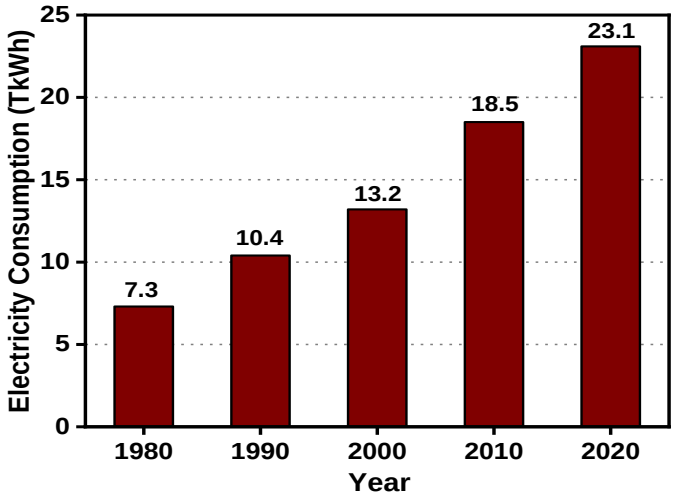

Figure 2.1 Global electric power consumption from 1980 to 2020.

21st century having an average annual increase in electric energy consumption of 3.4% [27]. Figure 2.1 shows the decade-wise distribution of annual global electric energy consumption from 1980 to 2020, whereas the Figure 2.2 shows the global electricity consumption of different regions across the globe in the years 2000 and 2020.

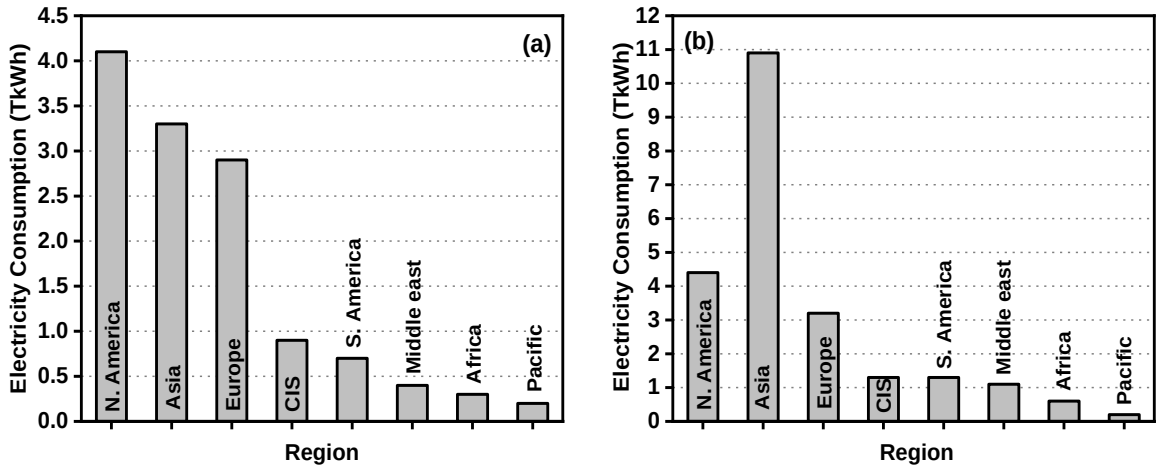

Figure 2.2 Region-wise annual electricity consumption in years (a) 2000 and (b) 2020.

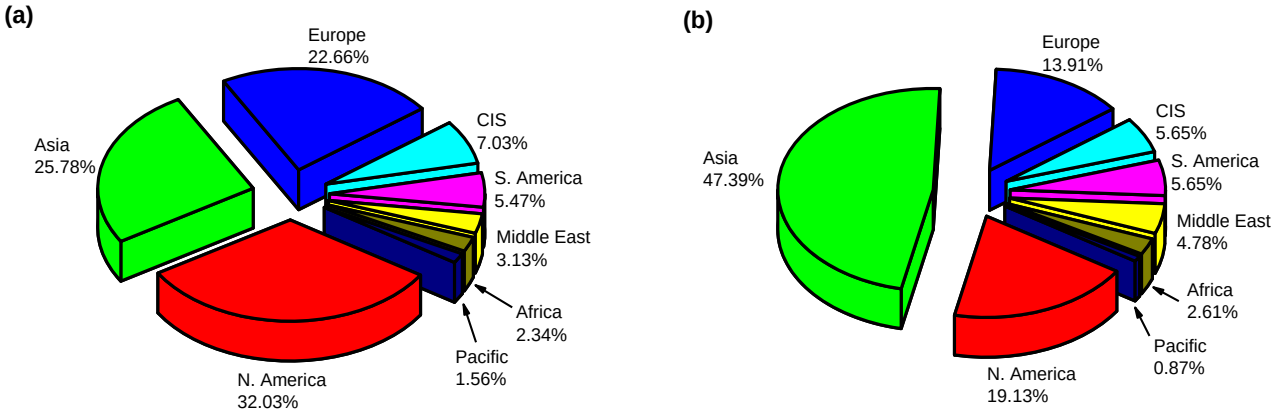

Figure 2.3 Region-wise share in annual electricity consumption in years (a) 2000 and (b) 2020.

The developing continents witnessed a far more increase in their electricity consumption as compared to the developed continents, the highest increase shown by Asia. This is due to the fact that the regions like southern Asia houses emerging economies like India, Pakistan, Malaysia, etc., which are on continuous path of adopting recent developments thus increasing their electricity consumptions. In terms of increase in global shares in electricity consumption of different regions

covering the entire globe in years 2000 and 2020, as is shown in Figure 2.3, the share of Africa, South America and Asia from 2000 to 2020 increased by 11.5%, 3.29% and 84%, respectively. The global shares of Middle East from 2000 to 2020 also increased by 34.5%. The regions which reported a decrease in their global shares of electricity consumption from 2000 to 2020 are North America, Europe, Pacific and CIS countries. Their respective global shares from 2000 to 2020 decreased by 40.2%, 38.61%, 44.2% and 19.6%, respectively.

This overall increase in the worldwide electricity consumption has resulted in a very high demand of electrical energy in both domestic as well as industrial sectors. In order to meet this demand with the most possible reliability, the electrical equipment need to be updated constantly right from the generating stations to the distribution stations and eventually up to the consumer ends. In terms of transformers, this updating means increasing their power handling capacity, i.e., their ratings, thus resulting in a significant increase in the ratings of transformers continuously without letting the engineers and researchers to put a final limit [28].

2.2 INCREASE IN TRANSFORMER RATINGS

After the discovery of the phenomenon of electromagnetic induction in 1831 by Sir Michael Faraday, the application of electricity was revolutionized to such a great extent that it finally led to the development of the most important component of any electrical system, i.e., the transformer. By 1883, secondary generators started to find their usage to light up a 12-kilometer section in the first a.c. distribution system in London Underground in Britain [29]. In 1884-85, a Budapest based company, known as The Ganz Company, manufactured a closed-core device which, in its patent, was called a “transformer”. In 1893, the first transformer production started in Paris and during the same year in Sweden, one of the first three-phase electric power was transferred commercially – from a hydro power plant to an iron ore mine about 10 km away [30]. It was again in Sweden in the early 1950s, when the world’s first 400 kV transmission with 500 MW capacity was developed over the span of about 1000 km. This was the first step into the world of extra high voltage (EHV). In later 1960s, a Canadian power company Hydro-Québec developed a 735 kV transmission system to transfer the electric power to far flung and geographically remote areas. In early 1970s, two giant electric companies, ABB Ludvika and American Electric Power, AEP, came together

with the goal of finding the highest possible feasible transmission voltage. For this research, they developed a full size three phase transformer network with a total capacity of 3000 MVA, the first transformer network of that capacity [30]. It was during this time the voltage level of 800 kV was achieved and the Grid Solutions developed the first 600 MVA generating transformer, thus onsetting the era of ultra-high voltage (UHV). Since then, transformers saw many modifications and upgrades but it was in 2006 when the first vegetable oil immersed 245 kV shunt reactor was developed. Table 2.1 gives a summarized timeline of evolution of transformers whereas Figure 2.4 shows the evolution of transformer ratings over the years.

Table 2.1 Evolution of transformers.

Year	*Achievement*
1831	The principle of Electromagnetic Induction is discovered by Sir Michael Faraday
1853	A spark inductor-based voltage transformer is developed by H. Ruhmkorff
1883	Secondary generators are used as a part of distribution system in London
1885	A machine called “Transformer” is patented by M. Deri and Co.
1893	First transformer production is started in Paris
1910-20	Voltage levels of 220 kV are achieved
1929	First 3.5 MVA, 100/27.7 kV transformer is developed
1933	First 40 MVA, 220/8.8 kV transformer is developed
1945	Voltage levels of 400 kV are achieved
1960-70	Generating transformers of 600 MVA ratings are developed
1985-90	Development of amorphous core type distribution transformers takes place
2006	Vegetable oil immersed 245 kV shunt reactors are manufactured
2007	The largest electric arc furnace transformer of rating 300 MVA is developed
2010	800 kV transformer prototype tested for UHVDC network

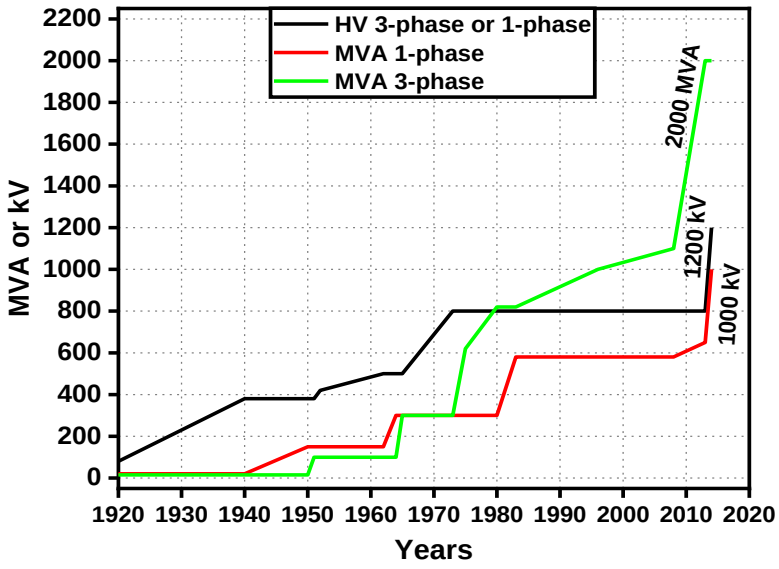

Figure 2.4 Increase in voltage and power rating of transformers over the years

2.3 USAGE OF MINERAL OIL IN TRANSFORMERS

Mineral oil has been the insulating oil of choice for every type of transformer over the past century. Even after the development of suitable alternative fluids like silicone oils and ester oils, mineral oil is still the most widely used insulating oil in transformers – from generating level to distribution level [10,11]. The reasons behind its common usage are well known as well. It has optimum breakdown voltage, is very cheap when compared to its alternative fluids and is readily available. It has relatively low viscosity making it a good coolant as well [12-15]. Mineral oil can be generally classified in two categories – paraffinic oil and naphthenic oil. Both types of oils are derived from base crude oil. During the early usage of mineral oil in transformers, paraffinic oils were widely used due to their easy processing as compared to the naphthenic oils. However, due to their high pour point and the presence of normal paraffins and wax, the oxidation stability of paraffinic oils was very low. The residue precipitate formed as the result of oxidation would settle down at the bottom of the tank and cooling ducts causing hinderance in the transformer's entire cooling system. This resulted in the switching of focus towards the naphthenic oils which would have low pour point and were mostly wax-free [31]. The dielectric properties of naphthenic oils are also superior to paraffinic oils [32]. The material compatibility of naphthenic oils with various transformer components like Styrene Butadiene Rubber (SBR) made gaskets and seals is also much better as compared to the paraffinic oils. Due to all these factors, naphthenic oils have

become the most widely used type of mineral oil in transformers [33]. Figure 2.5 shows a brief overview of two types of mineral oils used in transformers.

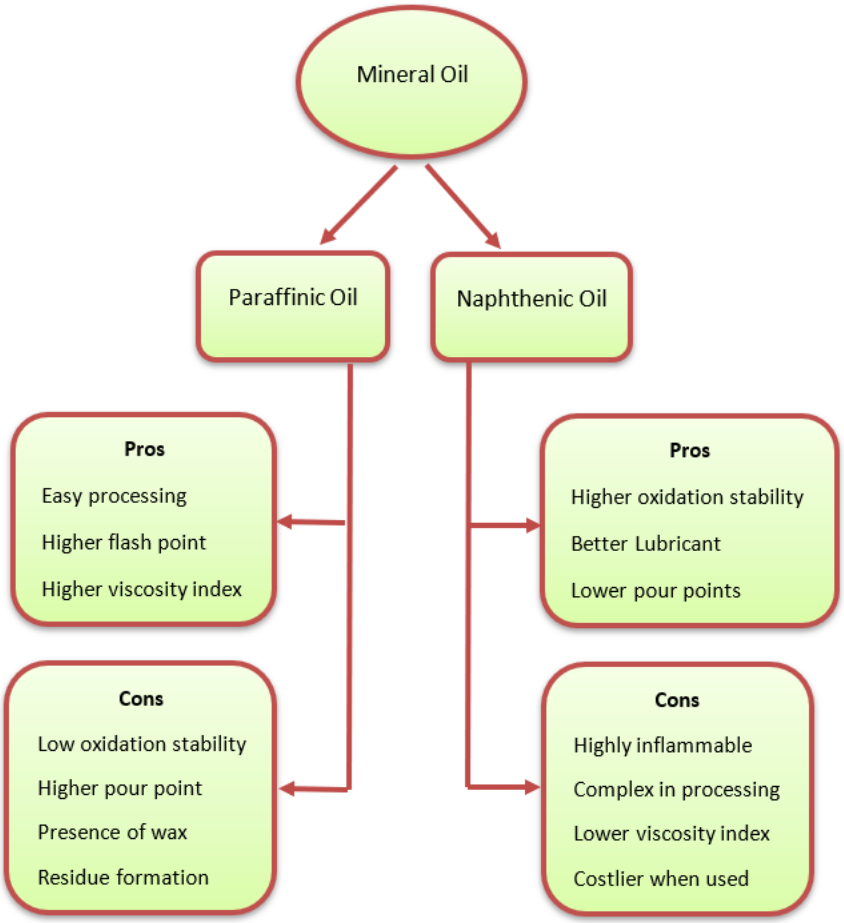

Figure 2.5 Types of mineral oil for transformer applications.

2.4 USAGE OF ESTER OIL IN TRANSFORMERS

2.4.1 General Composition of Ester Oils

Chemically, an ester can be defined as a chemical compound which is derived from an acid having at least one hydroxyl (-OH) group replaced by an alkoxy (O-alkyl) group [34]. In most of the cases, esters are derived from an alcohol and a carboxylic acid. Esters are formed by the process of esterification which is basically a condensation reaction between a carboxylic acid and alcohol

[35]. Vegetable oils are the primary source for the derivation of natural esters whereas a particular group of chemicals can be used to make the synthetic ester. The chemicals are selected as per the desired properties. The term “ester” is referred to various chemical compounds having particular chemical structures which fall in a particular category. For fatty acids, the structure is represented by the formula shown in Figure 2.6 [36].

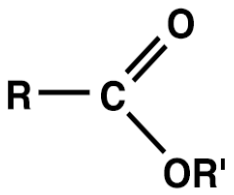

Figure 2.6 Structure of fatty acid in an ester.

The C represents carbon, O represents the oxygen, R´ denotes an aryl or alkyl group, which in every case, is attached to an oxygen atom. The single dash is representing a single bond whereas the double dash is representing the double bond. An aryl group is a particular type of group which consists of carbon atom and hydrogen atom in a particular pattern C_nH_{2n+1}. Here, the letter “n” is generally having any numerical value (number) and represents the molecular length of the structure. The aryl group, which in some cases is replaced by alkyl group, is obtained from its parent alkane. It is essentially a particular type of hydrocarbon, i.e., aromatic hydrocarbon having one atom of hydrogen less than the number of hydrogen atoms in their parent alkane. The name of the ester compound is taken from the parent acid and the parent alcohol. The esters which are derived from the simple carboxylic groups are named according to their traditional names, e.g., as acetate, butyrate, etc. On the other hand, the esters which are derived from complex carboxylic acids are named using their IUPAC nomenclature, e.g., as butyl ethanoate etc. the functional group of esters is –COO, and is known as ester link [37]. All the ester oils have one component in common, i.e., a triglyceride component [38]. In natural esters, common fatty acids are oleic acid and stearic acid which have eighteen carbon atoms in their chain. The fats and oils thus formed are also known as triglycerides [39]. The properties of all types of ester oils (natural or synthetic) mainly depend on the overall content of the fatty acid in the oil. Figure 2.7 shows the general structure of a triglyceride [37].

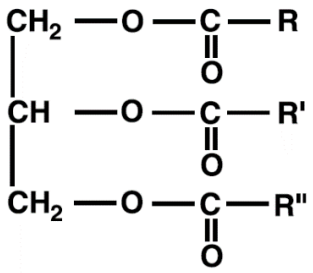

Figure 2.7 A triglyceride structure.

The R, R´, and R´´ are the fatty acid components. These are organic groups (made up of carbon, oxygen and hydrogen) and consist of chains of 8 to 22 carbon atoms. Fatty acids include linoleic acid, oleic acid, palmitic acid and stearic acid. There is a great effect of type of bonding on the properties of the oil. For example, oils with single bonds i.e., saturated fatty acids show better oxygen stability but at the same time, also raise the possibility of the higher pour point to an undesirable level such as 20-25°C. Similarly, multiple double bonded ester fluids are more prone to polymerization which again is a desirable quality in an insulating dielectric fluid, but at the same time, these fluids show a poor oxidation stability – something generally not wanted in a dielectric fluid to be used as an insulator in a power transformer.

2.4.2 Refining of Ester Oils

Natural esters, which are generally all the fats and oils extracted from plants and animal sources, are formed from condensation reaction between alcohol glycerol and fatty acids which are essentially long chain carboxylic acids [38]. For example, glycerol (IUPAC name propane-1,2,3-triol) whose structure can be drawn as shown in Figure 2.8a. Taking the case of propanol, ethanoic acid and their result propyl ethanoate, the structures of esters can be understood as shown in Figure 2.8b. The process of refining of ester oils is totally different in manner than that of the mineral oil. In the case of the conventional oil, i.e., mineral oil, the process of extraction of the crude oil from the ground is done by drilling, and is treated in air as well as vacuum through various distillation steps which is then followed by the treatment with the hydrogen at a certain pressure in the presence of a catalyst. In the case of natural ester, the source used to derive the oil from is crops.

So, natural esters are generally more attractive than mineral oils due to the renewability and biodegradability in their nature.

Multistep processes involving various techniques are used to manufacture the natural ester oil [40-42]. Generally, there are two basic techniques which are applied for the extraction of the natural ester oils in their crude form. Their respective oil seeds are used as the primary sources for the extraction of these oils. First technique is the bench pressing. It involves the application of hydraulic pressing on the crop seeds. Pressure is also applied on the pulp. In some cases, the use of a rotating screw or worm can also be made. Bench pressing technique is most profitably used on softer crops like rapeseed and sunflowers [43]. The second technique involves the crushing of seeds and the extraction of oil with a solvent like hexane. This technique is best suited for harder crops like soybeans. In order to remove other unwanted materials like chlorophyll from the oil, a degumming step is carried out by separating them physically. This physical separation becomes

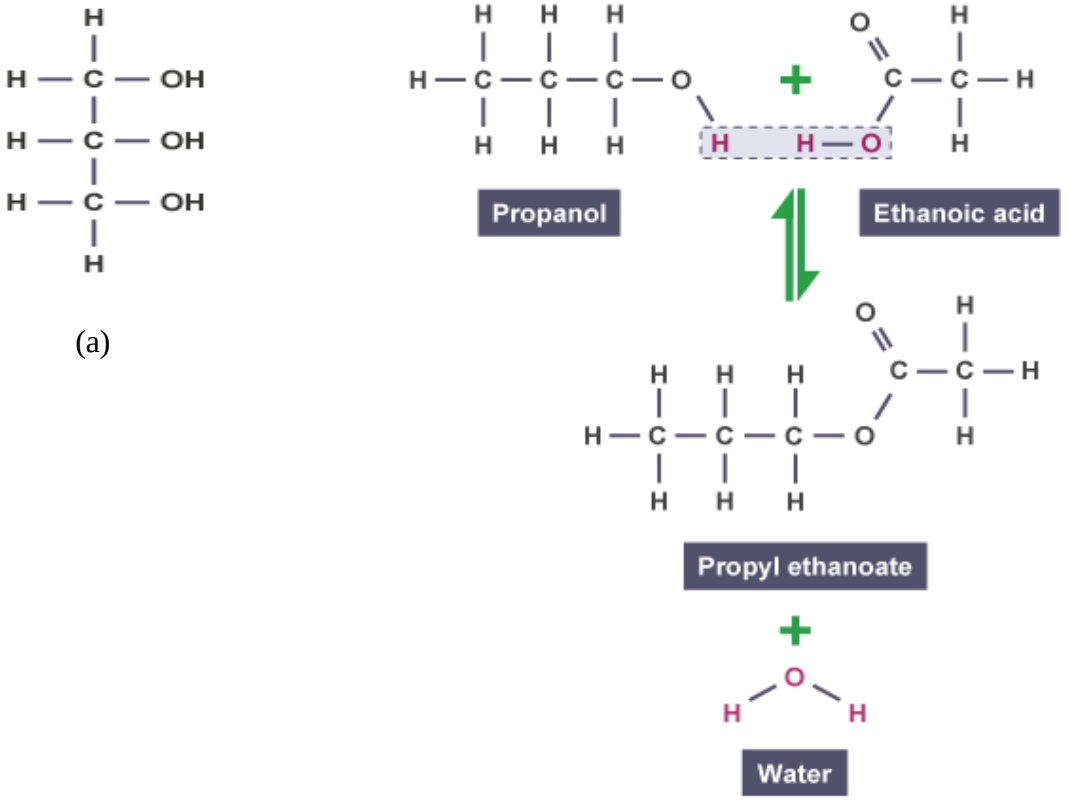

(a)

(b)

Figure 2.8 (a) Structure of glycerol and (b) Formation and basic structure of Propyl ethanoate (an ester).

tedious and time consuming. So, another degumming process is used in majority of the cases which consists of making a solute of material and a solvent, normally water. Any catalyst material can also be used to speed up the process. The next step which is the part of neutralization process is called as bleaching process. In this process, the oil is subjected to clay treatment in order to remove the polar compounds. Steam distillation in vacuum at a temperature of 200°C is done to remove the unwanted volatile compounds in order to deodorize the oil. Due to more controllable refining processes, a product which is more consistent is produced. The natural ester insulating oils differ from their predecessors in many aspects, like the early natural ester oils didn't have any additives; the new ester oils have a variety of additives which enhance their properties.

2.4.3 Ester Oil as Transformer Oil

In recent years, a lot of attention has been given to alternative insulating oils such as natural and synthetic ester oils [43-52]. Natural ester oils are considered to be the best alternative for mineral oils in coming years [53-65]. The main purpose of the transformer oil is to act as an insulator in the transformer and to dissipate the heat of the transformer. It also acts as a barrier between the atmospheric oxygen and cellulose paper, which is prone to oxidation. Various dielectric properties of natural ester fluids are comparable to those of mineral oils as shown in Table 2.2 [61-71]. The most important purpose for the preparation of such dielectric fluid is to manufacture a transformer insulation oil which on one hand has better dielectric properties, whereas on the other hand is bio-degradable to most of the extent when subjected to the conditions of outer environment. Due to natural esters' environmentally friendly nature, the leaks and spillages are most likely to be handled in a much easier way than the conventional oils used in power transformers. Since the time when these oils were developed for the very first time, many positive qualities of these oils are being explored continuously. In general, potential users of natural ester insulating fluids would expect various qualities to be present in the oil, some of which are:

- Biodegradability to most of the extent.
- Nontoxic in nature.
- Good material compatibility with other transformer components.
- High breakdown voltage.
- High thermal stability.
- Dielectric constant closer to the solid insulation.

• Relatively low pour point.

Table 2.2 Dielectric properties of various transformer oils [61-71].

Properties	***Mineral Oil***	***Silicone Oil***	***Synthetic Ester***	***Natural Ester***
Breakdown Strength (kV)	30-85	35-60	45-75	49-99
Dissipation factor % (25°C)	0.005-0.05	0.01	0.0006-0.001	0.001-0.003
Dissipation factor % (90°C)	<0.002	<0.001	0.005	<0.006
Relative Permittivity (20°C)	2.1-2.5	2.6-2.9	3.0-3.5	2.9-3.3
Kinematic viscosity, $mm^{2/s}$ (0°C)	<76	81-92	26-240	77-500
Kinematic viscosity, $mm^{2/s}$ (40°C)	3-16	35-40	14-29	16-50
Kinematic viscosity, $mm^{2/s}$ (100°C)	2-3	15-17	4-6	4-15
Flash point, °C	110-175	300-310	250-310	310-343
Fire point, °C	110-185	330-350	300-322	300-369
Pour point, °C	-30 to -63	-50 to -60	-40 to -60	-10 to -33
Biodegradability, OECD 301, % (at 28 days)	<10	<5	>80	>95
Fire hazard classification, IEC 61100	0	K_3	K_3	K_2

It is clear from the table above that from the ecological point of view, the main outstanding properties of the ester oils are biodegradability and flash point. For both natural as well as synthetic esters, their biodegradability is considerably much better than the mineral oil. Considering that

after a period of 28 days, both the esters decay in about 60%, making them a perfect biodegradable insulating fluid as per OECD 301 standards. So, it becomes much easier to use ester oils in the places where environmental regulations are restricted.

Flash point is another factor which specifies both the esters as the environmentally friendly fluids. The “open burner” test is generally performed on all the three dielectric fluids and confirms the data given in the table above. In case of mineral oil, an open fire is delivered from the acetyl burner following which there is a violent increase in the temperature of the oil. After a period of around 4 minutes, the conventional oil, i.e., the mineral oil gets ignited at a temperature of 130°C. The oil keeps burning without the open fire as well and emits a dense black smoke in the environment. On the other hand, in ester oil, the increase in the temperature of the oil takes place at a slower rate and the ignition takes place at a temperature above 250°C. Both the esters emit the smoke in smaller amounts with density much lower when compared to those of the mineral oils. In terms of percentages, the burned ester oils emit a volume of waste gases which is only about 15% of the total amount of the volume of gases emitted as a waste product by the burning mineral oil.

When measured as per IEC 60156 standard, the breakdown voltage (BDV) of a typical natural ester oil is also better than the conventional mineral oil. It is found out by using a special apparatus having profiled metal electrodes which can create a uniform electric field distribution. The liquid sample is put in the apparatus. The input AC voltage is increased resulting in increasing electric field. The oil sample is subjected to this increasing electrical field and the breakdown value is recorded. The average of six such breakdown voltage values is finally jotted down and recorded as the breakdown voltage of the sample. The BDV (breakdown voltage) value is mostly dependent upon the materialistic quality of the liquid to be tested, i.e., water and the content of the impurities present in the liquid.

Keeping in view the effect of the moisture content on the dielectric strength, the ester fluids behave in a better way as compared to the mineral oils. The reason behind this better behavior is that the ester fluids are tested and characterized by/under particular values of input breakdown voltages with respect to the moisture content up to the value of 600 ppm. Whereas in case of mineral oils, its strength decreases even at the small increase in the moisture content. At a 17 concentration of 20 ppm, the BDV, i.e., the breakdown voltage is about 40 kV whereas a well-tested ester oil has a breakdown voltage of around 65-75 kV. The better usage of ester fluids as

the insulating oils in power transformer can also be justified by looking at the other parameters of their dielectric properties. One such parameter is the electrical permittivity. The overall insulating system of any transformer winding consists of combined arrangement of dielectric liquid materials and dielectric solid materials like transformer-board or cellulose paper. This combination is connected in series arrangement, parallel arrangement or series-parallel arrangement. In the most commonly used system, i.e., the series system, the stress distribution is dependent inversely upon the dielectric permittivity of the material. More the stress distribution is uniform, higher the strength of the system. The electrical permittivity value of the esters is higher (3.0-3.5) than that of the mineral oil (2.1-2.5). This proves to be profitable for the stress distribution in the oil-cellulose system (electrical permittivity of cellulose being around 4). In spite of all the positive properties of ester oils, their lightning strength lacks behind when compared to the mineral oil. Lightning strength is the strength of a material to withstand the short pulses or spikes of voltage which have a steeper front (1.2 μs) and a comparatively long back (50 μs). The experimental considerations and studies over the processes of initiation as well as over the processes of propagation of electrical discharges in the insulating fluid under short voltage pulses (lightning pulses) indicate that only at 50% of their BDV, the electrical discharges start to develop in the ester dielectrics. With the increase in voltage, the electrical discharges grow stronger in ester dielectric fluids as compared to those in mineral oils. These strong and energetic electrical discharges are more hazardous for the solid (paper and transformer-board) as well as the liquid insulation of the power transformer, and can pose serious threats to the overall insulation system through the process of local carbonization. Thus, when ester oils are used as the dielectric fluids in the transformers, it is recommended to use wider insulation gaps in the transformer for the sake of lightning strength. It becomes even more important in the case of power transformers having the ratings equal to or higher than 110 kV.

On the other hand, the more viscosity of ester fluids doesn't let them circulate as freely as mineral oils. The oil flow velocity in case of ester fluids is slower in the cooling channels of the magnetic core and windings. This restricted flow doesn't allow the ester fluids to reach all parts of the insulating systems of a power transformer. So, the design of the insulation system in the power transformers should be in compatibility with the physio-chemical properties of the insulating oil so that the proper circulation of coolant is achieved both in forced as well as natural circulation.

This demands the insulating system in power transformers which are filled with ester oils to have wider oil channels as compared to the transformers filled with the mineral oil.

2.5 USAGE OF NANOFLUIDS IN TRANSFORMERS

The term “nanoparticle” or “ultrafine particle” is generally used in the same sense. Nanoparticles are generally particles in the size range of 1-100 nm. According to the ISO technical specifications 80004, a nanoparticle can be defined as a nano object having its all the three sides i.e., three dimensions in terms of nano-scale with no significant difference between its longest and shortest axes. In 2008, the ISO (International Organization for Standard) set the definition of nanoparticles on a discrete nano object having its all the three dimensions (Cartesian dimensions) less than 100 nm [72]. Similarly, the ISO set definition for two-dimensional nano objects (i.e., nanoparticles and nano-dimensions) and one-dimensional new object (i.e., nanotube and nanofiber). Later in 2011, a wide range and more technical definition was put forth by the commission of the European Union. It stated that a particle can be considered as a nanoparticle if at least one of its characteristic dimensions is in the range of 1-100 nm even if its other dimensions don’t fall within this size range. The reason behind using 1 nm as a lower limit is that the atomic bond length takes place at 0.1 nm [72]. Nanoparticles exist naturally in the environment and can be created through human efforts too. Their submicroscopic size enables them to possess outstanding material properties, as a result these nanoparticles find their applications in large variety of fields like engineering, medicine, environmental remediation etc.

Based upon the shape, size and choice of the material, nanoparticles can be classified into various types [73]. One of the bases of classifications is that whether the nanoparticles are organic or inorganic, though there are a very few organic nanoparticles which include liposomes and polymeric nanoparticles [74]. Inorganic nanoparticles are fullerenes, gold nanoparticles, quantum dots etc. Similarly, other basis of classifications divides nanoparticles into categories like ceramic based, polymeric based, conductors, semiconductors, etc. [75-77] Depending upon the structure, nanoparticles can also be classified as hard and soft nanoparticles [78]. Titanium dioxide, silica dioxide (silica), fullerenes etc. are hard nanoparticles whereas vesicles, liposomes and nanodroplets are the soft nanoparticles. So, the basis of their classification generally depends either

upon their applications (area where they are to be used) or upon the way in which the nanoparticles are produced. Figure 2.9 shows different classifications of nanomaterials while highlighting the basis of classification for this research within a box.

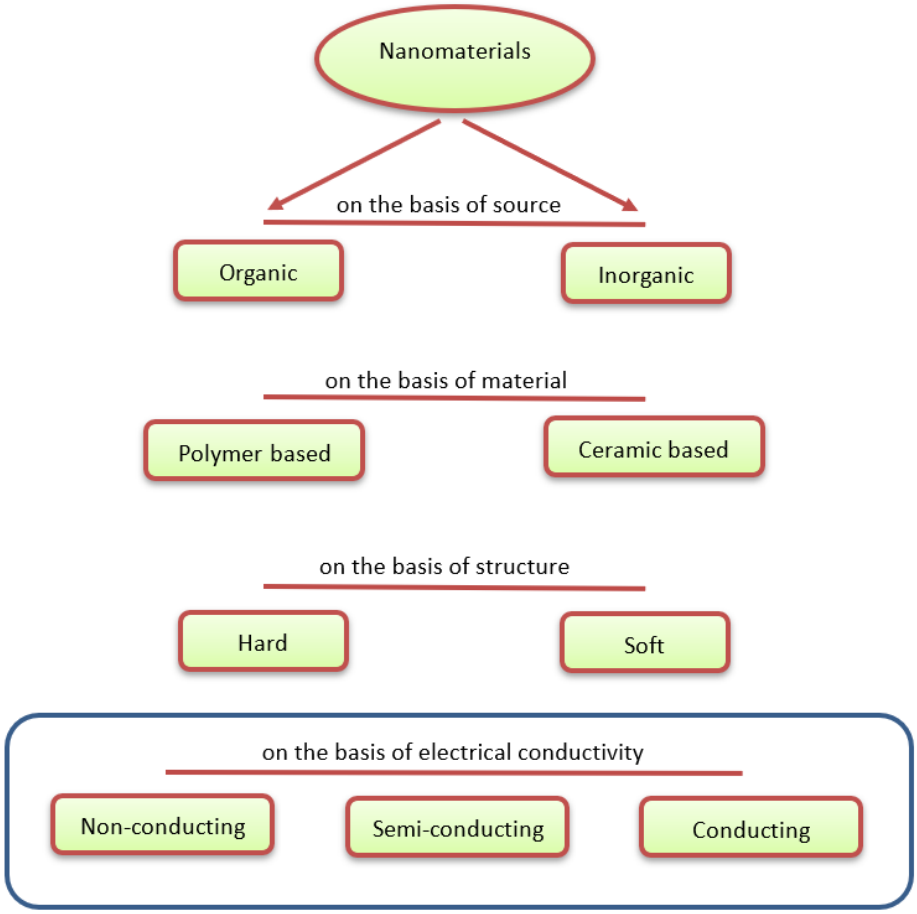

Figure 2.9 Types of nanomaterials and the basis of classification chosen for this research.

The major physical properties of nanoparticles due to which they are sought after in various fields are:

1. Their mobility in the free state is very high. For example, a nanoparticle of silica having 10 nm diameters possesses a sedimentation rate of 0.01 mm/day in water under normal gravity.
2. Their specific surface areas are large. For example, a teaspoon (6 ml) of silica nanospheres having 10 nm diameters has much more surface area than a dozen double sized tennis courts.
3. Nanoparticles are known to exhibit quantum effects.

4. Certain nanoparticles are known for their electron trapping capabilities which can be helpful in improving the dielectric properties of materials they are dispersed in.

There are many properties that are unique to nanoparticles because of their direct relation with the particle size. So, it has been a common trend to incorporate these properties into other materials (composite materials or liquid materials). An example of how the unique properties of nanoparticles are incorporated in base materials is rubber tires which have rubber (elastomer) as a base material and an inorganic filler like carbon black or silica as nanoparticle. Another example is to vary the dielectric properties of various insulating materials by varying the interfacial as well as inter-particle distances of the nanomaterials which are dispersed in the base insulating materials. Similarly, another example is the mineral oil based nanofluid which is used in the transformer as dielectric oil, and it consists of mineral oil as a base material and aluminum dioxide, silica dioxide, graphene etc. as nanoparticles.

In case of most of the nanocomposite materials, there are some complications in incorporating the nanoparticles into the base materials. Nanoparticles tend to agglomerate very easily, as a result there is formation of large clumps which are generally very difficult to redisperse [79-81]. Moreover, when nanoparticles are mixed with the base materials, their unique properties are lost in some of the cases; properties which are directly related to their size. Nevertheless, the use of nanoparticles has been growing rapidly since early 21^{st} century [82-91].

In the field of electrical insulation systems, researchers have started to further improve the dielectric and thermal properties of insulating oils by either using the blends of various oils or by mixing various nanoparticles in the oils to make nanofluids**.** For example, experiments are being carried out to study the behavior of blends of mineral oil and ester oil [92-96]. A blend containing 80% mineral oil and 20% ester oil has drawn a lot of attention from the researchers as this blend has shown some better electrical as well as thermal properties as compared to the base oils alone. Likewise, various blends having mineral oil and ester oil, mineral oil and silicone oil, natural ester and synthetic ester, etc. are being tested for their properties as well as the transformer solid insulation, i.e., pressboard has been studied for the ageing effects and creeping discharges [97, 99]. Similarly, various nanoparticles like SiO_2, Fe_2O_3, Fe_3O_4, BN, TiO_2, ZnO, Al_2O_3, etc. are being

used to make nanofluids for the insulation purposes [20, 100]. It has been shown that the addition of some of these nanoparticles in the base oils has led to an increase in breakdown voltage of the mixture. A recent experimental study conducted by R. Karthik et. al. has shown that the dielectric breakdown voltage of natural esters can be increased by 42% - 62% by adding SiO_2 nanoparticles of size 10-12nm [101]. Similarly, B. X. Du et. al. showed that the addition of small concentration (0.1 wt. %) of boron nitride. i.e., BN, in natural esters led to an increase in a.c. breakdown voltage (34%) and better heat transfer performance [102]. Likewise, the breakdown voltage of soybean and palm oil-based natural esters was increased by just adding ZnO nanoparticles as shown by W. Saenkhumwong et. al. [103]. The individual and joint researches conducted by Technical University of Lodz, Poland, North China Electric Power University, China, Texas A&M University, USA, University of Malaya, Malaysia, Aligarh Muslim University, India and University of Patras, Greece are the major contributors to the field of vegetable oil based dielectric nanofluid blends. In Malaysia, A. Mohamad et. al. examined the properties such as breakdown voltage and dielectric loss in Fe_3O_4, CuO and Al_2O_3 dispersed nanofluids and reported that these properties were greatly affected by the concentration of the nanoparticles; B.D.V increased and tan delta valued decreased at lower concentrations (0.01 g/L) [104]. It was also reported that the semi-conductive nanoparticles were more suitable options than conductive nanoparticles due to former's less vigorous influence of dielectrophoretic forces on vegetable oils. In Greece, V. P. Charalampakos et. al. concluded that the dielectric properties of vegetable oils were improved by incorporating conductive nanoparticles like Fe_2O_3 due to their free electron trapping property whereas the addition of insulting nanoparticles like SiO_2 failed to do so [105]. In Malaysia, N. S. Suhaimi et. al. prepared a Carbon Nanotube (C.N.T) filled mineral oil and palm oil blend and studied the effect of CNT on dielectric oil [106]. They showed that certain amounts of CNT's concentration can improve AC breakdown performance of mineral oil. It was also found that as the concentrations increased, the probability of breakdown failure gradually decreased. Similar patterns were observed for palm based CNT nanofluids. However, the presences of CNTs were inappropriate for palm oil. This was because the probability of AC breakdown of palm oil based CNT nanofluids dropped slightly for 0.01g/L and 0.05g/L and fell significantly for 0.2g/L concentrations. In Thailand, Potivejkul et. al. investigated the AC breakdown voltage and negative impulse breakdown voltage characteristics of the unmodified natural ester and the natural ester based TiO_2 and ZnO nanofluids [107]. It was found that the modified liquid AC breakdown

property was strongly influenced by the nanoparticles type. With the addition of nanoparticles, the AC breakdown voltage increased slightly above that of the unmodified natural ester. Additionally, TiO_2 and ZnO nanofluids demonstrated their exceptional properties to increase the negative lightning impulse breakdown voltage of the natural ester based nanofluids compared to the original natural ester. According to all results, it was found that the studied nanoparticles are good candidates to enhance the dielectric properties of the natural ester for dielectric applications. In Saudi Arabia, Khaled et. al. showed that the AC breakdown voltages of synthetic ester-based Fe_3O_4, Al_2O_3 and SiO_2 nanofluids based on synthetic ester nanofluids are improved [108]. The improvement is the best with conductive/magnetic nanoparticles (Fe_3O_4), about 48% at a concentration of 0.4 g/L. However, the addition of insulating nanoparticles with the smallest size also gave interesting results; the increase in AC BDV was of about 35% for 13 nm size at a concentration of 0.05 g/L; the decrease of nanoparticles size resulted in an increase of AC breakdown voltage. With such nanoparticles (Al_2O_3), the dielectric constant as well as dissipation factor were less impacted.

Another group of researchers from Greece, Charalampakos et. al. studied breakdown voltages of natural ester based nanofluid under ac voltage stress [109]. Graphene nanosheets of various sizes were inserted in to prepare the nanofluid. The diameter of nanosheets ranged from 50 nm to 500 nm. They concluded that the B.D.V. i.e., breakdown voltage was significantly reduced with the addition of graphene nanosheets concentration. After the first initial reductions, breakdown voltage remained constant between the values of 40 and 50 kV, and did not reduce further with increased concentration of nanoparticles. This indicates that it can be possible to have a positive effect, i.e., to increase the breakdown voltage by increasing the graphene nanosheet concentrations. The dielectric qualities of nanofluids were usually enhanced as the size of nanoparticles was reduced. The smaller sized nanoparticles also had a positive effect on agglomeration and sedimentation inside the fluids. Thus, the behavior of graphene nanofluid is expected to be improved if nanosheets of smaller dimensions are used and the reduction of breakdown voltage would not be so intense.

In India, a joint team from Research and Innovation Centre DRDO, IIT Madras and School of Mechanical, Materials and Energy Engineering, IIT Ropar collectively studied the dielectric behavior of graphene and Carbon Nano-Tubes (CNT) infused insulating nanofluids. P. Dhar et. al. showed how the natural convection and viscous effects are affected by adding the excessive

nanoparticles [110]. On increasing the concentration of nanoparticles, the viscous effects of the transformer oil increased which further led to deteriorated efficiency of the convection. This can be implied to say that the thermal conductivity decreased with the increase in the nanoparticle concentration. This is a very important point to focus on as most of the transformer systems which are generally oil cooled follow the convection process. Another joint team from Central Power Research Institute (CPRI), Bangalore and NIT Durgapur, West Bengal studied the dielectric and thermal conductivity of synthetic ester oil based TiO_2 nanofluids [111]. They showed that there was an increase of 15.3% in A.C. breakdown voltage whereas increase in Impulse Lightning Breakdown was 3.6% on adding the nanoparticles. Thermal conductivity as well as the flash and fire points showed a linear increase with the increase in the concentration of nanoparticles. Khan et. al. from Aligarh Muslim University researched upon the dielectric characterization of ester oil filled with Fe_2P nanoparticles [112]. The inferior dielectric properties of ester oil which is generally biodegradable and inflammable showed promising enhancement in their dielectric as well as thermal properties. The maximum increase in the breakdown voltage of the prepared nanofluid was obtained at 11mg solution. With further increase in the concentration of the nanoparticles, a sharp decrease in the values of BDV was recorded. One of the reasons for this can be the particle agglomeration.

Taro et. al. from NERIST, Arunachal Pradesh tested for silica (SiO_2) nanoparticles in MIDEL, ester oil and its effect on the lightning impulse breakdown voltage [113]. The lightning impulse breakdown voltage values were found to be higher in nanofluids as compared to the base oils. Moreover, the density of the fluid remained at a fixed value at all the volume fraction of silica (SiO_2) nanoparticles. On the other hand, the viscosity of the fluid showed an increase beyond 0.5 % volume fraction of silica nanoparticles in case of ester oil based nanofluids. Jacob et. al. from NIT Calicut analyzed the temperature dielectric spectrum of relative permittivity (ε) and dissipation factor (Tan δ) of cellulose paper which had been impregnated with ester oil filled with alumina nanoparticles at 0.1 g/L [114, 115]. The nanoparticles were surface modified with oleic acid to avoid any kind of agglomeration. They showed that at 50°C, ε of oil impregnated paper increased at first, but after a particular value as the temperature increased, the value of ε decreased. It was concluded that ε of ester oil impregnated paper was higher than that of mineral oil impregnated paper, due to which the overall structure of the transformer can me miniaturized. Also, the value of Tan-δ of oil impregnated papers showed an increase with the increase in

temperature at a frequency of about 50Hz. The increasing rate of dissipation factor, Tan-δ of mineral oil impregnated cellulose papers came out to be greater than that of ester oil impregnated papers, from which it can be concluded that the aging of transformer insulation can be slowed down in case of vegetable oil filled transformers. The breakdown strength of vegetable oil immersed paper was higher than that of mineral oil immersed paper, and the breakdown strength can further be increased by adding the alumina nanoparticles. The only drawback regarding the vegetable oil immersed paper was found out to be that the moisture content in the insulation paper was higher as compared to that of in the mineral oil immersed cellulose paper which can reduce the life of the cellulose paper of the transformer. However, it was proposed that the addition of alumina nanoparticles can lead to the reduction of the moisture content in the oil.

In terms of applications of graphene oxide in electrical insulations, a little research is available in the field of solid insulations. In 2022, Y. Zhao et. al. prepared hyperbranched graphene oxide structure based- epoxy nanocomposite as superior electrical insulation [116]. The synthesized EP/HPB-GO nanocomposite showed much better thermal conductivity as well as increased mechanical properties to broaden the application of GO based epoxy resin in electrical engineering. In 2021, H. Liu et. al. prepared graphene oxide/carbon composite aerogel and studied its thermal insulation properties [117]. The results suggested the better heat shielding performance with improved mechanical properties of the synthesized aerogel. In 2017, Y. Lei et. al. improved the mechanical properties as well as the thermal insulating properties of silica aerogels by dispersing the graphene oxide in silica matrix [118]. Their findings showed that the of the resulting mixture was lowered from 0.0089 W/mK to 0.0072 W/mK.

2.6 OUTCOMES OF LITERATURE SURVEY: GAPS IN RESEARCH

It has been realized that with respect to the application of vegetable oil based nanofluid in transformers, there are some areas which have not been explored at all, whereas there are some grey areas which need further research and comprehensive studies in order to obtain conclusive results. For example, till date, there are just few types of nanoparticles which have been extensively studied, like Fe_3O_4 (Iron Oxide), Al_2O_3 (Aluminum dioxide) and H.BN (Hexagonal Boron Nitride). The types of nanoparticles studied can be generally classified under two categories – conducting and semi-conducting nanoparticles. The researchers have focused on these two types

of nanomaterials due to their electron trapping properties which result in the enhancement of breakdown voltages, however, the application of non-conducting nanomaterials in vegetable-based oils have not been studied in detail. In the field of nanotechnology, graphene oxide is the most researched nanomaterial nowadays. Recently, graphene oxide has found its usage in almost every field of science like medicine, physics, bio-chemistry, etc., thus, serving as a boon in various needed applications leading to it being called as 'wonder material' of 21st century. However, due to its non-conductive nature, it has not been studied corresponding to the field of high voltage engineering. Its applications in the field of insulating materials, particularly for transformers, still remain unknown.

There are no conclusive studies on the application of ester oil/mineral oil blend based nanofluids in transformers. Furthermore, the study on the effect of such nanofluids on solid insulation structure of transformers still remains in the grey area. Since, the solid insulation structure plays a vital role in the overall service life span as well as the reliability of the transformer, the behavior of solid insulation when impregnated with these nanofluids needs to be studied extensively. Also, due to the higher ratio of the permittivity of oil to the permittivity of pressboard and insulating paper in case of natural ester oils as compared to that of mineral oils, the stress in liquid insulation decreases but meanwhile the stress in the solid insulation increases. This can lead to the deformation in solid insulation, thereby decreasing the life of the pressboard and impregnated paper. This is one of the main factors affecting the design parameters of any transformer. However, there are no conclusive reports on the electric stress distribution of oil blend based nanofluids which leads to the demands in the research to be vast which focuses on providing a solution to this problem.

2.7 OBJECTIVES OF THE RESEARCH

In order to overcome the issues related to the usage of mineral oil, an oil blend having ester oil/mineral oil composition is proposed for the dispersion of nanoparticles. The oil blend would be having a higher portion of ester oil in order to regain its bio-degradability whereas the mineral oil content could help in bringing down the viscosity of the blend. Non-conductive graphene oxide (GO) nanomaterial is proposed for the dispersion in the oil blend. For comparative analysis, the

semi-conductive titanium dioxide (TiO_2) and conductive zinc oxide (ZnO) nanomaterials are also chosen to be dispersed in the synthesized oil-blend. The dielectric as well as the physio-thermal properties of the non-conductive graphene oxide dispersed oil-blend will be studied and compared with the properties of the same oil blend when dispersed with the semi-conductive titanium dioxide and conductive zinc oxide nanomaterials. Similarly, the effects of non-conductive graphene oxide dispersed oil blend on the solid insulation of transformer, i.e., transformer pressboard, will be studied and compared with the effects of semi-conductive titanium dioxide and conductive zinc oxide nanomaterial dispersed blends on the solid insulation. The necessity of design analysis will be studied by observing the electric field stress distribution in the entire insulation structure due to the synthesized nanofluids. Thus, the main objectives of this research can be summarized in the following points:

1. To formulate and prepare an ester oil based nanofluid as a liquid insulation for power transformers.
2. To investigate the various aspects of electrical, mechanical and thermal properties of the developed insulating fluid through various characterization techniques.
3. To study the effect of nanofluid on the solid insulation of the power transformers.
4. To analyze the necessity of making required changes in the design of power transformers due to the behavior of nanofluid on various transformer components.

CHAPTER 3

SYNTHESIS OF MATERIALS

THE various materials for this research have been synthesized using different techniques. The synthesis of these materials has been divided into three parts – synthesis of nanomaterials, synthesis of nanofluids and synthesis of solid insulation. The various methods and techniques of their synthesis are explained below.

3.1 AVAILABILITY OF NANOMATERIALS

For this research, three types of nanomaterials were selected for dispersion in the base fluid – non-conductive graphene oxide (GO), which is the main focused nanomaterial for this research, semi-conductive titanium dioxide (TiO_2) and conductive zinc oxide (ZnO).

3.1.1 Synthesis of Graphene Oxide (GO)

GO was synthesized using modified Hummer's method in Advanced Nanomaterial Lab, TIET, Patiala [119, 120]. To begin with, about 92 ml of concentrated sulfuric acid (H_2SO_4) is taken as the base solvent in which about 2 g of powdered graphite and 2 g of sodium nitrate ($NaNO_3$) are dissolved. The entire solution is stirred in an ice bath for 4 hours. Keeping the solution continuously on stirring, about 12 g of potassium permanganate ($KMnO_4$) was added into it at a very slow rate. Subsequently, about 440 ml of distilled water (H_2O) was added dropwise into the solution followed by the dropwise addition of 20 ml of 30% hydrogen peroxide (30 % H_2O_2) while keeping the solution in an ice bath. The resultant solution is washed with 5% concentrated hydrochloric acid (HCl) followed by the washing with ethanol. The resulting precipitate is dried overnight in a hot air oven at a temperature of 40°C to obtain the GO nanoparticles. Sometimes, the precipitate can be needed to heat for longer duration till the moisture in it dries completely. The pictorial representation for synthesis of GO using modified Hummer's method is shown in Figure 3.1.

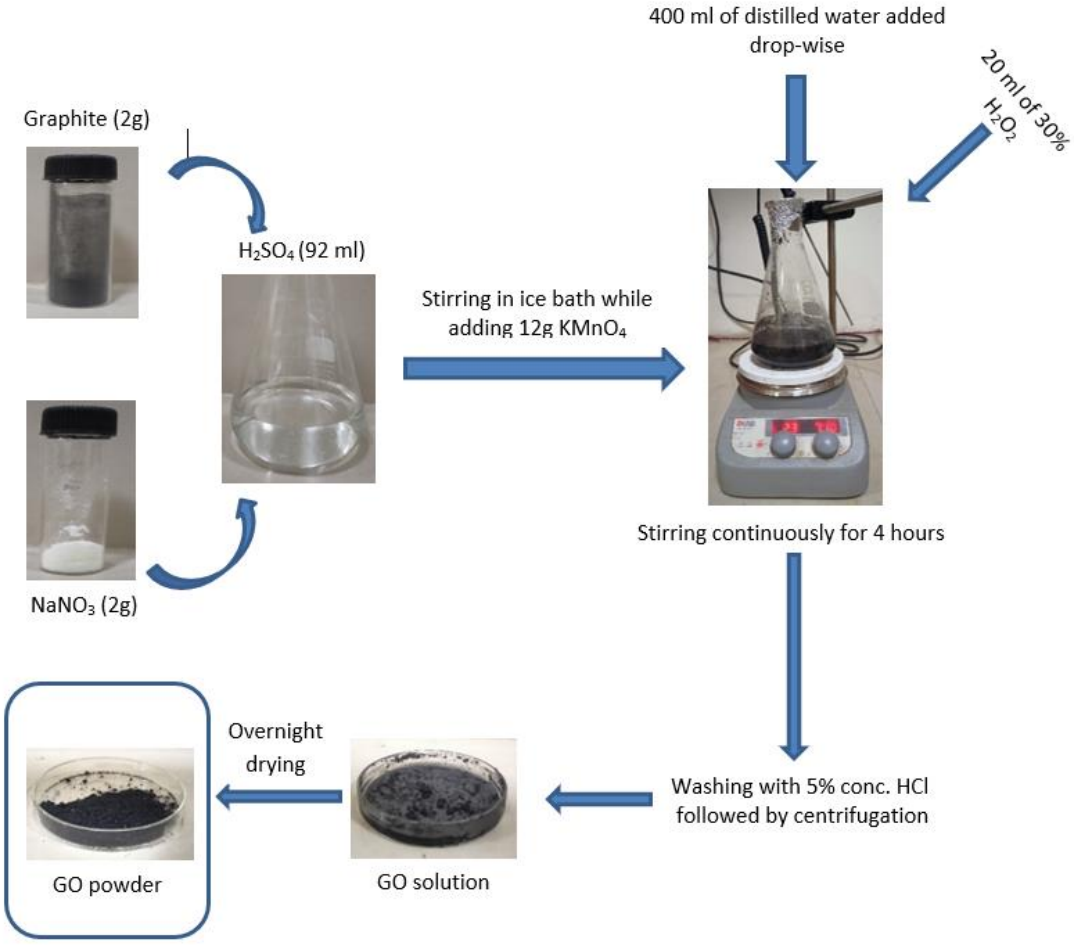

Figure 3.1 Pictorial representation of synthesis of graphene oxide nanoparticles using modified Hummer's method.

3.1.2 Synthesis of Zinc Oxide (ZnO)

ZnO nanoparticles are synthesized using traditional sol-gel method in Advanced Nanomaterial Lab, TIET, Patiala [121,122]. About 28 g of Zinc acetate ($ZnC_4H_6O_4$) was taken as a precursor and was added to 800 ml of ethanol. The solution was subjected to magnetic stirring for a period of 40 minutes at a constant temperature of 60°C. Meanwhile, in a separate beaker, 34 g of oxalic acid ($C_2H_2O_4$) and 500 ml of ethanol were vigorously mixed together and the entire resulting solution was heated up to 60°C. The solution was further stirred for 40 minutes. Both the resulting solutions were mixed together in one beaker and stirred magnetically for 4 hours while being heated up to a temperature of 80°C. This resulted in the formation of sticky white colored paste. This whitish paste like slurry was put in a centrifuging machine at 4500 rpm for 5 minutes. The

caused the ethanol to separate from the precipitate. After draining the ethanol, the leftover precipitate was dried in a hot air oven at 40°C to obtain ZnO nanoparticles in powdered form. The pictorial representation of the method employed for synthesis of ZnO nanoparticles is shown in Figure 3.2.

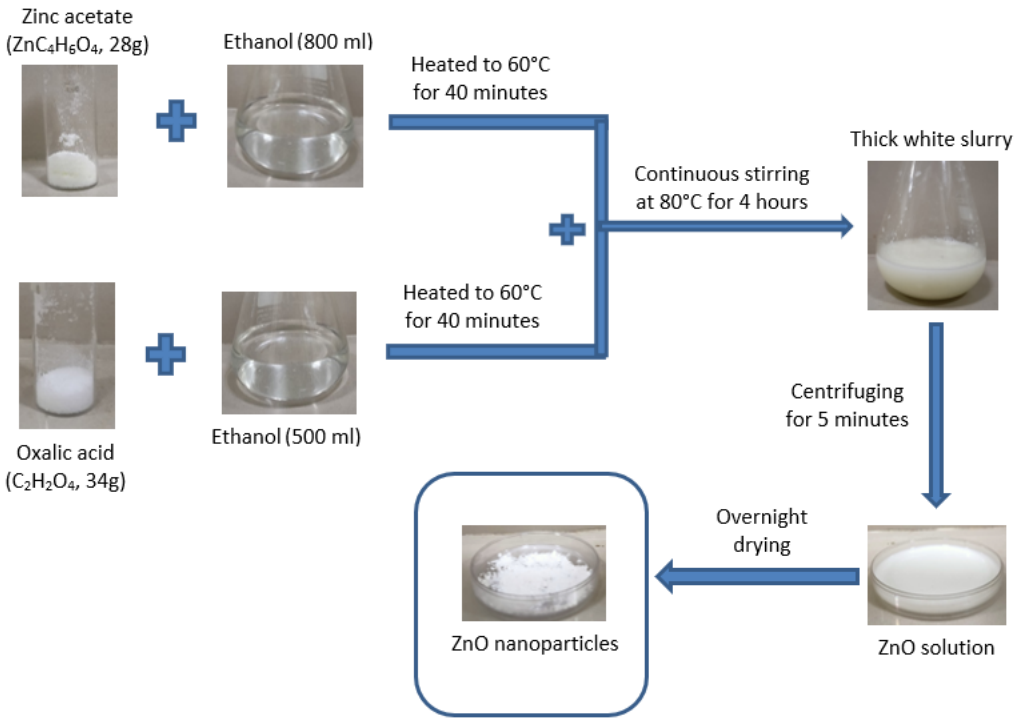

Figure 3.2 Pictorial representation of synthesis of zinc oxide nanoparticles using sol-gel method.

3.1.3 Availability of Titanium Dioxide (TiO_2)

TiO_2 was purchased commercially as TiO_2 P25 from Evonik Industries, Germany. The specifications of purchased TiO_2 were confirmed through characterization techniques which will be explained in further sections.

Figure 3.3 Commercially purchased P25 TiO_2 nanoparticles.

3.1.4 Surface Modification of Nanomaterials

The literature has suggested that the nanomaterials have repeatedly shown the tendency to form clusters in the base solvents. This is known as 'agglomeration of nanoparticles [122-125]. Various nanomaterials have different rates of agglomeration depending upon their molecular weights and the inter-molecular forces in them. Nevertheless, almost all of them undergo the process of agglomeration, i.e., sedimentation. This can cause serious issues when these nanomaterials are dispersed in the transformer fluids. The sedimentation of nanoparticles at the bottom of the transformer tank or cooling ducts can lead to the hinderance in the flow of oil in the transformer, thus, resulting in a poor cooling performance. It can also result in nullifying the desired outcomes which would have been expected from the insulating oil after the dispersion of nanoparticles in it. To overcome these issues, the nanomaterials are generally surface modified by either using stearic

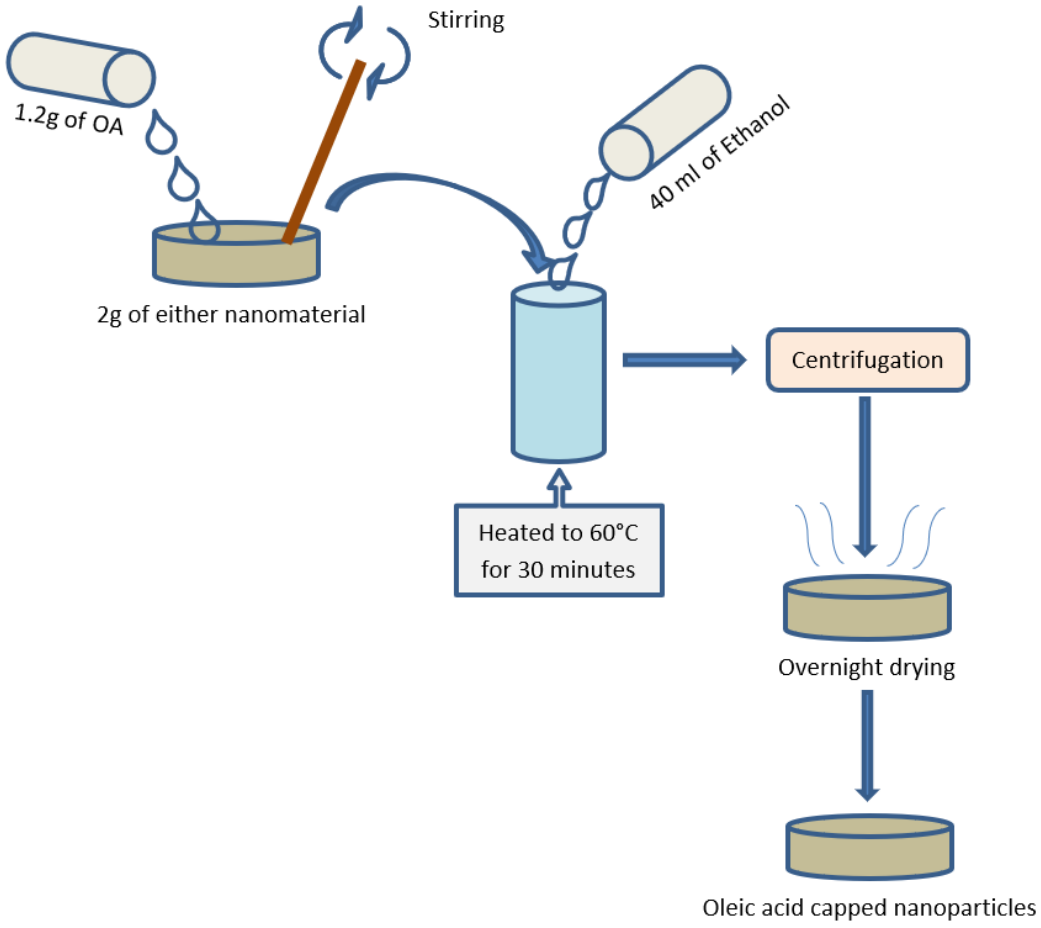

Figure 3.4 Pictorial representation of a Two-Step surface modification method used to cap the nanomaterials.

acid or oleic acid [126-128]. In this research, oleic acid (OA) has been chosen for the surface modification of these nanomaterials.

The surface modification of nanoparticles is explained as follows. About 2 g of either nanoparticles was added into 1.2 g of liquid OA. The mixture was stirred rigorously to form a thick paste which was, then, put into 40 ml of ethanol. The solution was magnetically stirred while being kept at a constant temperature of 60°C for a period of 30 minutes. The solution was, then, centrifuged at 5000 rpm for 5 minutes and the ethanol was distilled away. The remaining precipitate was dried in a hot air oven at 50°C till all the moisture of the precipitate dried away and the final product was obtained as oleic acid capped nanoparticles in powdered form. The pictorial representation of the procedure of surface modification of nanoparticles is shown in Figure 3.4. The same method was used with same quantity ratios of material composition to obtain oleic acid capped graphene oxide (OA-GO), oleic acid capped titanium dioxide (OA-TiO_2) and oleic acid capped zinc oxide (OA-ZnO) powders.

3.2 SYNTHESIS OF NANOFLUIDS

The availability of nanofluids for this research can be explained in two parts – making of base oil blend and synthesis of the nanofluids from that oil blend.

3.2.1 Preparation of Base Oil Blend

Two types of oils are selected for developing the required oil blend. One is the vegetable based natural ester oil whereas the other one is the conventional mineral oil. As for the vegetable based oil, BioTransol-HF has been used as natural ester oil and the primary component in the making of oil blend. BioTransol-HF was supplied by Savita Chemicals, India. It is a soyabean extracted natural ester based insulating oil. It is completely biodegradable as per the specifications put forth by US EPA OECD 301B, thus being environmentally friendly and non–toxic to the marine life. Electrical and Chemical properties of BioTransol-HF have been tested and certified by Central Power research Institute (CPRI), a reputed testing laboratory in India for insulating fluid testing. Whereas its bio-degradability and non-toxicity have been tested and certified by various laboratories of Intertek, a global Total Quality Assurance provider in the field of materials testing.

As for the conventional mineral oil, Transol-GE has been used as the secondary component in the making of oil blend. It was also supplied by Savita Chemicals, India. Table 3.1 shows the data listing various dielectric as well as physio-chemical properties of BioTransol-HF and Transol-GE as provided by the supplier. The dielectric properties of BioTransol-HF are found to meet the criteria set by 'IEEE Std C57.147-2018 - IEEE Guide for Acceptance and Maintenance of Natural Ester Insulating Liquid in Transformers', whereas the dielectric properties of Transol-GE fully meet with the 'IEEE C57.91-2011 - IEEE Guide for Loading Mineral-Oil-Immersed Transformers and Step-Voltage Regulators' standards.

Table 3.1 Comparative analysis of dielectric properties of transformer oils used in this research.

Parameter	***ASTM/IEC Standards***	***BioTransol-HF***	***Transol-GE***
Breakdown Voltage (kV)	IEC 60156	30-70	70
Dissipation Factor at 25°C	D924	-	0.15
Dissipation Factor at 25°C		0.5	0.02-0.03
Viscosity (mm^2/sec) at 40°C	D445	12	17.8
Biodegradation	OECD 301	Non-biodeg	Readily biodeg
Flash pint (°C)	D92	135	320-330
Density at 20°C (g/cm^3)	ISO 3675	0.89	0.92
Gassing tendency (mm/min)	D2300		-6.6
Water content (mg/kg)	IEC 60814	30-40	<50
Acidity (mgKOH/g)	IEC 62021-3	1.2	0.1

BioTransol-HF (now onwards referred to as EO, for natural ester oil) and Transol-GE (now onwards referred to as MO, for mineral oil) were mixed together in six different weight proportions to form six different samples of oil-blends. The weight proportions of EO:MO were 0:100, 20:80, 40:60, 60:40, 80:20, 100:0, respectively. Theses oil blend (OB) samples were named according to the weight proportion of the EO content in the blend, i.e., OB0, OB20, OB40, OB60, OB80, OB100 respectively, where OB0 represents pure mineral oil (0% EO in the blend) and OB100 represents pure natural ester oil (100% EO in the blend). The oil blend samples were subjected to magnetic stirring followed by sonication multiple times in order to achieve the uniform mixing of both fluids. All the six OB samples were tested for their ac breakdown voltages (BDV). The purpose for their testing was to obtain an optimized OB sample on the basis of EO content and the BDV value of that blend in order to use that OB sample as base solvent for nanoparticles. The BDV of all OB samples was measured at 25°C and 90°C as per the IEC 60156 specifications and the results are plotted in Figure 3.5.

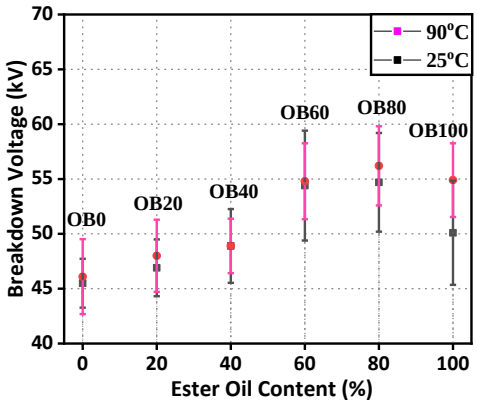

Figure 3.5 BDV values of synthesized oil-blends.

It is established that the ac BDV of oil blend is directly proportional to the EO content in the blend up to a certain value. The BDV of pure MO, i.e., OB0 is 45 kV and 46 kV at 25°C and 90°C respectively whereas the BDV of pure EO, i.e., OB100 is 50 kV and 55 kV at 25°C and 90°C, respectively. However, the peak value of ac BDV is achieved for OB80 sample which is 55 kV at 25°C and 56 kV at 90°C. Since, the approach is to optimize the OB on the basis of EO content and corresponding BDV, OB80 is considered as the most suitable OB sample for being used as the base solvent for dispersion of various nanomaterials. Figure 3.6 shows the MO (OB0), EO (OB100) and the optimized OB80.

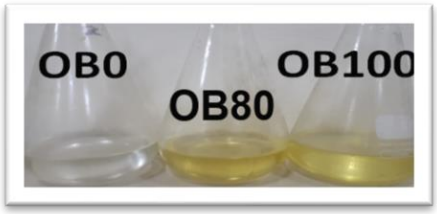

Figure 3.6 MO, EO as well as optimized blend, OB80.

3.2.2 Synthesis of Nanofluids

The nanomaterials were dispersed in five different concentrations in the base oil-blend, i.e., OB80 sample. The method of synthesizing the nanofluids from [1]GO, TiO_2 and ZnO nanomaterials is exactly same. For simplicity, only the procedure of synthesizing the GO dispersed nanofluid is explained here while considering the fact that the same procedure will be repeated for TiO_2 as well as ZnO nonmaterial dispersed nanofluids. Taking OB80 as the solvent, GO nanoparticles were dispersed in five different concentrations in five different flasks. The concentration values were 0.001 g/L, 0.003 g/L, 0.005 g/L, 0.007 g/L and 0.009 g/L. The names of the resulting nanofluid (now onwards referred to as NF) samples were kept on the basis of the first letter of the nanomaterial and the concentration value, i.e., GNF1, GNF3, GNF5, GNF7 and GNF9, respectively. The uniform dispersion of nanoparticles was achieved by the usage of magnetic stirrers and sonicator. Same procedure was used to obtain TiO_2 dispersed NF samples, i.e., TNF1, TNF3, TNF5, TNF7 and TNF9, and ZnO dispersed NF samples, i.e., ZNF1, ZNF3, ZNF5, ZNF7 and ZNF9.

3.3 PREPARATION OF SOLID INSULATION

The solid insulation material of any transformer primarily consists of cellulosic pressboard. The transformer pressboard required for this research was supplied by Mubasa Electrical Pvt. Ltd. Patiala, India. High-density cellulosic pressboard sheets having 1.2 mm thickness were provided which fulfilled the IEC 60641-1 specifications. Ten strips were cut from the delivered pressboard sheets. Each strip had a dimension of 70 x 10 x 2.5 mm. These sheets were first dried in vacuum

[1] It is to be understood that only the surface modified nanoparticles, i.e., OA-GO, OA-TiO_2 and OA-ZnO are dispersed even though short terms like GO, TiO_2 and ZnO are used for simplicity.

at a temperature of 120°C and at a pressure of 50 Pa for a period of 48 hours. Simultaneously, the base oil blend, i.e., OB80 and the NF samples, i.e., [2]GNF5, TNF5 and ZNF5 were heated in separate containers up to a temperature of 60°C and dried in a vacuum oven at 60°C at a pressure of 50 Pa for 48 hours. This preheating treatment of pressboard strips and oil samples was done in order to remove the moisture from the solid as well as liquid insulation materials. Preparation of different pressboard samples is explained as follows:

- Two pressboard strips were put in two empty air tight vessels.
- Two pressboard strips were put in two OB80 filled vessels.
- Two pressboard strips were put in two GNF5 filled vessels.
- Two pressboard strips were put in two TNF5 filled vessels.
- Two pressboard strips were put in two ZNF5 filled vessels.

Each vessel was filled only up to the $3/4^{th}$ of its total volume capacity in order to let some space for air so that the atmospheric conditions could be maintained inside the vessel. In order to further simulate the conditions inside the vessel similar to those of transformers, cut pieces of copper wires having length 20 mm and diameter 2 mm were immersed in the OB and NF filled vessels. All the vessels were air sealed and then put in hot air circulated oven preheated to a temperature of 130°C which was further maintained till the end of ageing process. One vessel from every two similar vessels was taken out of the oven after a period of 15 days whereas the other vessel was taken out after a period of 60 days. In other words, one vessel was subjected to 15 days of ageing period whereas the other vessel was subjected to 60 days of ageing period. The pressboard strips were taken out of the vessels and named on the basis of the fluid and the ageing period undergone by the strips. For example, the pressboard strip impregnated with OB80 and aged for 15 days was named as P-OB15 whereas the pressboard strip impregnated with OB and aged for 60 days was named P-OB60. Similarly, pressboard strip impregnated with GNF and aged for 15 days was named as P-GNF15 whereas the pressboard strip impregnated with GNF and aged for 60 days was

[2] The reason for selecting the GNF5, TNF5 and ZNF5 samples for impregnation of pressboard samples is their peak performances in terms of dielectric and physio-thermal properties amongst all the NF samples which will be explained in Chapter 4.

named as P-GNF60. Likewise, pressboard strips were named as P-TNF15 and P-TNF60 in case of TNF impregnated pressboard strips aged for 15 days and 60 days respectively and P-ZNF15 and P-ZNF60 in case of ZNF impregnated pressboard strips aged for 15 days and 60 days, respectively.

3.4 CHARACTERIZATION OF NANOMATERIALS

Synthesized nanomaterials were subjected to various characterization techniques which are explained below:

3.4.1 X-Ray Diffraction (XRD)

XRD patterns of GO, TiO_2 and ZnO nanoparticles are shown in Figures 3.7a, 3.7b and 3.7c, respectively.

GO: In XRD pattern of GO nanoparticles, the main peaks can be noticed; a major peak at 2θ=14° having plane values (002), a broader peak at 2θ=27° and a very sharp peak at 2θ=43°. The 14° peak is generally expected to appear at 10°, however it appears to be shifted by 4° due to the partial thermal reduction of GO nanoparticles. The main reason behind the reduction of nanoparticles is their longer exposure to heat during the drying process. The 27° peak corresponds to the residual graphite platelets in the GO nanoparticles. The 43° peak appears due to the turbostratic disorder in GO nanoparticles. Turbostratic disorder is caused by random rotations between each parallelly stacked adjacent layers of graphene [129].

TiO_2: In XRD pattern of TiO_2 nanoparticles, the diffraction peaks at 2θ = 25.4° (101), 2θ = 37.9° (004), 2θ = 48.3° (200), 2θ = 55.1° (211) and 2θ = 62.6° (204) collectively confirm the anatase structure of the P25 TiO_2 nanoparticles according to the JCPDS card no. 21-1272 [130]. The sharpness of these high intensity peaks represents the crystalline nature of the TiO_2 nanoparticles.

ZnO: In XRD pattern of ZnO nanoparticles, the diffraction peaks at 2θ = 30.2° (100), 2θ = 33.6° (002), 2θ = 35.2° (101), 2θ = 47.5° (102), 2θ = 51.9° (110), 2θ = 62.5° (103) and 2θ = 68.5° (112) collectively represent the hexagonal wurtzite structural arrangement of synthesized nanoparticles as per JCPDS card no. 36-1451 [131].

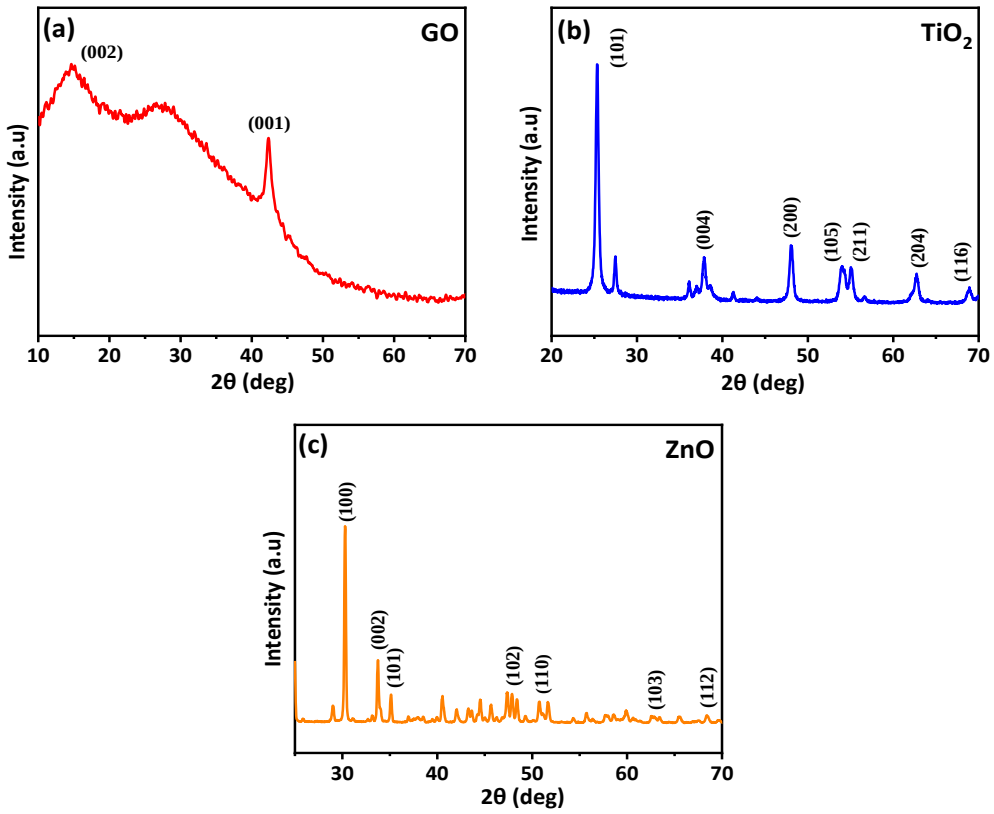

Figure 3.7 XRD pattern of (a) synthesized GO, (b) commercially purchased TiO_2 and (c) synthesized ZnO nanomaterials.

3.4.2 Fourier Transform Infrared Spectroscopy (FTIR)

Figure 3.8 shows the comparative analysis of FTIR spectroscopies of synthesized and surface modified nanomaterials. The FTIR spectroscopy of each nanomaterial as well as OA is explained below.

OA: In FTIR spectrum of OA, a wide band between 3012 cm^{-1} and 2500 cm^{-1} corresponds to the OH bond. The peaks at 2918 cm^{-1} and 2847 cm^{-1} are due to the angular deformation of C-O-H bond whereas the peak at 1285 cm^{-1} represents the C-O elongation [132].

GO: In FTIR spectrum of GO nanoparticles, a broad peak from 3400 cm^{-1} to 2400 cm^{-1} is due to the presence of absorbed water molecules. The peak at 1620 cm^{-1} is due to the C=C stretching of the unoxidized graphite. The peaks at 1727 cm^{-1} and 1170 cm^{-1} are representing the C=O

stretches of carboxyl group and C-OH stretches of alcoholic group respectively [133]. The peak at 1050 cm^{-1} is attributed to C-O stretching vibrations of C-O-C group.

TiO_2: In FTIR spectrum of TiO_2, a broad band around 3400 cm^{-1} and a small peak at 1621 cm^{-1}

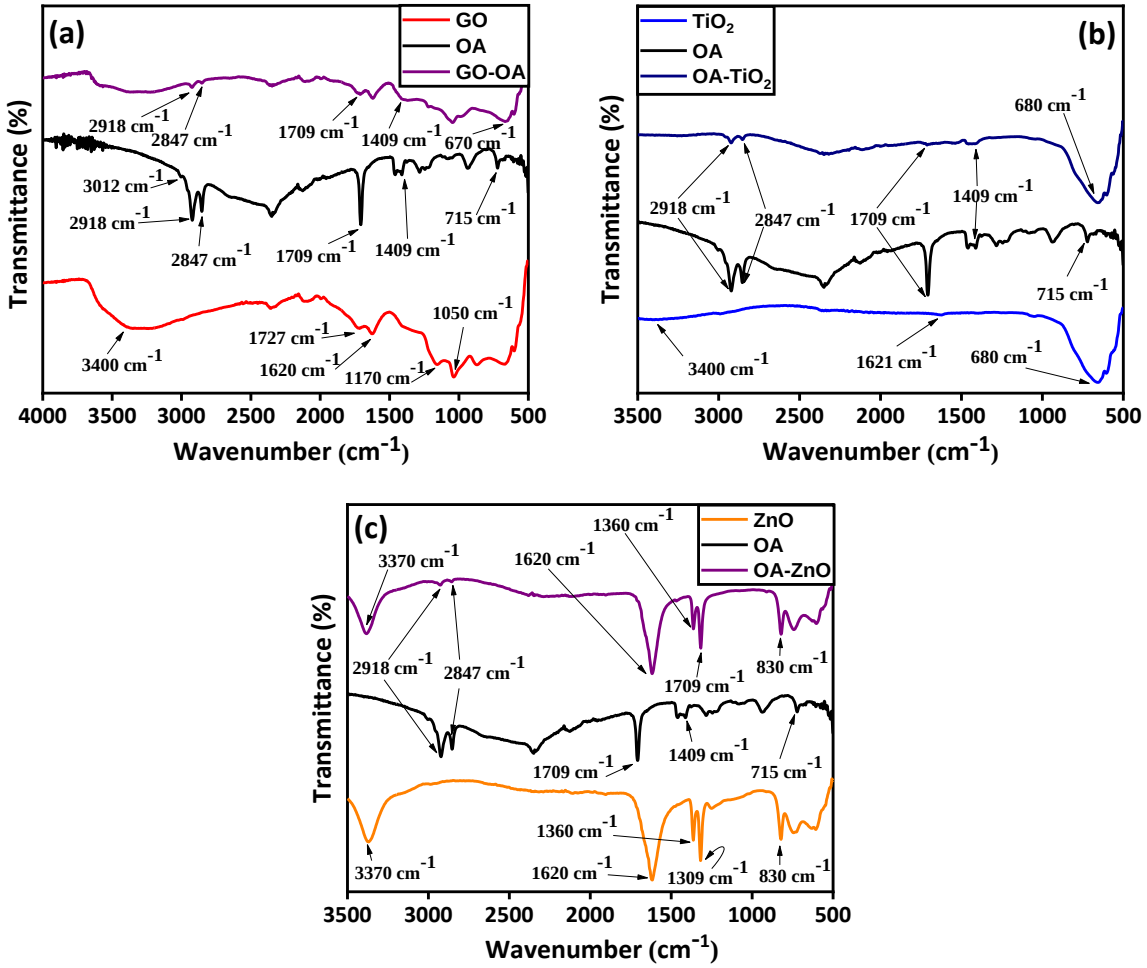

Figure 3.8 Comparative analysis of FTIR spectra of unmodified and surface modified nanoparticles: (a) GO and OA-GO, (b) TiO_2 and OA-TiO_2, (c) ZnO and OA-ZnO nanoparticles.

^{1} are due to the presence of absorbed water molecules and represent the hydroxyl group (OH). The peak at 680 cm^{-1} is representing the O–Ti–O bond [134].

ZnO: In case of FTIR spectrum of ZnO, a peak at 3370 cm^{-1} represents the stretching mode of hydroxyl group (OH). The peaks seen at 1620 and1360 cm^{-1} are due to the stretching of C=O and C-O in zinc carboxylate respectively [135]. This suggests the presence of impurities near ZnO surfaces. The peak at 1309 cm^{-1} is attributed to the in-plane bending of primary and secondary alcohol. The peak at 830 cm^{-1} represents the bending of C-O bond.

In surface modified nanomaterials, the effect of surface modification of nanoparticles by OA can be seen as extra induced peaks in their FTIR spectra. In case of OA-GO, the peaks at 2918 cm^{-1} and 2847 cm^{-1} are due to the CH stretching of the alkyl chain. The reduction in the intensity of peak shows the corresponding reduction in vibrations in case of OA-GO.

3.4.3 Field Emission Scanning Electron Microscopy (FE-SEM)

FE-SEM images of all the three pure as well as surface modified nanomaterials have been shown in Figures 3.9, 3.10 and 3.11. These images have been explained below.

GO: FE-SEM images of GO clearly reveal a three-dimensional layered structure as can be seen in Figure 3.9. In GO, the sheets are well defined and interlinked to one another forming a porous network. The images show that the agglomeration of layers can be the main reason behind the stacked structure of GO. The 3D sheets are structurally exfoliated which further indicates to the possibility of an increase in sheet dimensions and porosity with the increase in temperature. This again defines the larger specific surface area of GO as compared to that of the pristine graphite. In OA-GO, a slight deformation in the layered structure of GO can be seen due to the continuous exposure of heat during the process of surface modification. The entangling of the layers of GO sheets is clearly revealed by the FE-SEM images of the OA-GO.

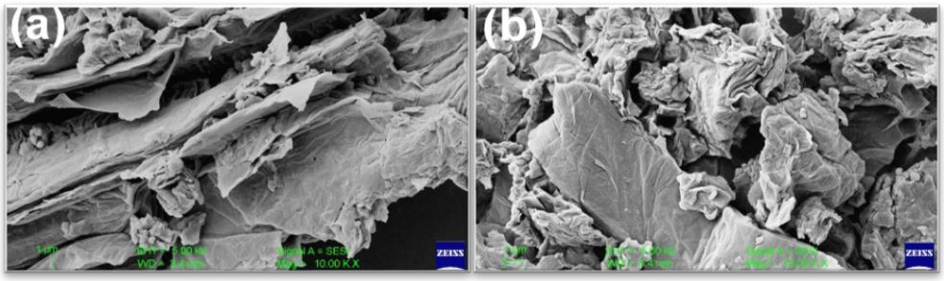

Figure 3.9 FE-SEM images of (a) GO and (b) OA-GO nanoparticles.

TiO_2: In case of TiO_2 nanoparticles, as shown in Figure 3.10, it can be seen that before the surface modification, TiO_2 nanoparticles have merged to form a crystalline structure. However, after modifying the nanoparticles with oleic acid, these OA-TiO_2 nanoparticles have further merged to form a larger structure. It can be due to the re-crystallization of the nanoparticles during the heating treatment involved in the process of surface modification.

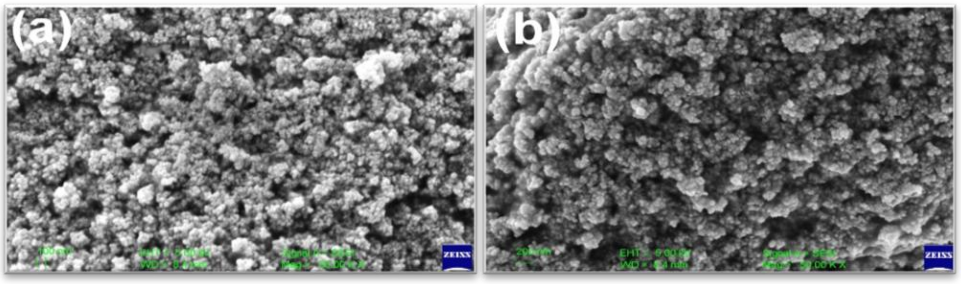

Figure 3.10 FE-SEM images of (a) TiO_2 and (b) OA-TiO_2 nanoparticles.

ZnO: In case of ZnO nanoparticles, as seen in Figure 3.11, a huge mesh of scattered grain like structures of ZnO nanoparticles can be seen. However, after their surface modification, the morphology of nanomaterial changed slightly. A cluster of OA-ZnO nanorods of shorter lengths can be seen. These structures are similar to the grain like structures resembling the broken rods of unmodified ZnO nanomaterial.

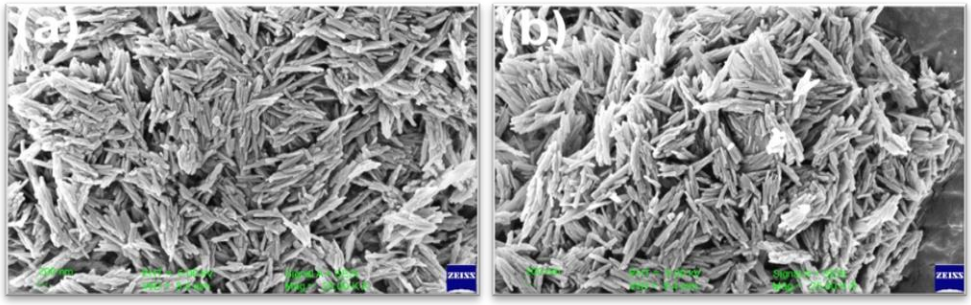

Figure 3.11 FE-SEM images of (a) ZnO and (b) OA-ZnO nanoparticles.

3.4.4 Brunauer-Emmett-Teller (BET) and Barrett-Joyner-Halenda (BJH)

In order to analyze the surface area and pore size, BET as well as BJH analyses of surface modified nanomaterials were carried out in the presence of N_2 gas. Figure 3.12 shows the N_2 adsorption-desorption isotherms as well as distribution of the pore sizes for synthesized surface modified nanomaterials. It is evident that all the three nanomaterials follow Langmuir type-IV isotherm exhibiting the properties of mesoporous nature. Furthermore, the presence of mesopores in these nanomaterials is confirmed by BJH-curve. The details about the specific surface area and the porosity of the three nanomaterials are shown in Table 3.2. OA-GO nanoparticles showed comparatively lowest specific surface area whereas OA-TiO_2 showed the largest. A mesoporous structure is a structure having pores with diameters between 2 nm to 50 nm. Larger pore diameters

can cause hinderances in the formation of shallow traps and thus reducing the electron trapping capability of the nanoparticles when dispersed in the insulating oils.

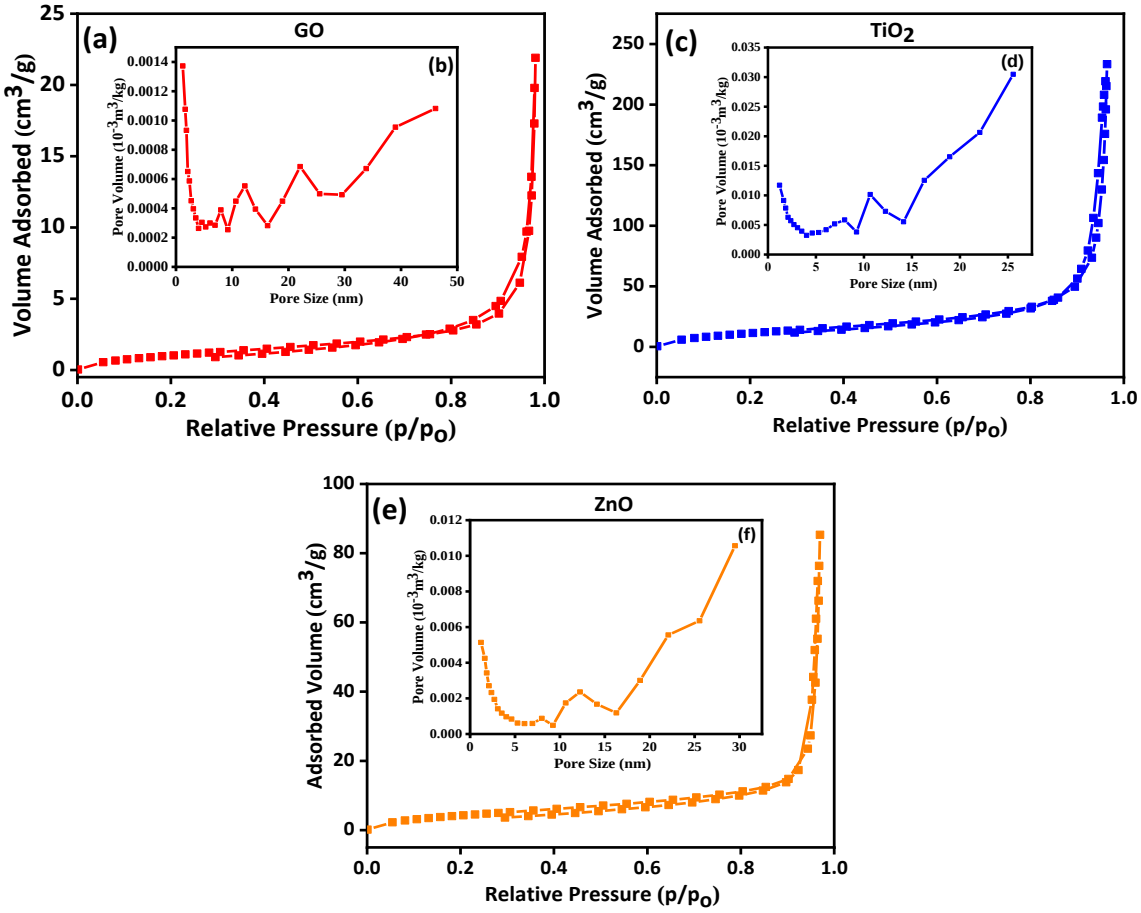

Figure 3.12 (a) and (b) BET and BJH for OA-GO, (c) and (d) BET and BJH for OA-TiO_2, (e) and (f) BET and BJH for OA-ZnO, respectively.

Table 3.2 Surface details of modified nanomaterials.

Samples	*Specific Surface Area (m^2/g)*	*Mean Pore Diameter (nm)*	*Mesopore Volume (cm^3/g)*	*Total Pore Volume (cm^3/g)*
OA-GO	4.39	30.86	0.032	0.981
OA-TiO_2	48.7	29.6	0.34	0.36
OA-ZnO	17.9	29.5	0.12	0.132

3.4.5 Thermo-gravimetric Analysis (TGA)

For transformer applications, it is of utmost necessity that the materials used in insulation purpose are thermally stable at transformer working temperatures under different conditions. For a typical transformer, this temperature range varies from 25°C under normally working conditions to 90°C under overload working conditions. The decomposition behavior of these nanomaterials is investigated by (TGA), thus giving the details about the thermal stability of these nanomaterials. TGA of all the three surface modified nanomaterials was carried out and the results are shown in Figure 3.13. OA-GO compound is found to be thermally stable throughout the process except a dip in its stability between 182°C - 250°C. The primary reason for this decrease in thermal stability is the emission of CO_2 gas and the decomposition of carboxylic group. OA-TiO_2 showed a steep increase of 7.3% in its weight loss during the temperature range of 120°C to 160°C and 14.2% during the temperature range of 400°C to 440°C. On the other hand, OA-ZnO showed a gradual increase of 5.4% in its weight loss from 120°C to 480°C. However, in terms of thermal stability, all the three synthesized nanomaterials are seen to be stable during the typical temperature limits of any transformer (25°C to 90°C) with overall stability of OA-ZnO being the greatest.

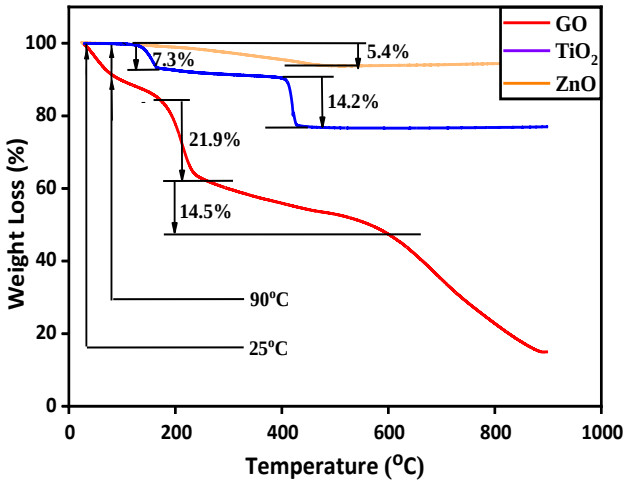

Figure 3.13 TGA of GO, TiO_2 and ZnO nanomaterials.

3.5 CHAPTER SUMMARY

All the three nanomaterials chosen for the dispersion in the base oil-blend in order to synthesize the desired nanofluids are selected on the basis of their electrical conductivities - non-conductive graphene oxide, semi-conductive titanium dioxide and conductive zinc oxide. GO and ZnO are prepared using conventional techniques like modified Hummer's method and Sol-Gel method respectively, whereas TiO_2 is purchased commercially as P25 nano-powder. All the nanomaterials are subjected to various characterization techniques in order to analyze their purity as well as surface details. The XRD analysis shows that the synthesized GO has unreacted graphite platelets as leftover residue, whereas in the case of TiO_2 and ZnO nanomaterials, their XRD spectra confirms their anatase and wurtzite structural arrangements, respectively. FTIR analysis also confirms the residual graphite in synthesized GO whereas the FTIR spectra of TiO_2 and ZnO nanoparticles show the absorbance of water molecules as well as the attachment of additional functional groups due to the mechanism involved in their synthesis and surface modification. FTIR spectra of surface modified nanomaterials show respective peaks with lower intensities as compared to the unmodified nanomaterials. It indicates the lesser vibrations in the surface modified nanomaterials. FE-SEM of GO shows its 3D layered structure whereas FE-SEM of TiO_2 nanoparticles shows their crystalline granular structure. On the other hand, FE-SEM of ZnO shows its rod like grains combined together to form a crystalline structure. BET and BJH techniques employed on these nanomaterials show that all the nanomaterials follow Langmuir type-IV isotherm. However, GO nanoparticles are having the least surface area of 4.3 m^2/g followed by ZnO nanoparticles having 17.9 m^2/g and TiO_2 nanoparticles are having the largest surface area of 48.7 m^2/g. When subjected to TGA technique, ZnO nanoparticles are found to be thermally most stable whereas GO nanoparticles are found to be least stable over the range of 0°C-1000°C. However, in the temperature range of a working transformer, i.e., 25°C-90°C, TiO_2 and ZnO nanoparticles are found to be almost equally thermally stable. Yet, all the three nanomaterials are thermally stable during a typical working temperature range of a transformer.

CHAPTER 4

STUDY OF DIELECTRIC PROPERTIES OF SYNTHESIZED NANOFLUIDS FOR TRANSFORMERS

IN this chapter, various insulating as well as physio-thermal properties of the synthesized nanofluids have been experimentally studied. The ASTM and IEC standards are chosen to conduct the experiments and measure these properties to ensure if the synthesized nanofluids possess better dielectric properties than the conventional mineral oil. The various properties studied and their ASTM/IEC specifications are shown in Table 4.1.

Table 4.1 Properties studied with their IEC/ASTM Standards.

Dielectric Properties	
AC Breakdown Voltage	IEC 60156
Impulse Breakdown Voltage	IEC 60897
Relative Permittivity	ASTM D924
Dissipation Factor	ASTM D924
Physio-Thermal properties	
Viscosity	ASTM D445
Interfacial Tension	ASTM D971
Flash Point	ASTM D93

4.1 EXPERIMENTAL APPROACH

The experimental approach for various insulating and physio-thermal properties has been explained as below.

AC Breakdown Voltage Test: AC breakdown voltage (BDV) is the most significant dielectric property of an insulator. BDV of all the prepared samples has been measured as per the IEC 60156

standards [136]. A semi-automated BDV test kit, shown in Figure 4.1, with maximum test voltage of 100 kV was used for measuring the BDV values. The test cell had two semi-spherical stainless-steel electrodes having body diameter of 50 mm. Spacing between the two electrodes was 2.5 mm and the applied step voltage was 2 kV/s. First, the BDV values of six oil-blend samples (OB0, OB20, OB40, OB60, OB80, OB100) were measured at 25°C and 90°C. The oil-blend having the optimum BDV out of the six blends was chosen for dispersing of surface modified GO, TiO_2 and ZnO nanomaterials and thus preparing three types of nanofluids (GNF, TNF and ZNF), each type having five different concentration levels. BDV values of all the three prepared nanofluid types, each having five concentration levels (NF1, NF3, NF5, NF7 and NF9), were measured at each concentration level and compared with the conventional mineral oil, pure ester oil as well as the base oil blend.

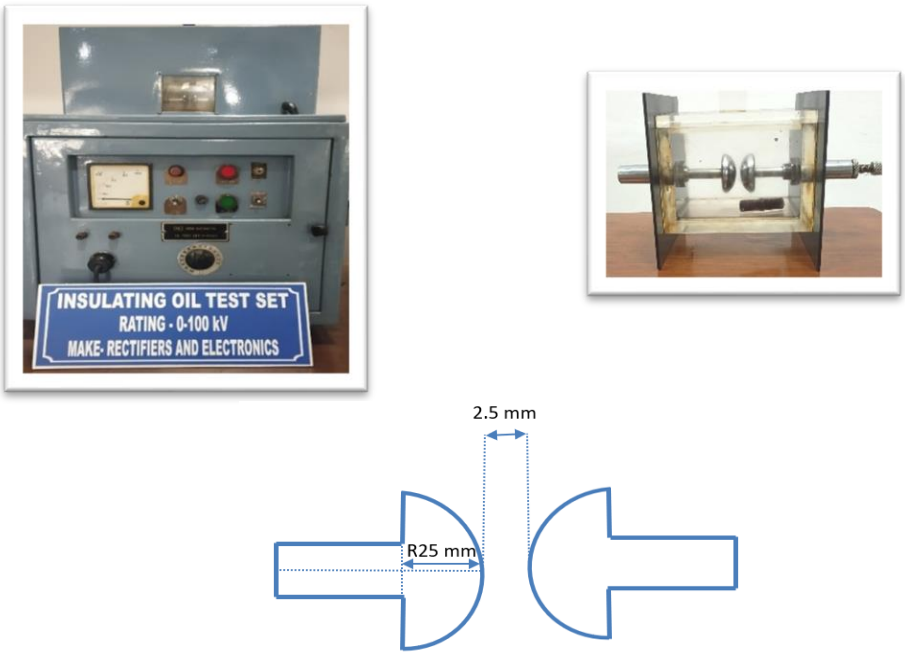

Figure 4.1 BDV test kit with its test cell as well as the dimensions of the electrodes used in the test cell.

Impulse Test: To simulate lightning strikes, standard positive lightning impulses (1.2/50 µs) were applied to the prepared OB and NF samples as per the IEC 60897 standards [137] and their effects were studied using the H.V Impulse generator as shown in Figure 4.2. The kit consisted of a pair of spherical electrodes capable of generating a maximum of 140 kV positive impulse. First, the impulse breakdown voltages (IBDV) of six oil-blend samples (OB0, OB20, OB40, OB60, OB80, OB100) were measured at 25°C. Thereafter, the IBDV values of prepared five nanofluid samples were measured at same temperature and compared with the mineral oil, ester oil and the base oil blend.

In order to increase the accuracy of BDV and IBDV tests and to obtain a wider probability range in Weibull distribution for these parameters, these tests were performed 15 times and their average values were taken as the final result values. Weibull distribution was carried out to obtain the reliability and sample failure probabilities. The values were plotted using 1-way ANOVA technique at 0.05 significance level. The BDV and IBDV data were modelled as per 2-parameter Weibull distribution model,

$$F(x) = 1 - \exp\{-(x/\alpha)^{\wedge}\beta\} \qquad (1)$$

where 'α' is the scale parameter which signifies the degree of failure, thus, defining the range of distribution of the function. 'β' is called as shape parameter because of the fact that it equals the slope of the line of the function in the probability plot. It also signifies the scattering of the data. Greater the shape parameter, wider the spread of the distribution of function.

Figure 4.2 Impulse generator kit used to measure impulse voltages.

Relative Permittivity and Tan δ Tests: The relative permittivity, also known as dielectric constant, is a non-sinusoidal parameter which depends upon the internal structure of the insulating fluid. The relative permittivity shows the ability of the material to change its polarity in the vicinity of an electric

field. Tan δ, also known as loss tangent, is a measure of dielectric losses in an insulator when subjected to an alternating electric field. Relative permittivity and loss tangent values of all OB and NF samples were measured as per IEC-61620 and ASTM D924 [138] standards respectively at 25°C and 90°C using the test kit shown in Figure 4.3. These temperature values correspond to the ambient temperature of a transformer in normal working conditions and in overload working conditions respectively. These tests have been performed 7 times for each sample and their average values have been taken as the final result values.

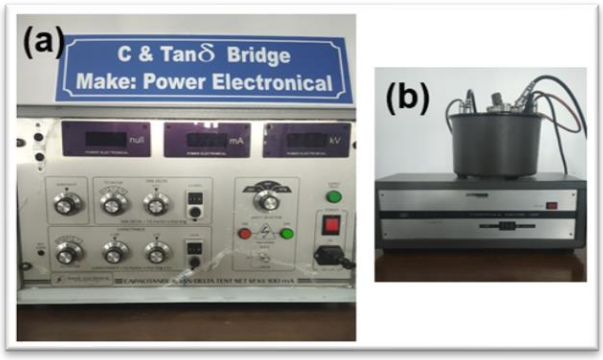

Figure 4.3 Test kit used to measure the relative permittivity and tan delta of the insulating fluids.

Viscosity Test: Viscosity of any transformer fluid can be defined as the oil resistance to shear, in other words, oil resistance to flow. It signifies the internal friction of the transformer oil, thus, giving a fair idea about the thermal conductivity of the oil. Viscosity of an oil is the most important governing factor to decide how properly the oil behaves as a coolant in the transformer. Viscosity values of the prepared OB and NF samples were tested in a viscometer as per the ASTM D445 standards [139] at 25°C and 90°C. The shear rate was applied in the range of 6/s to 120/s (at intervals of 6). The average viscosity was computed at a shear rate of 50.5/s.

Interfacial Tension Test: Interfacial tension (IFT) is defined as work done to increase the size of the common boundary between two adjacent materials which do not mix with one another. In case of transformer oils, this tension is measured at the surface of oil-water boundary, thus giving information about the status of the hydrophobic property of the oil. IFT tests of the samples were carried over in a tensiometer based upon Du-Nouy ring principle at 25°C as per the ASTM D971 standards [140].

Flash Point Test: Flash point of any transformer oil is the minimum temperature at which the oil

has vaporized enough to form an ignitable mixture in its surroundings. A lower flash point is a direct indication of the high flammability of any insulating oil. The flash point tests for the samples were done as per the ASTM D93 standards [141].

4.2 INSULATING PROPERTIES OF SYNTHESIZED NANOFLUIDS

The tests for dielectric properties were performed immediately after the ultra-sonification aided uniform dispersion of nanomaterials in order to avoid the effects of agglomeration and sedimentation of the nanoparticles.

4.2.1 AC Breakdown Voltage

OB: First of all, the BDV of synthesized OB samples are measured as already discussed in chapter 3, section 3.2.1. However, the results have been briefly discussed here once again in order to maintain the continuity. The BDV values of prepared OB samples at 25°C and 90°C are plotted in Figure 4.4. It can be seen that the BDV of the OB increases with increase in EO content in the blend. OB0 which represents the pure MO has a BDV of 45 kV at 25°C and 46 kV at 90°C. The BDV of OB100, which corresponds to the pure EO, is found to be 50 kV at 25°C and 55 kV at 90°C. For OB80, BDV attains a highest value of around 55 kV at 25°C and 56 kV at 90°C. Further increase of EO in the blend leads to a decrease in the BDV of the oil-blend.

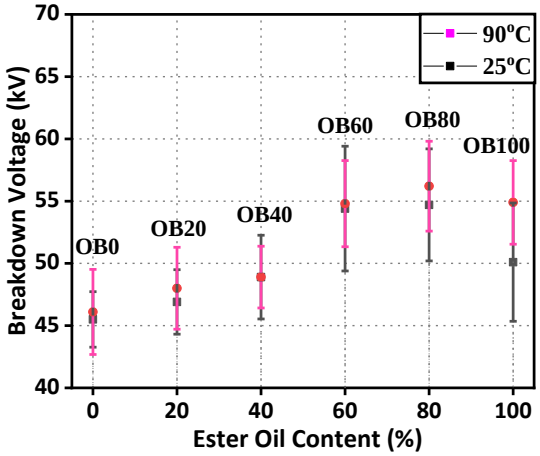

Figure 4.4 BDV values of oil blends.

The highest value of BDV along with the greater quantity of EO with respect to the MO makes

OB80 a good base oil-blend in order to disperse the synthesized nanomaterials to make NF samples, which has already been discussed in chapter 3 in great detail. The BDV of synthesized NF samples are discussed as below.

GNF: Figures 4.5a and 4.5b show the BDV of GNF samples at 25°C and 90°C respectively in comparison with the BDV of base oil-blend i.e., OB80. It can be clearly seen that the introduction of GO results in a decrease in the BDV of GNF sample. However, further addition of GO causes the BDV of the GNF to increase and the highest value of BDV is attained in case of GNF5 sample which is 61.14 kV at 25°C and 64.3 kV at 90°C. Addition of more GO nanoparticles results in the decrease of BDV once again. It is also noticed that the values of standard deviations are comparatively lower for GNF5 samples at both 25°C and 90°C which indicates to the better stability of the GNF5 sample in comparison with other GNF samples.

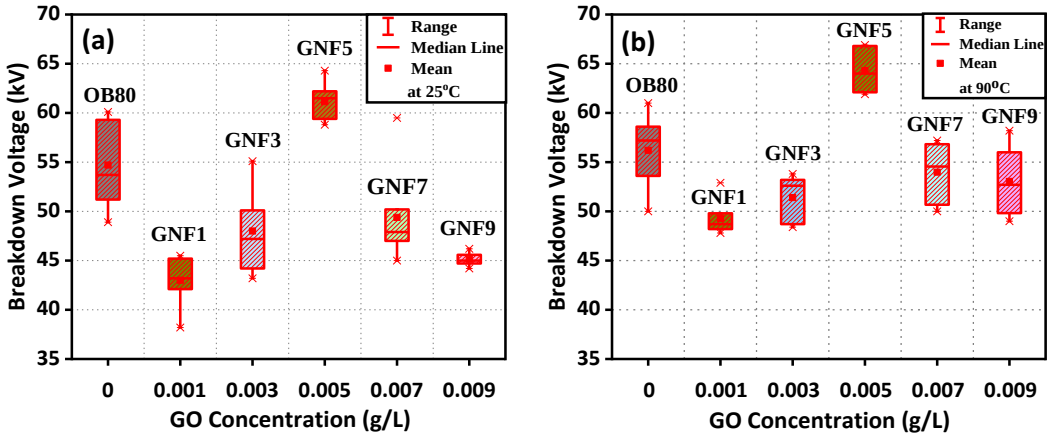

Figure 4.5 (a) BDV of GNF samples at 25°C, (b) BDV of GNF samples at 90°C.

Figure 4.6 shows the Weibull distribution of BDV values of GNF samples with 50% probability at different temperature values with the data listed in Table 4.2. The scattering of plot values can be clearly seen to be more in case of BDV of GNF sample at 25°C when compared to the BDV values at 90°C. However, at both temperature values the GNF5 sample continuously maintains the highest values of BDV. When the BDV values of GNF samples are combined over the entire temperature range as shown in Figure 4.6c, GNF5 sample, once again, shows the least scattering of data plots of respective BDV samples as compared to the GNF samples having other concentration values. The increase in the slope of line for GNF5 sample also signifies the stability of the sample at both temperature values.

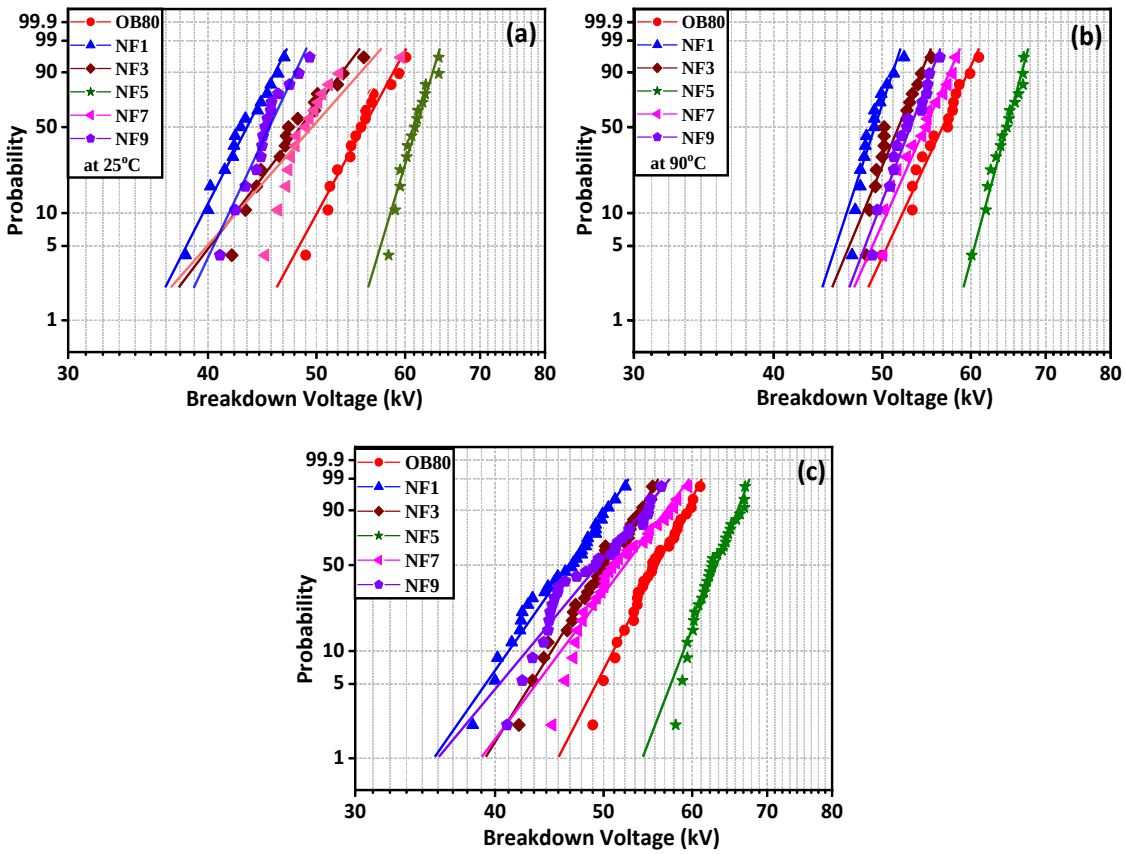

Figure 4.6 Weibull distribution plots for BDV values of GNF samples at (a) 25°C, (b) 90°C and (c) combined temperature values.

Table 4.2 Minimum and maximum BDV values of GNF samples with their scale and shape parameters at 50% probability values

SAMPLES	U_{50}			
	BDV (kV)		α	β
	Min	Max		
OB80	54.7	57.0	56.86	20.67
GNF1	45.26	47.83	47.66	15.26
GNF3	48.92	51.39	51.22	17.14
GNF5	62.11	64.03	63.90	27.75
GNF7	50.73	53.89	53.62	14.25
GNF9	47.84	51.11	50.88	12.82

TNF: Figure 4.7 shows the BDV of TNF samples at 25°C and 90°C in comparison with the BDV of base oil-blend i.e., OB80. Data shows that at both temperature values, BDV of TNF increases on dispersing the TiO_2 nanoparticles in OB80. However, with further increase in the concentration of nanoparticles, the BDV keeps on increasing till it reaches its maximum value in TNF5 sample which is recorded to be 64.2 kV at 25°C and 68.2 kV at 90°C. Addition of more TiO_2 nanoparticles results in the decrease of BDV in TNF samples. The pattern followed by the changes in the BDV values of TNF samples at different concentrations levels differs from the pattern followed by the GNF samples for the fact that in case of GNF samples, an initial decrease at lowest concentration level, i.e., GNF1 can be noticed whereas in case of TNF, the BDV increases directly with the addition of the TiO_2 nanoparticles.

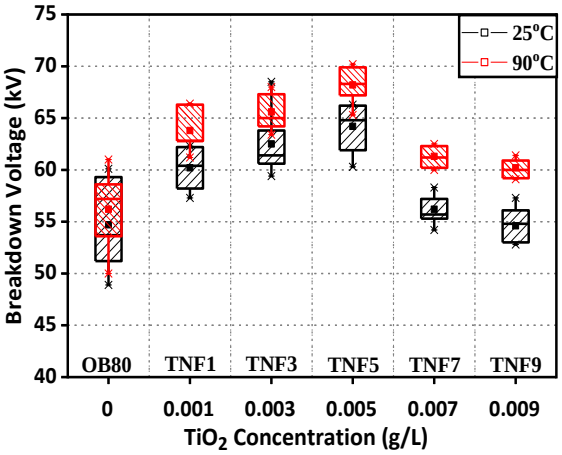

Figure 4.7 BDV values of TNF at 25°C and 90°C.

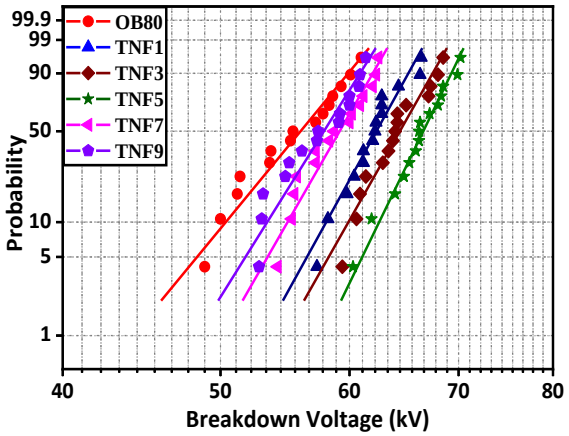

Figure 4.8 Weibull distribution plots for BDV values of TNF samples at combined temperature values.

Figure 4.8 shows the Weibull distribution of BDV values of GNF samples with 50% probability at different temperature values with the data listed in Table 4.3. It can be seen that the shape parameter (β) is lowest for is OB80, thus, resulting in the minimum steepness in the line corresponding to OB80 sample. However, the data scattering keeps on varying with the increase in concentration levels of TiO_2 nanoparticles up to a limit corresponding to TNF5 for which the slope of the line becomes maximum and the scattering of data values becomes minimum. Weibull distribution further confirms the increase in failure probability for BDV values of TNF samples after increasing the concentration of TiO_2 nanoparticles in the oil blend, i.e., in the case of TNF7 and TNF9 samples.

Table 4.3 Minimum and maximum BDV values of TNF samples with their scale and shape parameters at 50% probability failure.

	U_{50}			
SAMPLES	***BDV (kV)***		***α***	***β***
	Min	***Max***		
OB80	54.1	57.9	57.1	17.8
TNF1	60.9	63.7	63.1	26.5
TNF3	62.9	65.9	65.3	25.8
TNF5	65.3	67.3	67.4	30.1
TNF7	57.8	60.6	60	25.6
TNF9	56.4	59.3	58.7	23.5

ZNF: Figure 4.9 shows the BDV of ZNF samples at 25℃ and 90℃ in comparison with the BDV of base oil-blend i.e., OB80. The data shows that at both temperature values, BDV of ZNF increases on dispersing the ZnO nanoparticles in OB80 but only up to a certain concentration value. With initial increase in the concentration of ZnO nanoparticles, the BDV keeps on increasing till it reaches its maximum value in ZNF5 sample which is recorded as 62.9 kV at 25°C and 67.2 kV at 90°C. Addition of more ZnO nanoparticles results in the decrease of BDV in TNF samples. When compared with the patterns followed by the BDV values of other nanofluids, the BDV pattern of ZNF is almost similar to the BDV pattern of TNF samples. As seen in the case of GNF samples, no initial decrease in the BDV of ZNF samples is noticed.

Figure 4.10 shows the Weibull distribution of BDV values of GNF samples with 50% probability at different temperature values with the data listed in Table 4.4. In Weibull plot, the scattering of data plot values of BDV of ZNF samples tends to increase as soon as the ZnO nanoparticles are introduced in the oil blend. The slope of the line corresponding to ZNF1 sample also increases. However, as the concentration level of ZnO nanoparticles is increased in the oil blend, the scattering of the BDV plots decreases whereas the slope of the corresponding lines increases which is further confirmed by the increase in the shape parameter given in Table 4.4. This overall increase indicates towards the enhanced BDV voltages for the ZNF5 sample with better stability when compared the ZNF samples having other concentration values. The Weibull

plot also confirms the decrease in BDV with further increase in the concentration of ZnO nanoparticles.

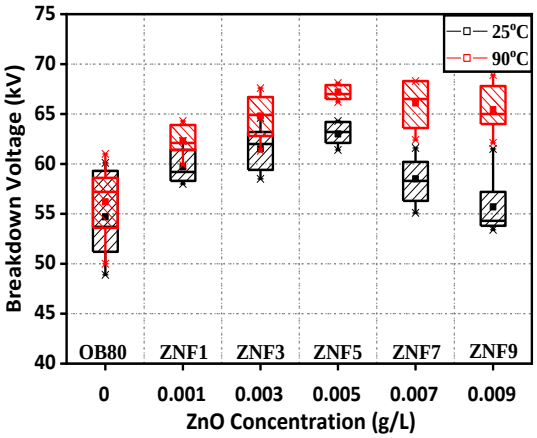

Figure 4.9 BDV values of ZNF at 25°C and 90°C.

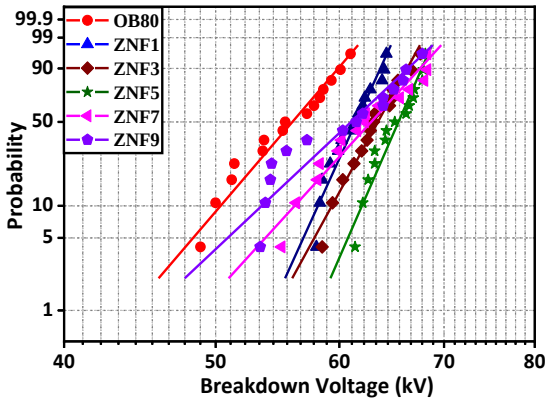

Figure 4.10 Weibull distribution plots for BDV values of ZNF samples at combined temperature values.

Table 4.4 Minimum and maximum BDV values of ZNF samples with their scale and shape parameters at 50% probability failure.

	U_{50}			
SAMPLES	***BDV (kV)***		***α***	***β***
	Min	***Max***		
OB80	54.1	57.9	57.1	17.8
ZNF1	60.4	62.5	62.1	33.5
ZNF3	62.1	64.8	64.3	27.8
ZNF5	64.3	66.5	66.1	35
ZNF7	60.6	65.1	64.2	16.7
ZNF9	58.5	63.6	62.6	14.3

4.2.2 Impulse Breakdown Voltage

OB: The IBDV values of OB samples at 25°C are plotted in Figure 4.11. It can be seen that the IBDV for the oil blend increases with the increase in the content of EO in the blend. IBDV of OB0,

i.e., pure MO is 54 kV. This value increases with the increase in EO content in oil-blend till OB80 sample for which IBDV hits the peak value of 75.5 kV. With further addition of the EO, the IBDV starts to decrease resulting in the lowering of IBDV of OB100, i.e., pure EO to 72.5 kV. This once again confirms the optimization of OB80 blend out of all the oil-blends.

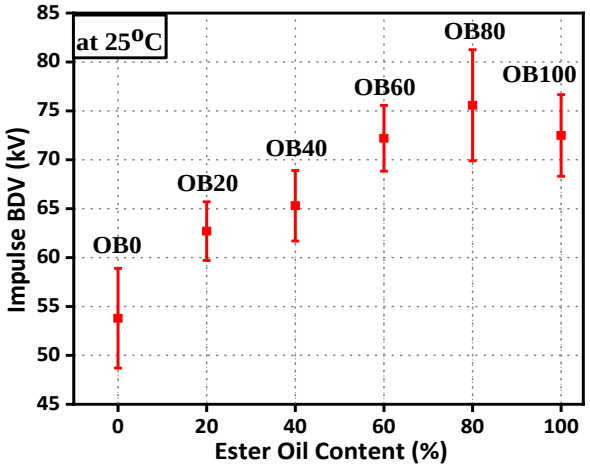

Figure 4.11 IBDV values of oil blend samples at 25°C.

GNF: Figure 4.12a shows the IBDV values of prepared GNF samples in comparison with the value of OB80. It is evident that at first, addition of GO nanoparticles causes a slight dip in the IBDV of the GNF just like the initial dip noticed in the BDV values of GNF samples on introducing the GO nanoparticles. As the concentration of GO nanoparticles is increased, IBDV value of the GNF keeps on increasing till it hits the peak value of 84.35 kV corresponding to the GNF5 sample.

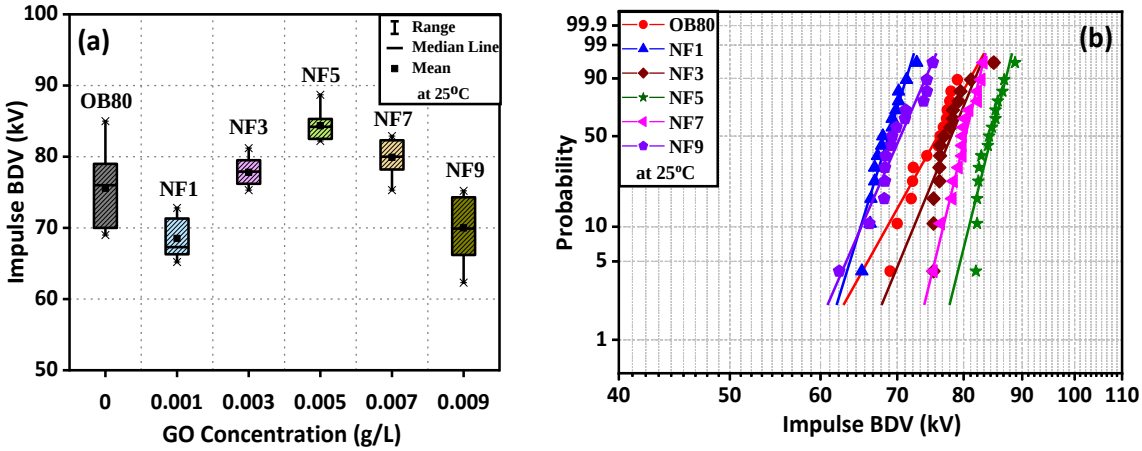

Figure 4.12 (a) IBDV values of GNF samples and (b) Weibull distribution plot for IBDV values of GNF samples.

A further increase in the concentration of GO in the GNF results in a decrease in the IBDV of the sample. The standard deviations of IBDV values also change according to the IBDV values which again confirms the stability of GNF5 sample as compared to other samples. Figure 4.12b shows the Weibull distribution of IBDV values of GNF samples with 50% probability at different temperature values with the data listed in Table 4.5.

Table 4.5 Maximum and minimum values of IBDV for GNF samples at 50% probability failure.

	U_{50}			
SAMPLES	***IBDV (kV)***		***α***	***β***
	Min	***Max***		
OB80	73.55	78.43	77.47	18.51
GNF1	67.57	70.01	69.53	33.64
GNF3	76.19	79.89	79.17	25.06
GNF5	83.40	85.82	85.36	41.59
GNF7	79.13	81.39	80.95	42.52
GNF9	63.73	72.25	71.56	23.90

TNF: IBDV values of TNF samples are plotted in Figure 4.13a. Addition of TiO_2 leads to an increase in the IBDV of TNF samples up to a particular concentration. The highest value of IBDV for TNF samples is recorded in case of TNF5 sample which is 92 kV. Increasing the TiO_2 nanoparticle concentration beyond this value, i.e., the limit of 0.005 g/L of said nanoparticles, leads to a decrease in the IBDV values of TNF samples. This decrease in IBDV values continues even more with more addition of nanoparticles. Figure 4.13b shows the Weibull distribution of IBDV values of TNF samples with 50% probability with the data listed in Table 4.6a.

ZNF: IBDV values of synthesized ZNF samples are plotted in Figure 4.13a. Addition of ZnO nanoparticles results in an increase in the IBDV of ZNF samples up to a particular concentration. The peak value of IBDV for ZNF samples is recorded in case of ZNF5 sample which is 98 kV. Increasing the ZnO nanoparticle concentration beyond this value leads to a decrease in the IBDV

values of ZNF samples. Figure 4.13c shows the Weibull distribution of IBDV values of ZNF samples with 50% probability with the data listed in Table 4.6b.

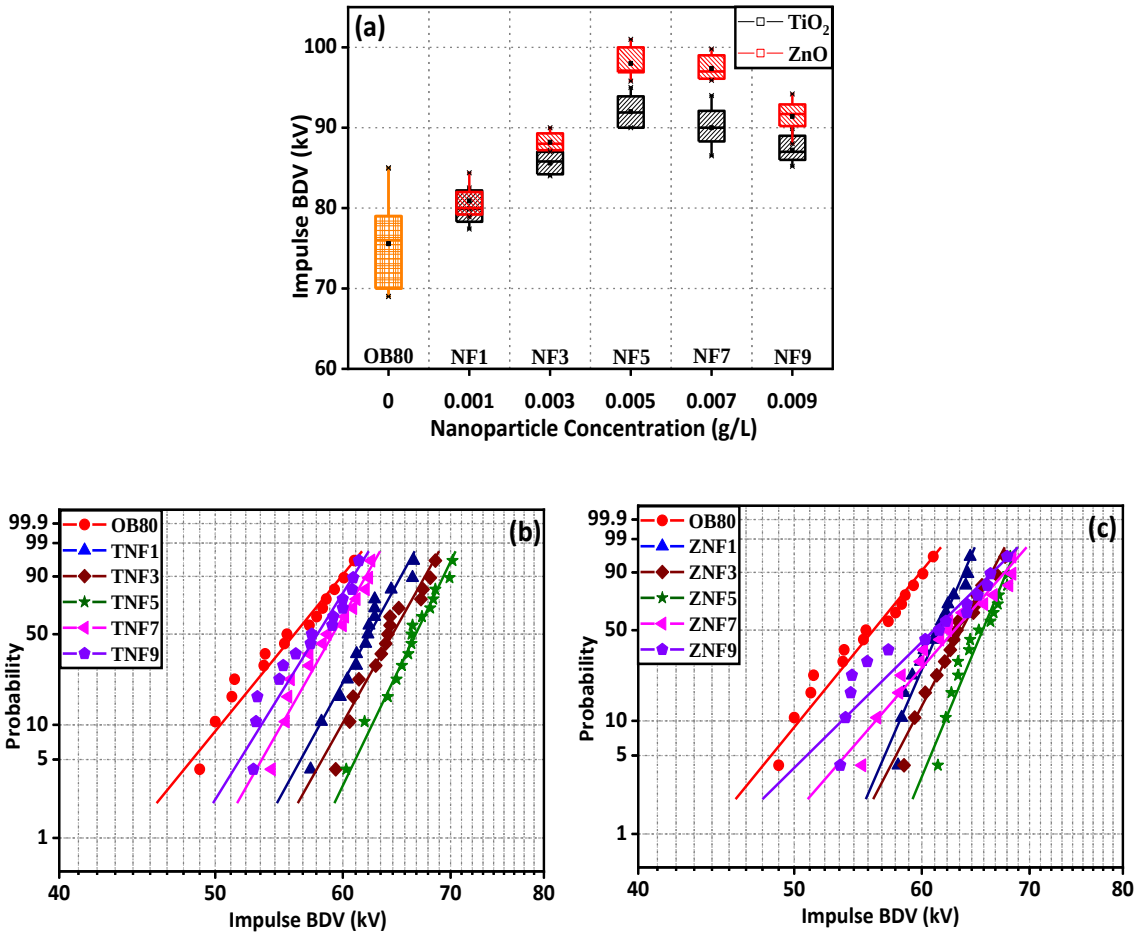

Figure 4.13 (a) IBDV values of TiO_2 and ZnO nanoparticles at 25°C, (b) and (c) Weibull distribution of IBDV values of TiO_2 and ZnO nanoparticles respectively at 50% probability failure.

The Weibull distribution plots of IBDV values of all the three nanofluids confirm the behavior of these nanofluids at different concentration levels as shown by their respective data graphs. GNF samples have shown the maximum steepness in the lines, i.e., maximum shape parameters as compared to the TNF and ZNF samples. However, for all the three cases, the concentration level of 0.005 g/L which corresponds to the NF5 concentration (GNF5, TNF5 and ZNF5) is seen to enhance the IBDV of oil blend to the maximum values as compared to the other concentration levels. Like the Weibull plots of BDV values for these three nanofluids, the data scattering in IBDV for GNF5, TNF5 and ZNF5 samples is minimum, thus signifying the overall stability of these nanofluid samples over the entire temperature range.

Table 4.6 Minimum and maximum limits of IBDV values for (a) TNF and (b) ZNF samples at 50% probability failure.

(a)

SAMPLES	U_{50}			
	IBDV (kV)		α	β
	Min	Max		
OB80	73.5	78.4	77.4	18.5
TNF1	79.2	81.1	80.7	50.1
TNF3	85.2	86.4	86.1	85.4
TNF5	91.2	93.2	92.8	55.5
TNF7	89	91.5	91	43.5
TNF9	86.5	88.2	87.9	63.9

(b)

SAMPLES	U_{50}			
	IBDV (kV)		α	β
	Min	Max		
OB80	73.5	78.4	77.4	18.5
ZNF1	79.4	82.9	82.2	27.5
ZNF3	87.4	89.4	89	53.1
ZNF5	97.2	99.3	98.9	54.8
ZNF7	96.8	98.4	98.1	74.9
ZNF9	90.8	92.3	92	70.2

4.2.3 Relative Permittivity and Dissipation Factor

OB: The relative permittivity values of the OB samples measured at 25°C and 90°C are plotted in Figure 4.14a. The relative permittivity (or dielectric constant) of the OB samples keeps on increasing continuously with the increase in EO in the blend. Although, the relative permittivity of OB100, i.e., pure EO, is found to hit the peak values at 2.1 at 25°C and 2.4 at 90°C, however the relative permittivity values of OB80 are of our concern since this OB80 has been used as the base oil for the dispersion of nanomaterials due to its highest BDV and IBDV values. Moreover, the dielectric constant of OB80 was measured to be 1.9 at 25°C and 2.3 at 90°C which lie closer to the dielectric constant values of the OB100 sample. The data for dissipation factor for OB samples were also measured at 25°C and 90°C is shown in Figure 4.14b. In case of OB samples, the dissipation factor starts to increase with the increase in EO content in the oil-blend at both temperature values indicating that the pure mineral oil has lower dissipation factor as compared to that of the pure ester oil. But OB80 and OB100 show a very sharp increase in the values of the dissipation factor especially at 90°C. OB80 had a dissipation factor of 0.08 at 25°C which increased to 0.15 at 90°C. OB100, i.e., pure EO, had a dissipation factor of 0.15 at 25°C and 0.3 at 90°C. Since, OB80 has

been selected for making the NF samples, its comparatively lower dissipation factor than OB100 serves a good purpose.

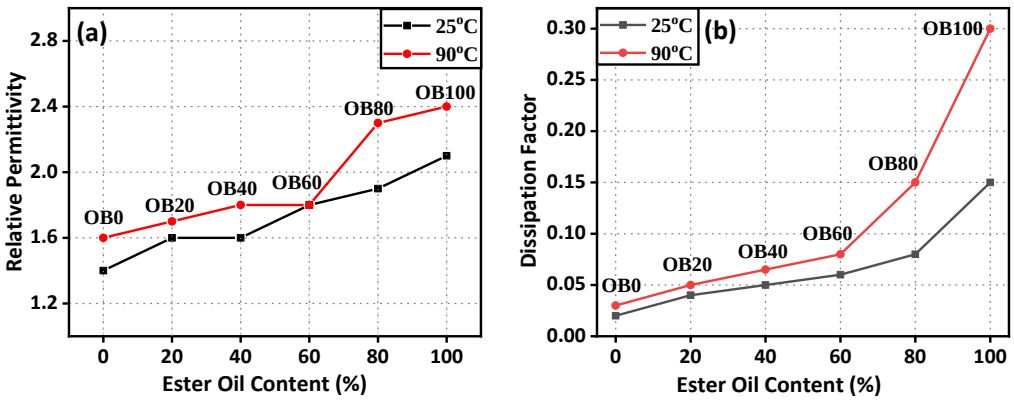

Figure 4.14 (a) Relative Permittivity and (b) Dissipation of oil blend samples at 25°C and 90°C.

GNF: In case of GNF samples, the relative permittivity is seen to follow a different trend as compared to that in OB samples as shown in Figure 4.15a. At first, the relative permittivity of the GNF increases with the addition of GO nanoparticles at both temperatures. At 25°C, the peak value is hit for GNF7 after which the permittivity starts to decrease. On the contrary, at 90°C, the peak value is hit for GNF3 after which the permittivity starts to decrease sharply and attains the values much lower than the values of the base OB80. It represents the poor performance of GNF samples dispersed with higher concentrations of GO nanoparticles at higher temperature.

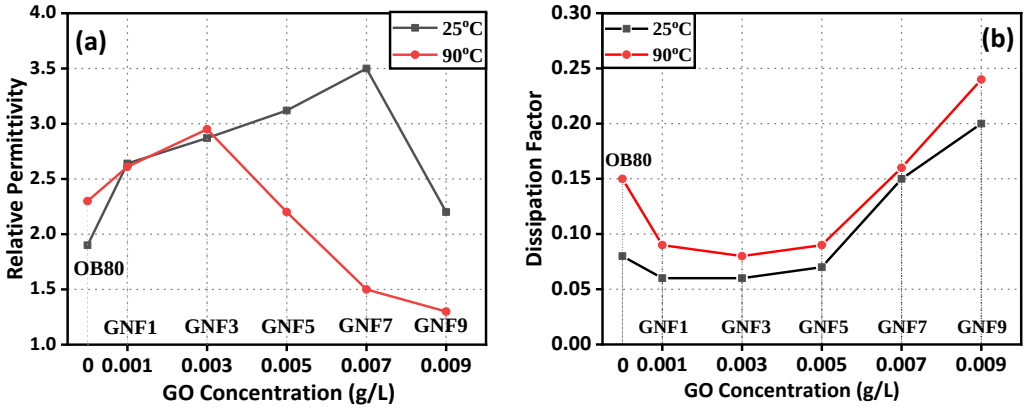

Figure 4.15 (a) Relative Permittivity and (b) Dissipation of GNF samples at 25°C and 90°C.

The dissipation factors for GNF samples are plotted in Figure 4.15b. The dissipation factor of the GNF decreases with the addition of GO nanoparticles and the minimum values corresponding to both the temperatures are obtained for GNF3 sample which are recorded as 0.06 at 25°C and

0.08 at 90°C. Further addition of GO causes the dissipation factor of GNF to increase drastically resulting in the values of 0.2 at 25°C and 0.24 at 90°C. This increase in the dissipation factor at higher concentration of GO nanoparticles is further justified by the trend followed by the relative permittivity values of GNF samples at higher GO concentrations especially at 90°C.

TNF: Figure 4.16a shows the relative permittivity of TNF samples at 25°C and 90°C. With the addition of TiO_2 nanoparticles in OB80, the values of dielectric constant of TNF samples were increased up to a certain concentration. For TiO_2 dispersed NF samples, the maximum value of dielectric constant at both temperatures was achieved for TNF3 which was 2.7 at 25°C and 2.9 at 90°C. After the concentration levels beyond TNF3, the dielectric constant started to decrease.

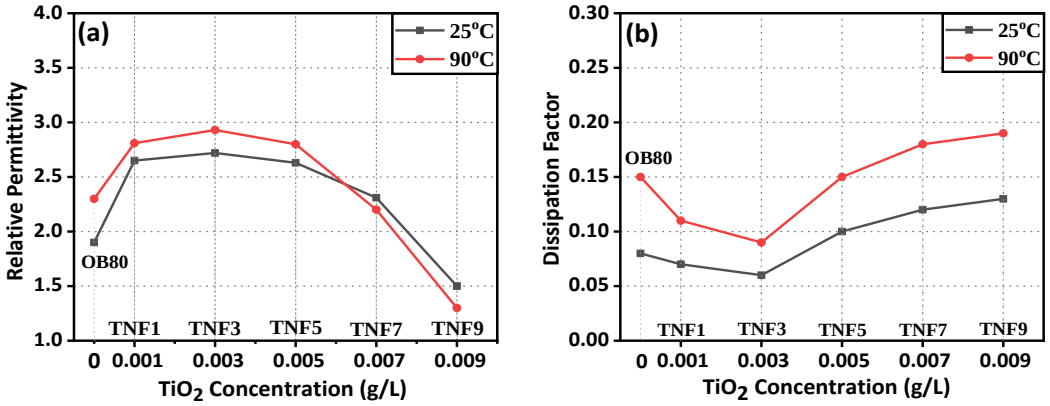

Figure 4.16 (a) Relative Permittivity and (b) Dissipation of TNF samples at 25°C and 90°C.

The dissipation factors for TNF samples are plotted in Figure 4.16b. It can be seen that by dispersing the TiO_2 nanoparticles in the oil-blend, the dissipation factor for TNF samples was found to decrease up to a certain concentration level, after which its value started to increase with the increase in the nanoparticle concentration. In the case of TNF samples, the minimum value was achieved for TNF3 which was 0.059 at 25°C and 0.09 at 90°C.

ZNF: Figure 4.17a shows the relative permittivity of ZNF samples at 25°C and 90°C. as soon as the ZnO nanoparticles are dispersed, the relative permittivity of resulting ZNF samples started to increase. The maximum value at both temperatures were recorded for ZNF5 which was 2.8 at 25°C and 2.9 at 90°C. With the addition of more ZnO nanoparticles, the values of dielectric constant started to decrease once again.

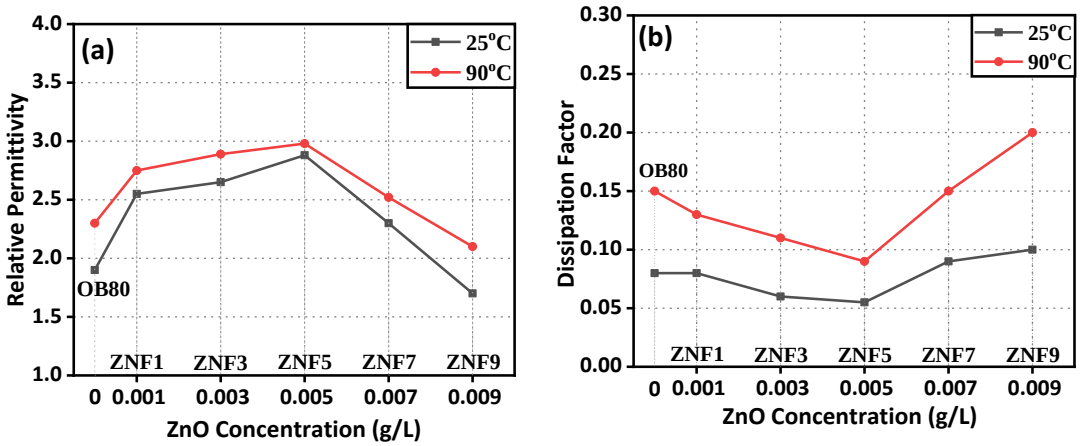

Figure 4.17 (a) Relative Permittivity and (b) Dissipation of ZNF samples at 25°C and 90°C.

The dissipation factors for ZNF samples are plotted in Figure 4.17b. For ZNF samples, the minimum value of dissipation factor was measured corresponding to ZNF5 sample and it was recorded to be 0.054 at 25°C and 0.089 at 90°C.

For any particular insulating material, the values of its dielectric constant as well as its dissipation factor are interrelated. The greater the dielectric constant, the more the capacity of the insulator to withhold the charge in itself, which further leads to the lower dissipation factor. This can also be seen by comparing the dielectric constant and dissipation factor data plots of both types of NF samples.

4.3 PHYSIO-THERMAL PROPERTIES OF SYNTHESIZED NANOFLUIDS

The various tested physio-thermal properties of different synthesized fluid samples are explained below.

4.3.1 Viscosity

The viscosity measured for the fluid samples is dynamic viscosity having units in centipoise, cP, (mPa-s). The viscosity of synthesized fluids is explained below.

OB: The viscosity values of OB samples have been plotted in Figure 4.18. As expected, the viscosity of the samples decreases tremendously with the increase in temperature. Viscosity of

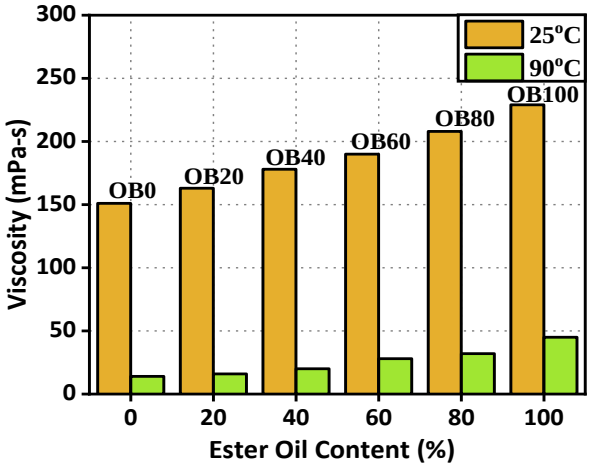

Figure 4.18 Viscosity of oil blend samples at 25°C and 90°C.

OB0, i.e., pure MO was 150 cP at 25°C which lowered down to 15 cP at 90°C. The viscosity of OB100, i.e., pure EO was 225 cP at 25°C and 45 cP at 90°C. However, the blend used for dispersion of nanomaterials, i.e., OB80 had viscosity of 210 cP at 25°C and 25 cP at 90°C.

GNF: The viscosity values of GNF samples have been plotted in Figure 4.19. It is clear that there is hardly any significant change in the viscosity of GNF samples at a particular temperature. However, a very slight decrease in viscosity can be noticed in GNF3 and GNF5 samples at 25°C as well as at 90°C. Both these samples had viscosity of 200 cP at 25°C and 25 cP at 90°C which were lower than other GNF samples but with a very minute margin. This can be due to the more inter-spatial distance between the nanoparticles as well as due to the alignment of nanoparticles in the direction of flow. However, further research needs to be done to prove these claims.

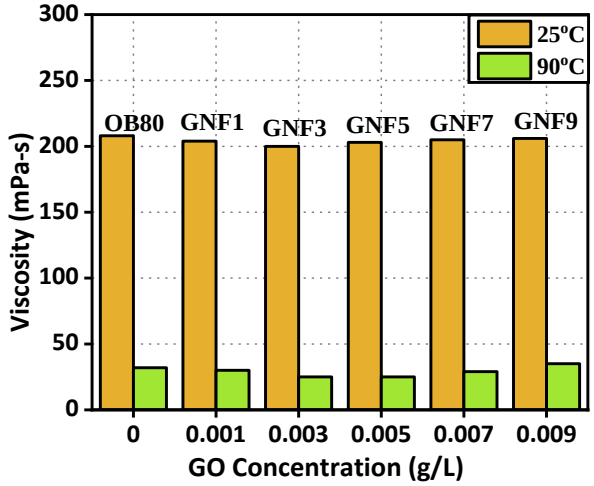

Figure 4.19 Viscosity of GNF samples at 25°C and 90°C.

TNF: The viscosity values of TNF samples have been plotted in Figure 4.20. It is evident that the viscosity of TNF sample decreased slightly with the addition of TiO_2 nanoparticles and almost attained a constant value at higher concentration levels. The lowest value of viscosity was achieved for TNF5 sample which was 180 cP at 25°C and 22 cP at 90°C, after which the viscosity of TNF samples attained almost a constant value.

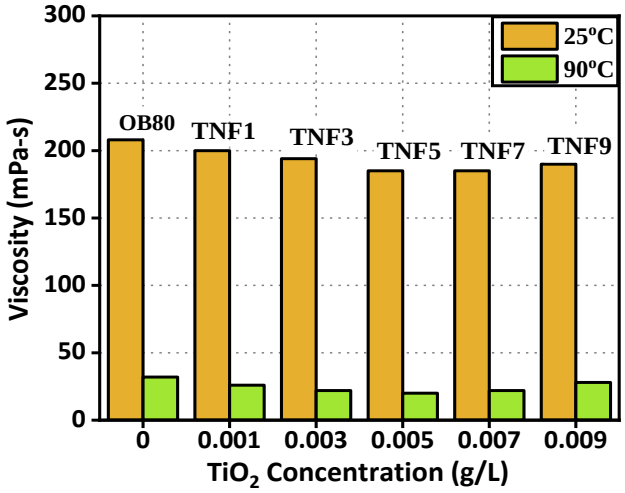

Figure 4.20 Viscosity of TNF samples at 25°C and 90°C.

ZNF: The viscosity values of ZNF samples have been plotted in Figure 4.21. The viscosity of ZNF sample is increased considerably with the addition of ZnO nanoparticles. However, following a similar trend, the viscosity values of particular ZNF samples are lower at a temperature of 90°C as compared to 25°C for obvious reasons.

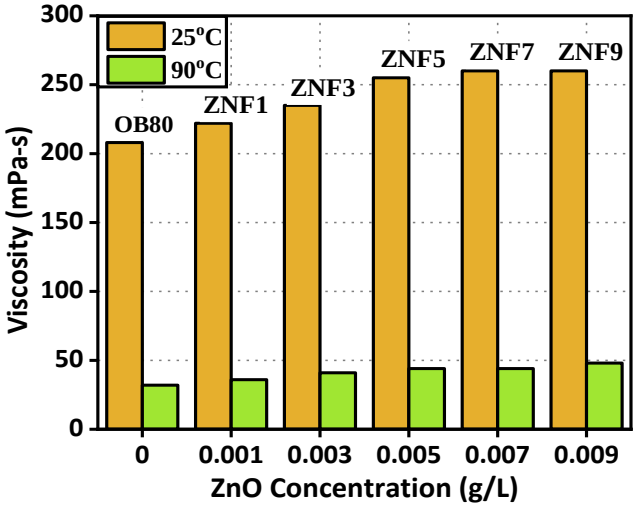

Figure 4.21 Viscosity of ZNF samples at 25°C and 90°C.

4.3.2 Inter-Facial Tension

IFT values of base oil-blend, i.e., OB80 and various NF samples were measured and compared as explained below.

OB80: The IFT values of OB80 sample and different NF samples as measured at 25°C are shown in Figure 4.22. IFT value of OB80 sample was 50 mN/m. Thus, OB80 shows IFT value corresponding to a 'good' insulating oil.

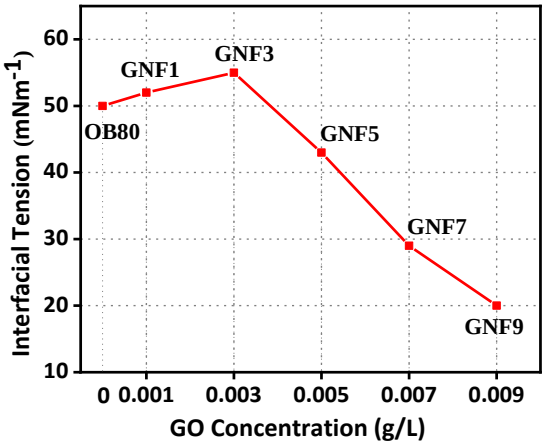

Figure 4.22 IFT values of GNF samples with respect to OB80.

GNF: The IFT value of GNF samples increases with the addition of GO nanoparticles up to the GNF3 sample, as shown in Figure 4.22, which was recorded as 55 mN/m, after which these values decreased sharply to very low readings corresponding to 'extremely bad' insulating oil in terms of IFT values, especially in cases of GNF7 and GNF9 samples, which were recorded as 28 mN/m and 20 mN/m, respectively.

TNF: In case of TNF samples, as shown in Figure 4.23, the IFT values increased after dispersing TiO_2 nanoparticles in the base oil-blend. The peak values of IFT were attained at a concentration level of TNF3 which was 56 mN/m, after which a decrease in the IFT values was noticed with further concentration of TiO_2 nanoparticles. At higher concentration values, IFT value was recorded to be very poor, i.e., 28 mN/m corresponding to the TNF9 sample.

ZNF: For ZNF samples, the IFT values increased after dispersing ZnO nanoparticles in the base oil-blend as shown in Figure 4.23. However, IFT for ZNF samples remained in 'good' category up to the concentration level corresponding to ZNF5 sample, after which there was extremely sharp decline in the IFT values leading to the 'poor' oil conditions. The worst IFT value was recorded to be 25 mN/m corresponding to the highest concentration value of ZnO nanoparticles in ZNF9 sample.

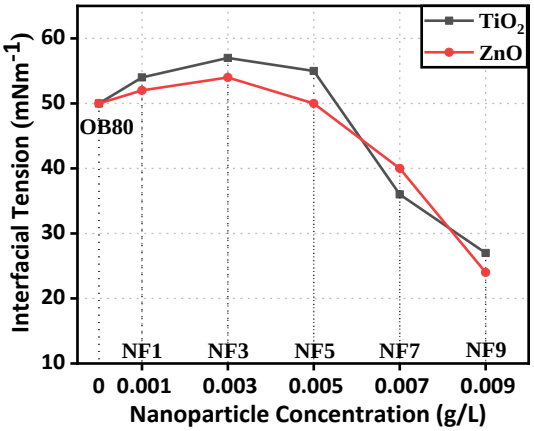

Figure 4.23 IFT values of TNF and ZNF samples with respect to OB80.

4.3.3 Flash Point

Flash points of base oil-blend, i.e., OB80 and various NF samples were measured and compared as explained below.

OB80: The flash points of OB80 sample and different NF samples are shown in Figure 4.24. Flash point of OB80 was recorded to be at 220°C.

GNF: Increase in GO nanoparticles leads to an increase in the flash point of GNF samples till it reaches the peak value in the case of GNF5, after which the flash point of GNF samples starts to decrease as shown in the Figure 4.24. The maximum value of flash point for GNF5 is recorded to be 280°C which then decreased to 240°C for GNF9 sample, which is still better than the flash point of the base oil-blend. This increase in flash point is a clear indication of the improvement in the non-inflammability for GNF samples.

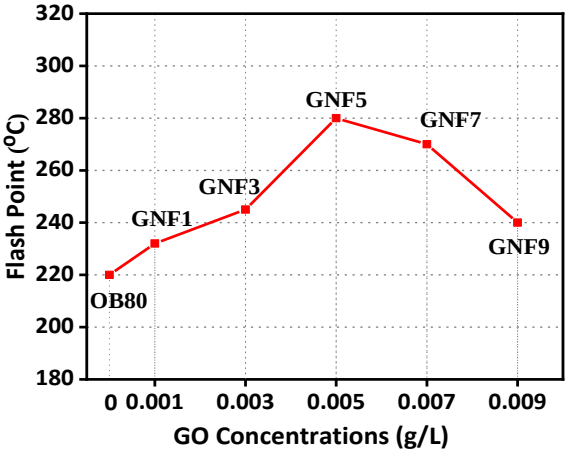

Figure 4.24 Flash point values of GNF samples with respect to OB80.

TNF: Addition of TiO_2 nanomaterials caused an increase in the flash point of the oil blend which is shown in Figure 4.25. The highest value of flash point in case of TNF samples was recorded as 269°C corresponding to TNF5 sample. The further addition of TiO_2 nanoparticles resulted in deterioration of flash point of NF samples, thus, lowering the flash point of TNF9 sample to 250°C.

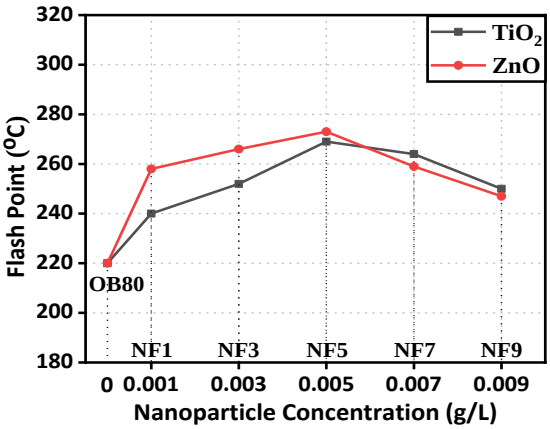

Figure 4.25 Flash points of TNF and ZNF samples with respect to base oil blend OB80.

ZNF: Dispersion of ZnO nanomaterials also caused an increase in the flash point of the oil blend. The highest value of flash point in case of ZNF samples was found to be 273°C, after which this value lowered down to 248°C corresponding to ZNF9 sample as can be seen in the Figure 4.25.

4.4 MECHANISM OF IMPROVEMENT

For GNF samples, the overall increase in the dielectric properties of NF samples can be due to the hydrophilic nature of GO leading to the absorption of moisture from the oil by nanoparticles. In case of TNF and ZNF samples, one of the most important reasons for the improvement in dielectric properties of the NF samples when compared to the base oil is the transferring of charge to the pathway served by the Gouy-Chapman-Stern layer which is former at an interface between the oil and nanoparticles due to the by-products formed over the passage of time [142]. This layer is responsible for the increased conductive path through the interface. In NF samples, the conduction along the interface of oil and nanoparticles can lead in higher shallow trap density. These shallow traps can be held responsible for the accumulation of charge carriers which are generated at higher voltage levels. This further enhances the electron trapping phenomenon in NFs when compared to the base oils. These shallow traps lead to a slower de-trapping of electrons in NFs leading to better dielectric properties.

4.5 CHAPTER SUMMARY

In this chapter, the important dielectric properties of OB samples as well as the synthesized NF samples have been studied. The dielectric properties of GO, TiO_2 and ZnO based NFs have been investigated and compared with the base oil-blend (OB80) in which the different nanomaterials have been dispersed. Addition of all the three nanomaterials in the natural ester based oil blend leads to considerable increase the breakdown values of NF samples up to a particular concentration limits. However, addition of non-conductive GO in base oil blend first leads to a decrease in BDV and IBDV values at lower concentration values of 0.001 and 0.003 g/L. However, on increasing the concentration of GO to 0.005 g/L, the peak breakdown values are measured with about 15% increase in BDV and 11.7% increase in IBDV as compared to the base oil-blend. Dispersion of semi-conductive TiO_2 and conductive ZnO also follow a similar trend of hitting the peak values of BDV and IBDV at 0.005 g/L concentration level. When compared to the base oil-blend, the increase in BDV and IBDV due to the addition of TiO_2 nanoparticles is 17% and 17.4% respectively, whereas, the increase in BDV and IBDV due to the addition of ZnO nanoparticles is 16% and 22.4% respectively. Dispersion of GO, TiO_2 and ZnO nanoparticles also leads to a

significant improvement in relative permittivity and dissipation factor of NF samples. However, the peak values are achieved at different concentration values for different nanomaterials. In GNF and TNF samples, the optimized peak performances are shown by samples corresponding to concentration levels of 0.003 g/L whereas, in case of ZNF samples, the peak values are achieved by sample having concentration level of 0.005 g/L.

The physio-thermal properties like interfacial tension and flash point of NF samples are also enhanced due to the dispersion of the nanomaterials. In terms of IFT, all the three nanomaterials based NF samples show the peak performances at concentration values of 0.003 g/L whereas, in terms of flash point, all the three nanomaterials based NF samples show the peak performances at concentration values of 0.005 g/L. However, no significant change in the viscosity of nanofluids with respect to the concentration of GO nanoparticles is noted except for a very minute reduction in the viscosities of GNF3 and GNF5 samples. On the other hand, the best performance in terms of viscosity is shown by the TNF samples having lowest viscosity corresponding to TNF3 sample, whereas, the ZNF samples shows the worst performance with the viscosity of the ZNF samples increasing on adding the ZnO nanoparticles. After a threshold value, further increase in NP concentration leads to the increased inter-molecular forces thus resulting in the agglomeration at higher loadings. This causes the dielectric properties to dip after hitting the peak value. In future, low synthesis cost and large-scale production will enable these nanomaterials dispersed ester oil based oil blend to be effectively used as insulating oils in transformers.

CHAPTER 5

ANALYSIS OF AGEING EFFECTS ON SYNTHESIZED LIQUID INSULATION FOR TRANSFORMERS

IN this chapter, the ageing effects on the transformer liquid as well as solid insulation impregnated with synthesized fluids have been studied. These effects have been investigated under two categories: mechanical effects and electrical effects.

5.1 EFFECTS OF AGEING ON SYNTHESIZED NANOFLUIDS

Whenever any new insulating fluid is developed and tested for its dielectric properties, it cannot be used for insulation purposes in transformers straightaway. The process of ageing plays a vital role in effecting the dielectric, thermal and chemical properties of insulating oils. It is well established that with the passage of time, the insulating properties of any particular dielectric fluid keep on deteriorating [141]. So, it becomes of utmost importance that the insulating properties of a newly developed dielectric fluid are studied after subjecting that fluid to the ageing conditions in laboratory. If the insulating properties of the developed fluid after ageing fall within the acceptable range as specified by the IEC standards for insulating oils for transformers, only then the developed oil can be used in transformers. The synthesized nanofluids were subjected to ageing conditions as described in chapter 3, section 3.3 and their dielectric and physio-thermal properties were measured after being aged for 15 and 60 days. These properties were compared with the properties of the newly developed respective nanofluid samples and their rates of deterioration were compared with the base oil OB80. Various properties that have been studied are analyzed below.

5.1.1 Dielectric Properties of Aged Nanofluids

(a) Ac BDV

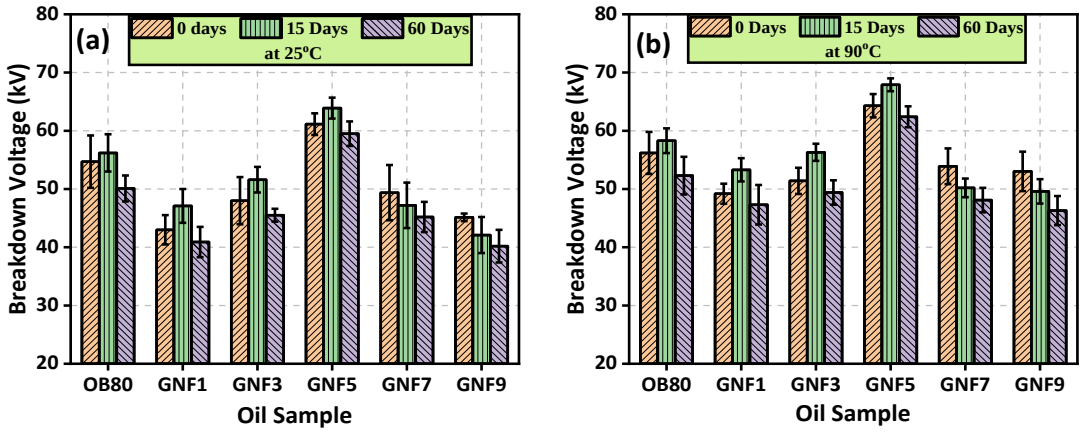

Figure 5.1 BDV values of unaged and aged GNF samples with respect to OB80 at (a) 25°C and (b) 90°C.

OB80: The ac BDV of OB80 as well as NF samples is shown in Figure 5.1. When measured at 25°C, the BDV of new unaged base oil OB80 is measured to be 54.7 kV which increases to 56.2 kV after 15 days of ageing and then drops to 50.1 kV after 60 days of ageing. Similarly, the BDV of new OB80 at 90°C is 56.2 kV which increases to 58.3 kV after 15 days of ageing and then reduces to 52.3 kV after 60 days of ageing.

GNF: At 25°C, the BDV of lower GNF samples, i.e., up to the concentration limits corresponding to GNF5 sample increased after 15 days after which it decreased at 60 days of ageing as can be seen in Figure 5.1. The BDV values of GNF7 and GNF9 started to deteriorate directly with the ageing period. The BDV values of GNF samples when measured at 90°C also follow a similar pattern where the BDV of lower concentrated GNF samples increased slightly at the end of 15 days and then decreased significantly at the end of 60 days of ageing. At both the temperature values, the maximum BDV after ageing is reported for GNF5 sample, i.e., 63.9 kV and 59.5 kV after the ageing periods of 15 and 60 days respectively when measured at 25°C, and 67.9 kV and 62.4 kV after 15 and 60 days of ageing respectively when measured at 90°C. Figure 5.2 shows the Weibull distribution plots of BDV values of unaged as well as aged GNF samples with respect to OB80 samples. The data plot scattering for the sample corresponding to 0.005 g/L concentration of graphene oxide, i.e., GNF5, is found to be minimum in all the cases of unaged as well as aged conditions. The maximum slope of the line corresponding to the unaged as well as aged GNF5 sample is also maximum showing its enhanced stability even after being subjected to the ageing conditions.

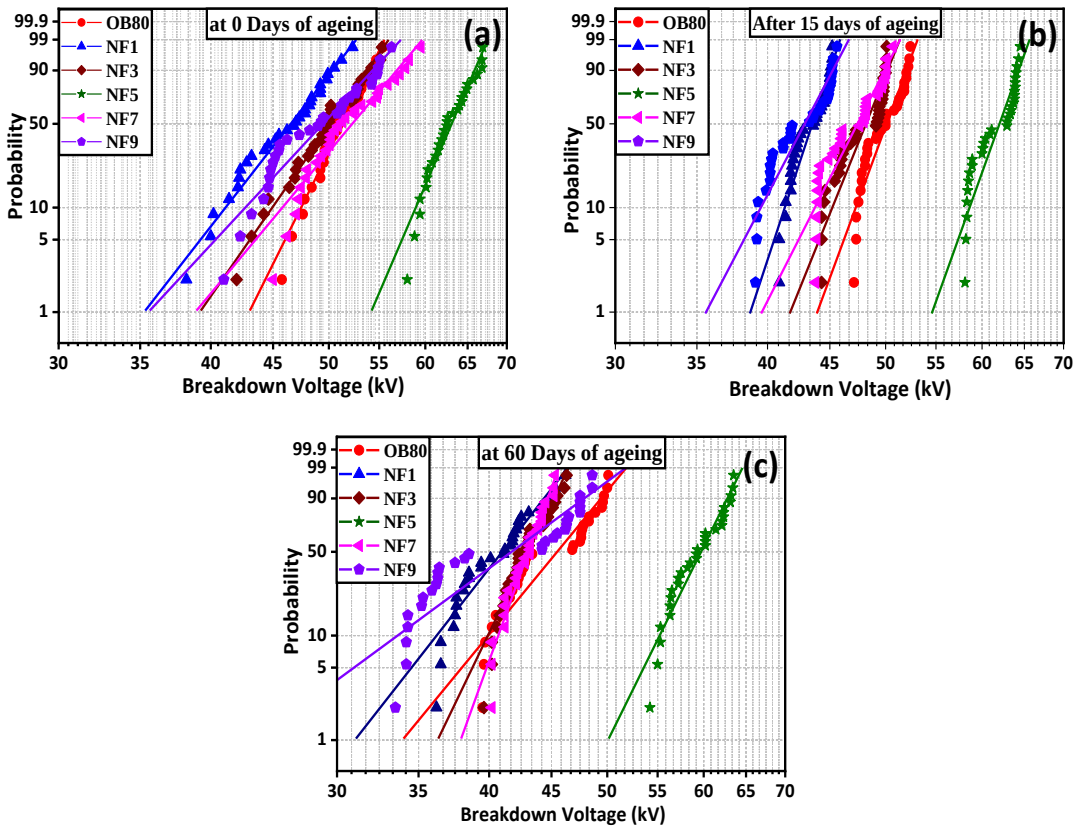

Figure 5.2 Weibull distribution plots for BDV values of GNF samples (a) at unaged conditions, (b) after 15 days of ageing and (c) after 60 days of ageing.

TNF: Unlike GNF, the BDV of new unaged TNF samples increased directly with respect to the OB80 sample as discussed already in previous chapters. However, this caused an overall increase in the BDV values of aged TNF samples as well. As a result, at both the temperature values, aged

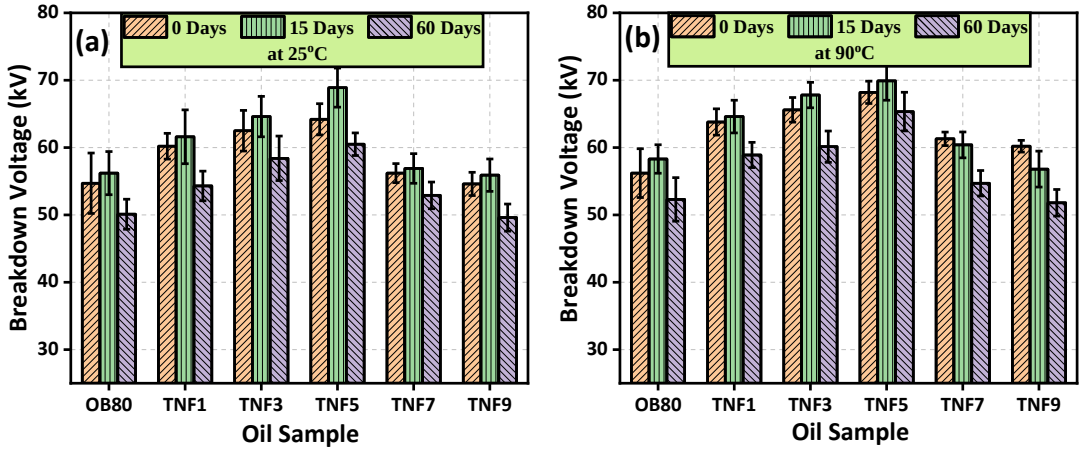

Figure 5.3 BDV values of unaged and aged TNF samples with respect to OB80 at (a) 25°C and (b) 90°C.

TNF samples reported higher BDV values when compared to the BDV of aged OB80 base oil as shown in Figure 5.3. The trend of increased BDV after 15 days of ageing and then decreased BDV after 60 days of ageing was also reported in TNF samples, However, at 90°C, the BDV values of TNF7 and TNF9 samples decreased directly with the ageing process indicating the poor dielectric performance of higher concentrated TNF samples at higher temperatures. In case of aged TNF samples as well, the peak value of BDV at both the temperatures is achieved for TNF5 which is recorded to be 68.9 kV after 15 days of ageing and 60.5 kV after 60 days of ageing at 25°C and 69.9 kV and 65.3 kV after 15 and 60 days of ageing respectively at 90°C.

ZNF: An exact similar pattern of increased BDV after 15 days and then decreased BDV after 60 days of ageing was reported in lower concentrated aged ZNF samples as can be seen in Figure 5.4. However, the higher concentrated ZNF samples showed a direct decrease in their BDV values as soon as the ageing process starts. At 25°C, ZNF7 and ZNF9 samples whereas at 90°C, ZNF9 sample reported no increase in their BDV after 15 days of ageing. Nevertheless, the peak values of BDV at both the temperatures were reported for ZNF5 which were measured to be 64.9 kV and 61.5 after 15 and 60 days of ageing respectively at 25°C, whereas these values were 69.9 kV and 65.2 kV after 15 and 60 days of ageing at 90°C.

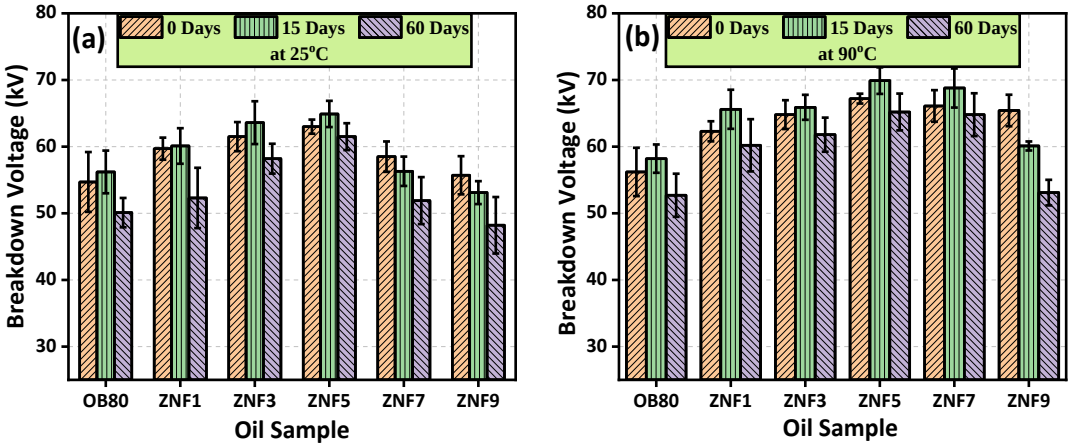

Figure 5.4 BDV values of unaged and aged ZNF samples with respect to OB80 at (a) 25°C and (b) 90°C.

(b) IBDV

OB80: As shown in Figure 5.5, unlike the BDV pattern, the IBDV values followed a different trend for new and aged OB80 samples. A continuous decrease was reported in the IBDV values

of OB80 samples as the samples were aged. The IBDV of aged OB80 dropped from 75.5 kV corresponding to new sample to 73.2 kV and 70.1 kV after 15 and 60 days of ageing, respectively.

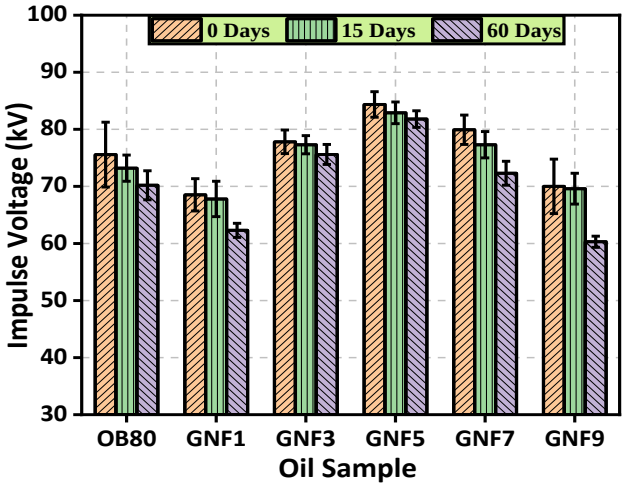

Figure 5.5 IBDV values of unaged as well as aged GNF samples with respect to OB80 samples.

GNF: In terms of Impulse BDV as shown in Figure 5.5, the IBDV of aged GNF samples follows the same pattern as that of aged OB80 samples. However, when compared to the base oil blend, OB80, the GNF samples with lower concentration of GO nanoparticles show a comparatively lesser decrease in the IBDV values even after 60 days of ageing. But, at higher concentrations corresponding to GNF7 and GNF9, the decrease in the IBDV values is even greater than the decrease in OB80 sample.

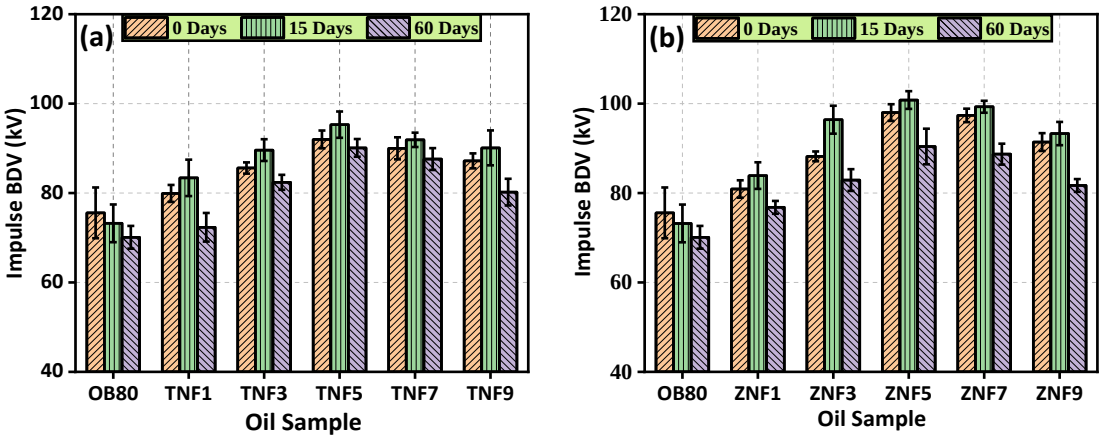

Figure 5.6 IBDV values (a) unaged and aged TNF values, (b) unaged and aged ZNF values.

TNF: The IBDV of TNF samples is shown in Figure 5.6a. These IBDV values follow a similar trend as that of the BDV values of NF samples. An increase in the IBDV of TNF samples was

recorded after 15 days of ageing after which an overall decrease is recorded after 60 days of ageing period. However, unlike BDV values, the IBDV values of 60 days aged TNF samples settled down at values closer to the IBDV of new unaged TNF samples. The peak value of IBDV of aged TNF samples was reported for TNF5 which was 95.3 kV and 90.1 after 15 and 60 days of ageing respectively.

ZNF: The IBDV values of unaged and aged ZNF samples are shown in Figure 5.6b. The IBDV values of aged ZNF samples show a similar type of behavior as shown by the IBDV values of aged TNF samples. IBDV of ZNF samples also increased at the end of 15 days of ageing after which the values started to decrease and settled down at much lower values after 60 days of ageing as compared to the new unaged ZNF samples. The peak IBDV values for aged ZNF samples were recorded for ZNF5 samples which were 100.8 kV and 90.4 kV after 15 days and 60 days of ageing.

(c) Relative Permittivity and Dissipation Factor

OB80: Figure 5.7 shows the relative permittivity and dissipation factor values of OB80 and GNF samples at 25°C and 90°C. The relative permittivity of OB80 samples decreased with the ageing process at both temperature values. At 25°C, the relative permittivity of new OB80 sample was measured to be 1.9 which decreased to 1.8 after 15 days of ageing and further to 1.5 after 60 days of ageing. At 90°C, the relative permittivity of new OB80 sample was 2.3 which decreased to 2.1 after 15 days of ageing and further to 1.8 after 60 days of ageing period. The overall permittivity value of unaged as well aged OB80 was higher at 90°C when compared to the permittivity at 25°C. At 25°C, the dissipation factor of unaged OB80 was recorded to be 0.08 which increased to 0.14 after 15 days of ageing and further to 0.32 after 60 days of ageing. Therefore, a considerable increase in the dissipation factor of base oil sample was noticed. However, this increase in dissipation factor was lower when measured at 90°C where the unaged OB80 had a dissipation factor of 0.15, the 15 days aged OB80 had a dissipation factor of 0.16 and 60 days aged OB80 had a dissipation factor of 0.26.

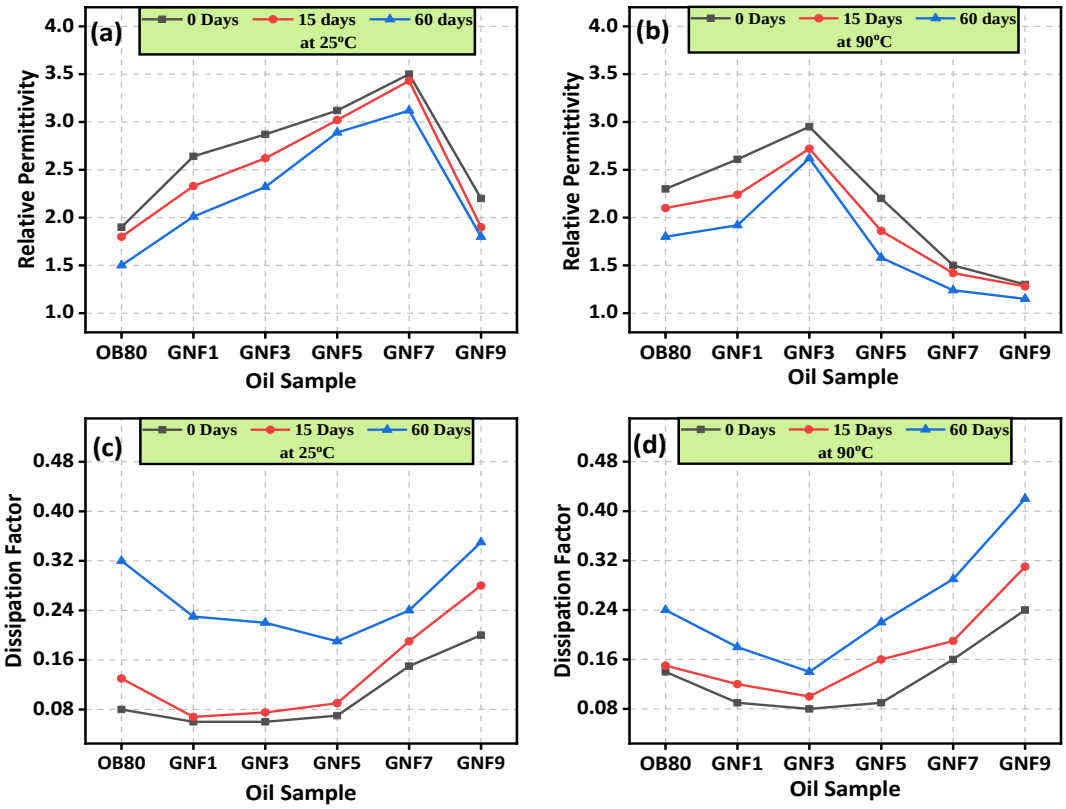

Figure 5.7 (a) and (b) Relative permittivity of unaged and aged GNF samples with respect to OB80 (a) at 25°C and (b) at 90°C, and dissipation factor of unaged and aged GNF samples with respect to OB80 (c) at 25°C and (d) at 90°C.

GNF: As shown in Figure 5.7, the relative permittivity values of GNF also showed a significant decrease with the increase in ageing period almost in a similar way as shown by the OB80 samples. AT 25°C, the peak value for aged GNF samples was measured at concentration level corresponding to the unaged sample, i.e., GNF7. The relative permittivity dropped from 3.5 to 3.43 after an ageing period of 15 days after which it further dropped to 3.12 at the end of 60 days of ageing period. Whereas, at 90°C, the peak relative permittivity values of GNF samples were recorded for GNF3 samples the values of which decreased from 2.95 to 2.72 after 15 days of ageing and further to 2.62 after 60 days of ageing period. The dissipation factor of GNF, when measured at 25°C, showed very negligible decrease till GNF3 in case of unaged samples. However, as the ageing process proceeded, this decrease in the dissipation factor values became higher. After an ageing period of 15 days, the minimum value of dissipation factor was reported for GNF3 sample which was 0.06 whereas, after an ageing period of 60 days, the minimum dissipation factor was reported for GNF5 which was 0.19. At 90°C, the minimum values of dissipation factor were recorded for

GNF3 sample in all the cases of aged as well as unaged samples. These values were 0.08 for unaged sample, 0.1 for 15 days aged sample and 0.14 for 60 days aged sample. The dissipation factor of GNF fluid increased drastically at higher concentration levels at both temperature values in case of unaged as well as aged conditions, thus indicating the poor performance of the nanofluid at higher concentrations.

TNF: As shown in Figure 5.8, the relative permittivity values of TNF samples decreased after undergoing thermal ageing treatment except in the cases of TNF1 and TNF3 samples where the permittivity values spiked up after 15 days of ageing when compared to the respective unaged samples. This increase in the relative permittivity values for TNF1 and TNF3 samples after 15 days of ageing was noticed at both the temperature values. At 25◦C, the highest relative permittivity was recorded for TNF3 as 2.7 for unaged, 3.2 after 15 days of ageing 2.6 after 60 days of ageing. Whereas at 90C, the highest relative permittivity was recorded for TNF3 samples as 2.9 for unaged and 3.2 after 15 days of ageing and for TNF1 as 2.4 after 60 days of ageing period.

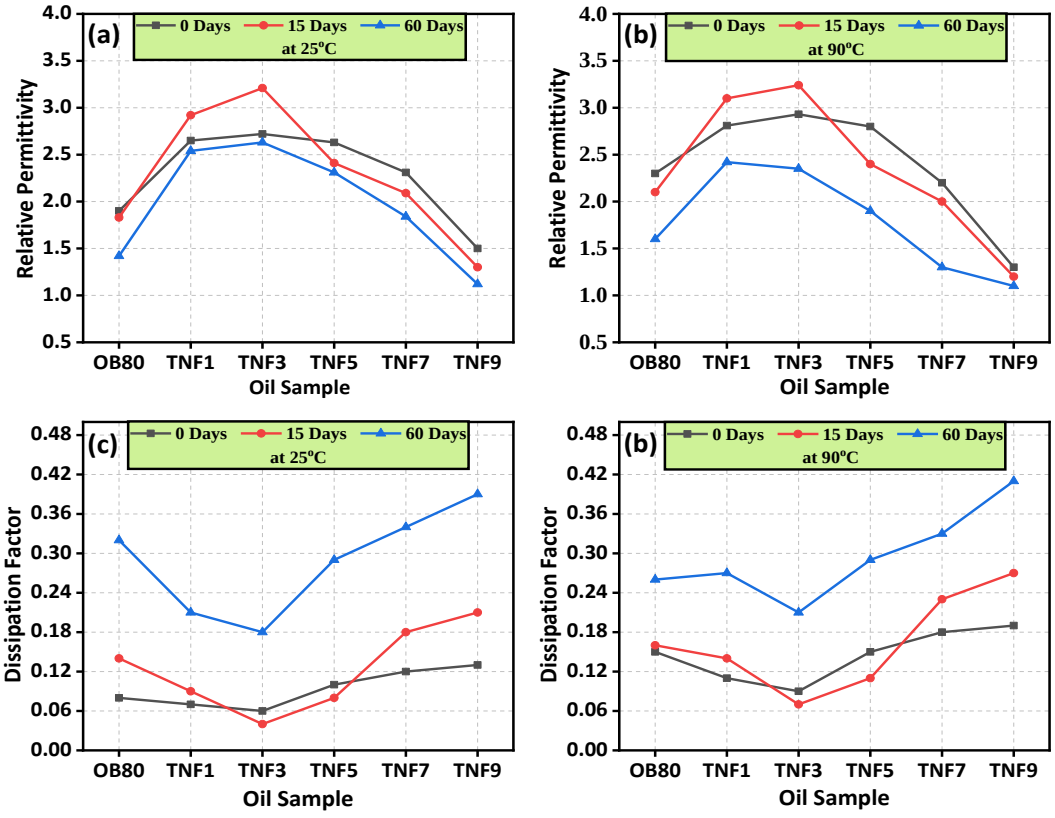

Figure 5.8 (a) and (b) Relative permittivity of unaged and aged TNF samples with respect to OB80 (a) at 25°C and (b) at 90°C, and dissipation factor of unaged and aged TNF samples with respect to OB80 (c) at 25°C and (d) at 90°C.

The dissipation factor values of TNF samples showed an interesting pattern. Whereas at both the temperature values, the minimum recorded dissipation factor was corresponding to the TNF3 sample, however, after 15 days of ageing, the dissipation factor of TNF3 samples further decreased below the values of unaged TNF3 sample. The minimum values recorded were 0.06 for unaged TNF3, 0.04 for 15 days aged TNF3 and 0.18 for 60 days aged TNF3 at 25°C, and 0.09 for unaged TNF3, 0.07 for 15 days aged TNF3 and 0.21 for 60 days aged TNF3 samples. The increase in the dissipation factor values of TNF samples with higher concentrations after hitting the peak minimum was reported to be much higher in aged samples when compared to the unaged samples.

ZNF: The ZNF samples also followed the trend of increasing permittivity values up to certain concentration limit as can be seen in Figure 5.9. At both temperatures, the maximum permittivity was attained for ZNF5 for each unaged and aged sample. The peak permittivity at 25°C of unaged ZNF5 was measured to be 2.9 which dropped to 2.6 after 15 days of ageing and further to 2.4 after 60 days of ageing. At 90°C, the peak permittivity value was measured to be 2.9 for unaged ZNF5,

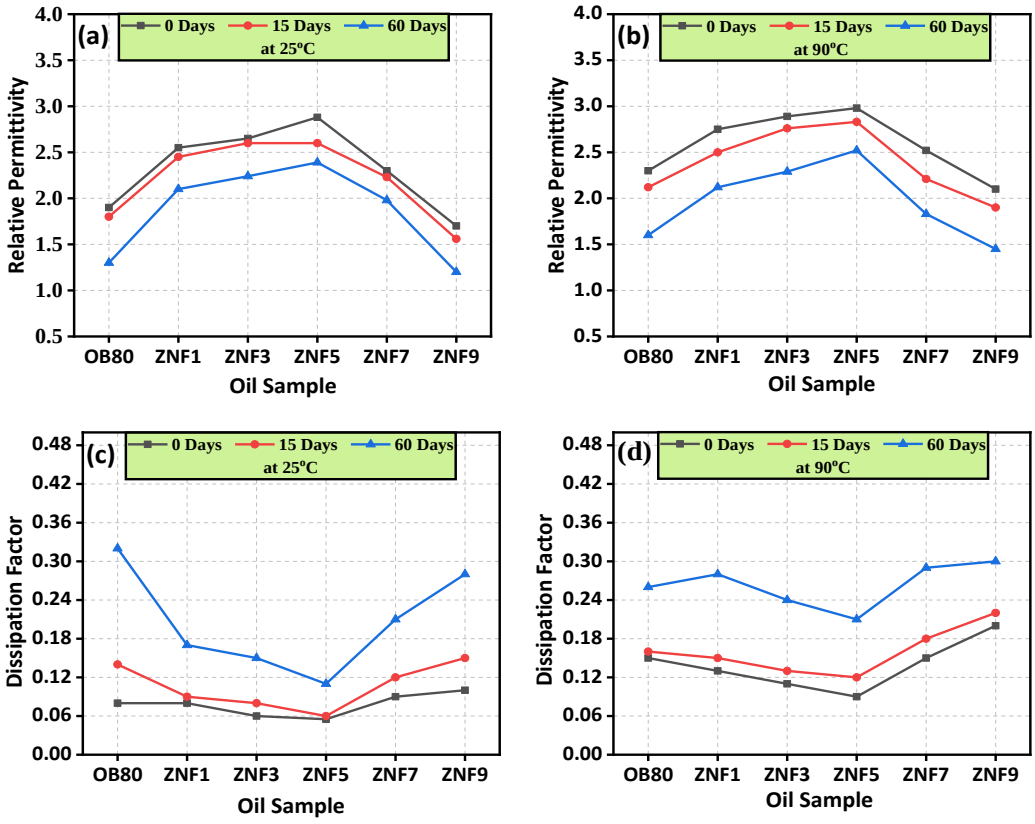

Figure 5.9 (a) and (b) Relative permittivity of unaged and aged ZNF samples with respect to OB80 (a) at 25°C and (b) at 90°C, and dissipation factor of unaged and aged ZNF samples with respect to OB80 (c) at 25°C and (d) at 90°C.

2.8 for 15 days aged ZNF5 and 2.5 for 60 days aged ZNF5 sample. Unlike TNF samples, no sudden increase in the permittivity values of 15 days aged ZNF samples was recorded.

The dissipation factor values of ZNF fluid followed an expected pattern of increased values with the corresponding increase in ageing period. At both temperature values, the minimum peak values were obtained for ZNF5 sample. These values were recorded to be 0.05 for unaged sample, 0.06 for 15 days aged sample and 0.11 for 60 days aged sample at 25°C whereas at 90°C, these values were 0.09 for unaged sample, 0.12 for 15 days aged sample and 0.21 for 60 days aged sample. In all the cases, the dissipation factor values increased significantly at higher concentration levels after hitting the peak minimum.

5.1.2 Physio-thermal Properties of Aged Nanofluids

(a) Viscosity

OB80: The viscosity of the base oil-blend OB80 increases significantly with the corresponding increase in the ageing period as can be seen in Figure 5.10. When compared to the increase in the viscosities of other nanofluids, OB80 showed relatively highest increase in its viscosity. In unaged conditions the viscosity of OB80 at 25°C was 208 mPa-s which increased to 217 mPa-s after 15 days of ageing and further to 245 mPa-s after 60 days of ageing. At the temperature of 90°C, the recorded viscosity values were 32 mPa-s for unaged OB80, 34 mPa-s for 15 days aged OB80 and 39 mPa-s for 60 days aged OB80.

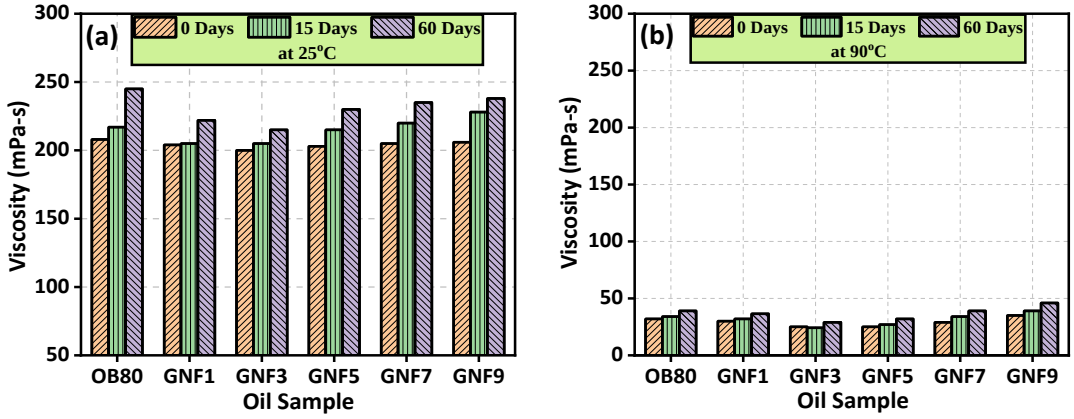

Figure 5.10 Viscosity of GNF samples with respect to OB80 (a) at 25°C and (b) 90°C.

GNF: As shown in Figure 5.10, the viscosity values of GNF samples remained almost constant

at every concentration level except a very minute dip in case of GNF3 sample at both the temperatures. However, aged GNF samples showed comparatively higher changes in their viscosity values. At 25°C, the viscosity of unaged GNF3 was recorded to be 200 mPa-s which increased slightly to 205 mPa-s after 15 days of ageing and further to 215 mPa-s after 60 days of ageing period. At 90°C, these values were recorded to be 25 mPa-s for unaged GNF3, 24.2 mPa-s for 15 days aged GNF3 and 29 mPa-s for 60 days aged GNF3. The interesting point to be noticed is the slight dip in viscosity of GNF3 at 90°C after 15 days of ageing where the viscosity drops slightly below the viscosity value of unaged GNF3 sample.

TNF: Like GNF, the viscosity of TNF samples also showed a decrease up to a particular concentration level as shown in Figure 5.11. At both temperature values, the viscosity kept decreasing up to the concentration level corresponding to TNF5 sample for which the minimum viscosities were recorded at 25°C as well as 90°C. Also, the increase in viscosity after ageing periods was lower in TNF5 as compared to other samples. At 25°C, the viscosity of unaged TNF5 was recorded to 185 mPa-s, 190 mPa-s after 15 days of ageing and 215 mPa-s after 60 days of ageing. On the other hand, at 90°C, the values of viscosities were 20 mPa-s for unaged samples, 23 mPa-s for 15 days aged samples and 25 mPa-s for 60 days aged samples.

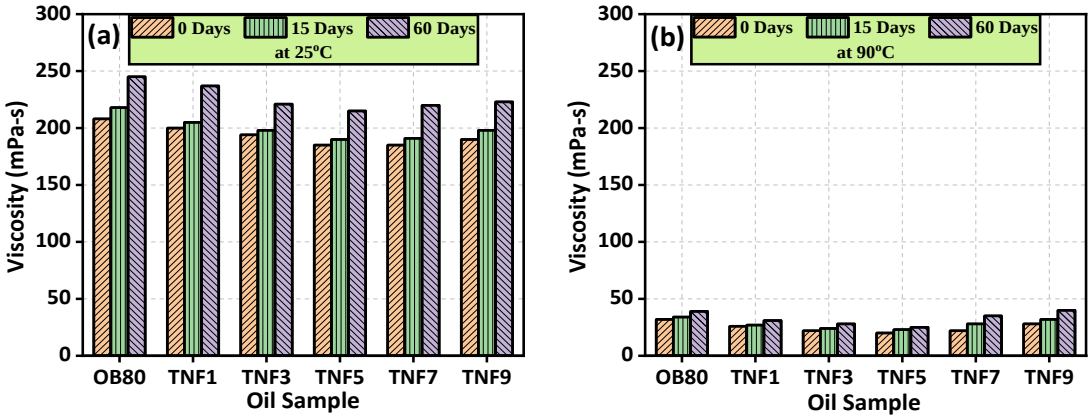

Figure 5.11 Viscosity of TNF samples with respect to OB80 (a) at 25°C and (b) 90°C.

ZNF: Unlike any other fluid, ZNF samples showed a totally different trend for their viscosity values as can be seen in Figure 5.12. The viscosity of ZNF samples kept on increasing with the increase in concentration level at both temperature values. After the ageing period, the viscosity of respective samples increased considerably. However, the increase in the viscosity of aged

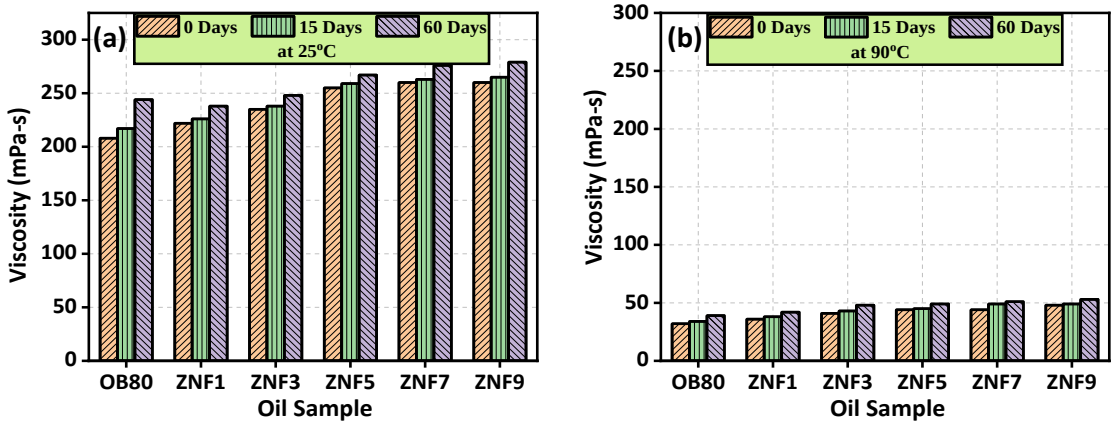

Figure 5.12 Viscosity of ZNF samples with respect to OB80 (a) at 25°C and (b) 90°C.

samples when measured at 90°C was higher than the increase in viscosity of aged samples when measured at 25°C.

(b) Inter-facial Tension (IFT)

OB80: The IFT values of OB80 are plotted in Figure 5.13. It can be seen that the IFT values of OB80 sample decreased with the increase in the ageing period. The IFT value of unaged OB80 was measured to be 50 mNm^{-1}, 48.1 mNm^{-1} for 15 days aged sample and 40 mNm^{-1} for 60 days aged sample as shown in Figure 5.11. All these values fall within the acceptable limits for IFT parameter for any transformer dielectric fluid.

GNF: As shown in Figure 5.13, addition of GO nanoparticles led to an increase in the IFT of GNF samples up to a particular concentration level. The IFT of unaged as well as aged GNF

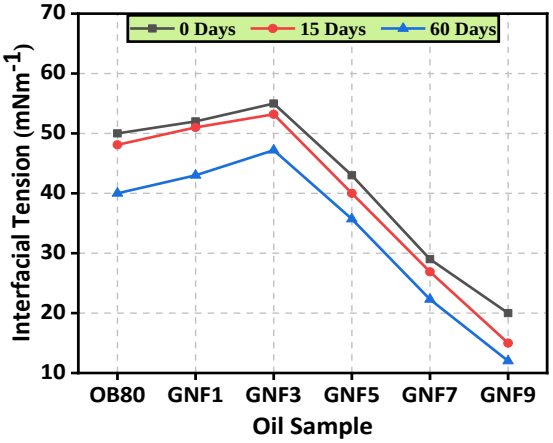

Figure 5.13 IFT values of GNF samples with respect to OB80.

samples increased up to the concentration limit corresponding to the GNF3 sample after which the IFT dropped drastically. The unaged GNF3 sample had an IFT value of 55 mNm^{-1}, 53.2 mNm^{-1} for 15 days aged GNF3 and 47.2 mNm^{-1} for 60 days aged GNF3 sample.

TNF: The IFT values of TNF samples are shown in Figure 5.14a. These values also increased up to a particular concentration level, after which the IFT values started to decrease. However, the IFT values hit the maximum peak at different concentration levels for unaged and aged TNF samples. The maximum IFT for unaged sample was achieved for TNF3 to be 57 mNm^{-1} whereas for 15 days and 60 days aged TNF samples, the maximum values were recorded for TNF1 to be 57 mNm^{-1} and 49 mNm^{-1}, respectively. Also, the IFT value of 15 days aged TNF1 increased to a value slightly higher than the unaged TNF1 sample.

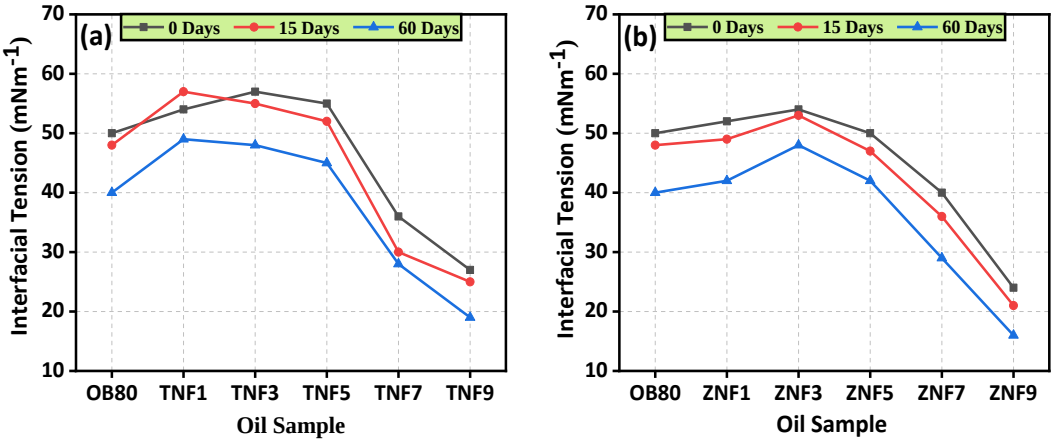

Figure 5.14 IFT values of (a) TNF and (b) ZNF samples with respect to OB80.

ZNF: The IFT values of ZNF samples are shown in Figure 5.14b. In case of ZNF fluids, the IFT values of unaged as well as aged samples kept on increasing up to the concentration level corresponding to ZNF3 sample after which the IFT values started to decrease sharply. The maximum peak was hit for ZNF3 sample in case of all the unaged as well as aged samples. The IFT values measured for ZNF3 samples were recorder to be 54 mNm^{-1} for unaged sample, 53 mNm^{-1} for 15 days aged sample and 48 mNm^{-1} for 60 days aged sample.

(c) Flash Point

OB80: It can be seen in Figure 5.15 that the flash point of the base oil-blend decreased with the increase in ageing period. The flash point of unaged OB80 was reported to be 220°C which decreased to 215°C after an ageing period of 15 days and further to 190°C after an ageing period of 60 days.

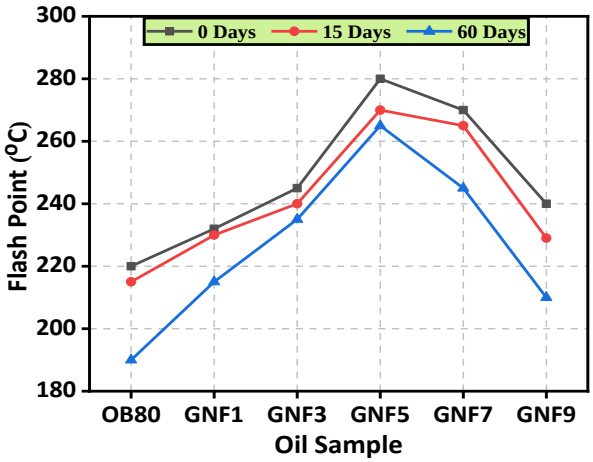

Figure 5.15 Flash point values of GNF samples with respect to OB80 samples.

GNF: The flash point values of GNF are shown in Figure 5.15. These values increased with the increase in GO nanoparticles till the values reach a maximum in the case of GNF5 sample. With the further increase in concentration, the flash point starts to decease again. This peak value was achieved for GNF5 sample at every stage of ageing period. For unaged GNF5, the maximum value of flash point was recorded at 280°C which decreased to 270°C after 15 days of ageing and further to 265°C after 60 days of ageing. The interesting thing to note is that the reduction in the flash point of aged GNF samples at peak values is much lower than that in the case of base oil blend OB80.

TNF: In case of TNF samples, the flash point values followed almost a similar pattern as shown by the GNF samples as can be seen in the Figure 5.16a. The flash point of unaged as well as aged TNF samples increased up to the concentration level corresponding to the TNF5 sample after which the flash point values decreased with the increase in concentration levels. The maximum values recorded in case of TNF5 samples were measured to be 269°C for unaged TNF5, 263°C for

15 days aged TNF5 and 240°C for 60 days aged TNF5.

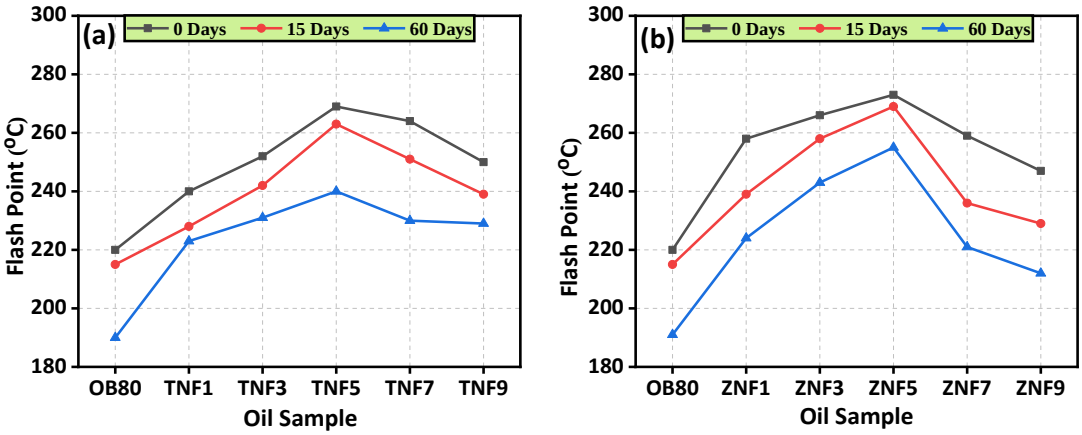

Figure 5.16 Flash point values of (a) TNF samples and (b) ZNF samples with respect to OB80 samples.

ZNF: A similar trend of flash point values can be seen for ZNF samples in Figure 5.16b. The Flash point values of ZNF samples increased during the ageing conditions up to the concentration level corresponding to ZNF5 sample after which the values started to decease again. The peak values recorded in case of ZNF5 samples were 273°C for unaged.

5.2 CHAPTER SUMMARY

In this chapter, the synthesized nanofluids have been subjected to accelerated thermal ageing process. The temperature value throughout the ageing has been set to 130°C and two samples per each nanofluid sample have been studied – one after 15 days of ageing and another after 60 days of ageing. In all the three nanofluids, i.e., GNF, TNF and ZNF, the ac BDV is seen to be increased slightly at the end of 15 days of ageing whereas after 60 days of ageing the BDV decreases considerably. However, in case of GNF and TNF samples, the increase in the BDV of samples after 15 days of ageing is reported only up to nanoparticle concentration level of 0.005 g/L (GNF5 and TNF5) when measured at both 25°C and 90°C except for the TNF samples at 90°C for which the BDV was increased after 15 days of ageing for every concentration level. after which the BDV decreased directly with respect to the increase in the ageing process. For ZNF samples, the increase in BDV after 15 days of ageing could be seen up to ZNF5 sample at 25°C and ZNF7 sample at 90°C. When measured at 25°C, the IBDV of GNF samples keeps on decreasing right from the

beginning of the ageing process where as the IBDV of aged TNF and ZNF samples follow a similar trend as shown by the BDV values. However, the rate of decrease in the BDV and IBDV values of aged nanofluid samples is lower than the rate of decrease in the BDV and IBDV values of base oil blend. Thus, directly indicates to the superior dielectric strength of synthesized nanofluids even after subjected to extreme ageing conditions. Other dielectric parameters like relative permittivity and dissipation factor also keep decreasing with the increase in ageing process in case of GNF and ZNF samples, whereas in case of TNF samples, these parameters show slight enhancement at the end of 15 days of ageing after which the decrease in these parameters could be seen.

Viscosity of all the nanofluids increases with the increase in the ageing process. This is expected due to the addition of residual products as a result of the thermal stress during ageing. However, ZNF samples shows lowest rate of increase in the viscosity as compared to the GNF and TNF samples at a particular concentration level. Interfacial tension and flash points of these nanofluids also decrease considerably with the ageing period. However, the peak values of these parameters after ageing are achieved for the same concentration levels corresponding to the samples having peak values for these parameters before ageing.

CHAPTER 6

ANALYSIS OF AGEING EFFECTS ON PREPARED SOLID INSULATION FOR TRANSFORMERS

DURING practical conditions, the solid insulation material like transformer pressboard remains continuously immersed in transformer dielectric oil. While such operating conditions, the dielectric as well as mechanical properties of the impregnated solid insulation materials are greatly affected by the type of the transformer oil used for the impregnation of such solid insulation materials [143]. In this chapter, the effects of synthesized nanofluids on mechanical and dielectric properties of transformer solid insulation are investigated by using various characterization as well as dielectric tests as explained in the following sections. The procedure of synthesis and ageing of these solid insulation samples has already been discussed in chapter 3, section 3.3 along with the basis of their nomenclature.

6.1 EXPERIMENTAL APPROACH

6.1.1 Mechanical Behavior of Solid Insulation

The mechanical behavior of oil impregnated solid insulation was studied using various techniques. XRD was used to analyze the crystallinity of the aged and unaged pressboard samples. SEM (Scanning Electron Microscopy) technique was used to obtain high resolution magnified images of pressboard samples in order to study the structural behavior of solid insulation under different ageing conditions. Both these techniques were used to analyze the deterioration of the solid insulation material over the course of ageing period. To measure the tensile strength, the dumbbell shaped pressboard specimens were cut with the dimensions as 125 mm length and 25 mm breadth as shown in Figure 6.1b and the tensile strength of the impregnated aged and unaged pressboard samples was measured as per the ASTM-D828 [142] specifications as shown in Figure 6.1c and compared with the raw pressboard samples. These techniques helped in understanding the overall mechanical behavior of oil impregnated solid insulation system.

6.1.2 Dielectric Behavior of Solid Insulation

AC Breakdown Voltages (BDV) of unaged and aged solid insulation samples were measured as per the IEC 60243-1 specifications [143] using a BDV test kit having applied step voltage of 2 kV/s. The pressboard samples were sandwiched between two stainless-steel semi-spherical electrodes having radius of 25 mm. A total of seven BDV values were measured for each sample at 25°C and their average was chosen as the final result value. The ac BDV test cell is shown in Figure 6.1a. Relative Permittivity and Dissipation factor of unaged and aged solid insulation samples were measured as per the ASTM D-150 specifications [144] using a three-electrode model in which the solid insulation samples were put between the H.V electrode and the test electrode. The diameter of H.V electrode was 80 mm and the diameter of test electrode was 60 mm whereas the diameter of guard electrode was 78 mm. A total of seven values were measured for each parameter at 25°C and their average values were taken as the result values.

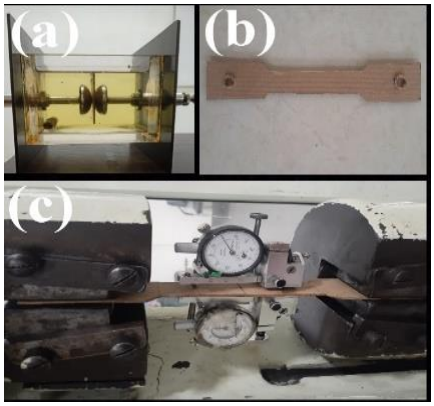

Figure 6.1 (a) BDV test cell with transformer pressboard specimen between the electrodes, (b) dumbbell shaped specimen of pressboard for measuring of tensile strength and (c) tensile strength measuring machine working on the principle of elongation method.

6.2 MECHANICAL EFFECTS ON TRANSFORMER PRESSBOARD

6.2.1 XRD Analysis

The crystalline nature of solid insulation material is the key feature which governs its electrical performance. During the thermal ageing process, the cellulose fibers of solid insulation experience a lot of stress due to which the fibers start to degrade leading to the deterioration of entire insulation

system. The number of atoms along with their structure decide the life of the crystalline material of test samples. A comparative XRD analysis has been used to study the degradation of crystal structure of cellulose fibers in transformer pressboard. The degradation of pressboard is studied by analyzing the relative intensity and the size of their crystalline domains. Both these parameters are responsible for changes in the solid insulation material over a certain period of time under ageing conditions. The sharp peaks and the smooth peaks in the XRD spectra of pressboard samples indicate the presence of both crystalline and amorphous regions in unaged pressboard specimen. However, over a period of time under thermal ageing conditions, the sharp peaks corresponding to the crystalline structure start to distort indicating the degradation of the crystalline structure of both types of specimens. The degradation is studied by comparing the relative crystallinity of the aged samples with that of the unaged samples. Relative crystallinity of pressboard is calculated using Equation 1:

$$C_r = \left\{\frac{I_{max} - I_{min}}{I_{max}}\right\} * 100 \qquad (1)$$

where C_r is the relative crystallinity of the samples, I_{max} and I_{min} are the highest and lowest peaks of the corresponding XRD spectra respectively. The crystallites sizes of different pressboard samples are calculated using Scherrer's Equation 2.

$$D = \frac{k\lambda}{\beta\cos\theta} \qquad (2)$$

where D is the mean crystallite size, k is the shape factor, λ is the wavelength of incident X-ray is the line broadening at half of maximum intensity in radians and θ is the Bragg angle. The XRD

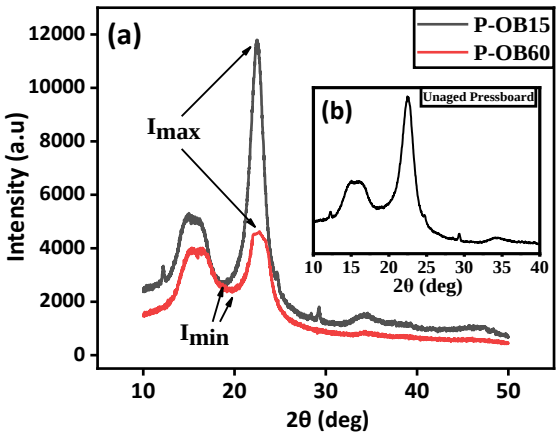

Figure 6.2 XRD pattern of (a) OB impregnated pressboard after 15 and 60 days, (b) raw unaged pressboard.

patterns of various pressboard samples have been explained as below.

P-OB: Figure 6.2a shows the XRD patterns of P-OB15 and P-OB60 samples along with the XRD pattern of a typical raw unaged pressboard sample in Figure 6.2b. Figure 6.3b shows the crystallite size of OB and GNF impregnated pressboard samples (P-OB and P-GNF) after 15 days and 60 days of ageing. Raw pressboard had relative crystallinity of 82.1% and crystallite size of 3.21 nm. The relative crystallinity and the crystallite size value of P-OB15 sample reduced to 68.9% and 2.82 nm respectively, whereas for P-OB60, these values further reduced to just 30.2% and 0.32 nm respectively, indicating the damage of more than half of the pressboard.

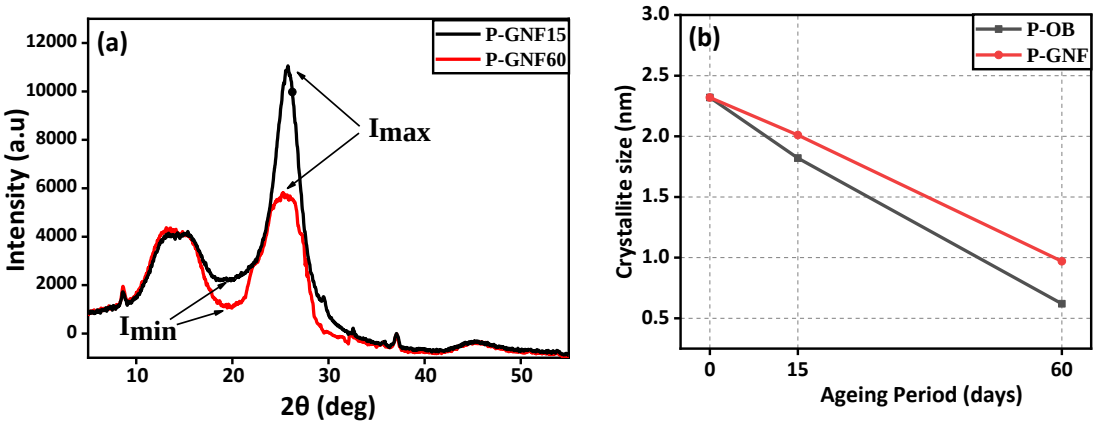

Figure 6.3 (a) XRD pattern of GNF impregnated pressboard after 15 days and 60 days of ageing (b) crystallite size of OB and GNF impregnated pressboard samples after 15 days and 60 days of ageing.

P-GNF: Figure 6.3a shows the XRD patterns of P-GNF15 and P-GNF60 samples. Figure 6.3b shows the crystallite size of P-GNF15 and P-GNF60 samples. It can be seen that there is no significant difference in the XRD patterns of P-GNF15 and P-OB15 which means that, apparently, the deterioration level of P-GNF after 15 days of ageing is similar to that of the P-OB sample.

However, the relative crystallinity as well as the crystallite size of P-GNF15 sample is slightly lower than P-OB15 indicating the slightly worse condition of P-GNF15 sample. However, after 60 days of ageing, P-GNF60 sample showed much better mechanical endurance than the P-OB60 samples aged after 60 days. Relative crystallinity and crystallite size values of P-GNF15 sample were 67.8% and 2.01 nm respectively whereas for P-GNF60, these values were 56.55 and 0.97 nm, which are considerably higher than the P-OB60 sample.

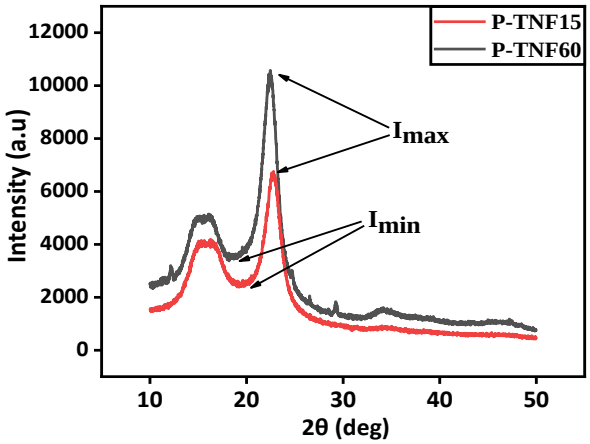

Figure 6.4 XRD pattern of TNF impregnated pressboard after 15 days and 60 days of ageing.

P-TNF: Figure 6.4 shows the XRD patterns of P-TNF15 and P-TNF60 samples. Figure 6.5 shows the crystallite size of P-TNF15 and P-TNF60 samples. The relative crystallinity and crystallite size values of TNF15 samples were calculated to be 80.5% and 2.92 nm respectively whereas for P-TNF60 sample, these values were found to be 62.7% and 1.83 nm. These values were much higher than the values corresponding to the OB impregnated pressboard under similar ageing conditions, in fact, even surpassing the values corresponding to the GO impregnated pressboard samples indicating better mechanical endurance of the P-TNF samples.

P-ZNF: Figure 6.5 shows the crystallite size of P-ZNF15 and P-ZNF60 samples and Figure 6.6 shows the XRD patterns of P-ZNF15 and P-ZNF60 samples. The relative crystallinity and

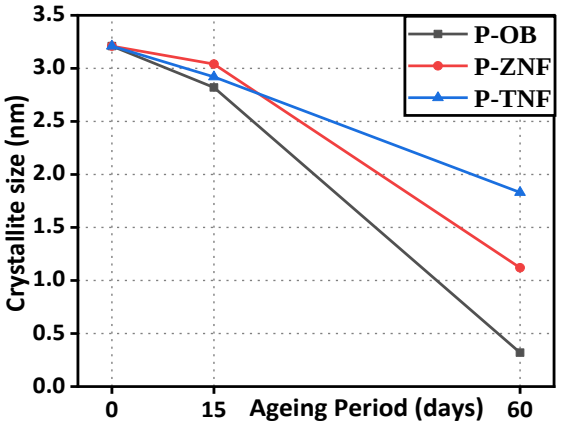

Figure 6.5 Crystallite size of P-TNF and P-GNF samples with respect to P-OB samples after 15 days and 60 days of ageing.

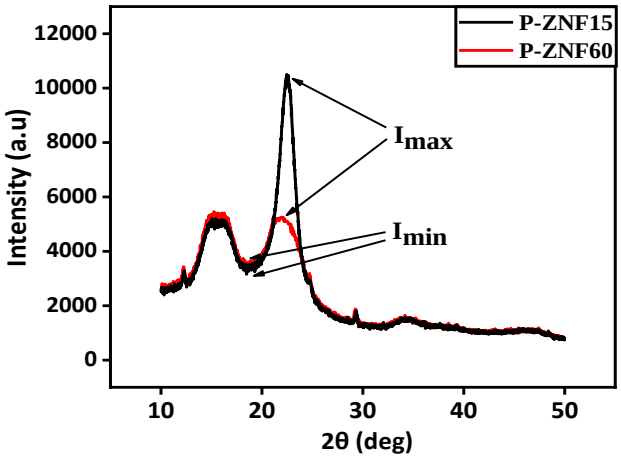

Figure 6.6 XRD pattern of ZNF impregnated pressboard after 15 days and 60 days of ageing.

crystallite size values of ZNF15 samples were calculated to be 77.9% and 3.04 nm respectively, whereas for P-ZNF60 sample, these values were found to be 46.8% and 1.12 nm as are shown in Table 6.1.

Table 6.1 Comparative analysis of the relative crystallinity and crystallite sizes of all the pressboard samples.

PRESSBOARD	UNAGED	AFTER 15 DAYS OF AGEING				AFTER 60 DAYS OF AGEING			
	Raw	P-OB	P-GNF	P-TNF	P-ZNF	P-OB	P-GNF	P-TNF	P-ZNF
Crystallinity (%)	82.1	68.9	67.8	80.5	77.9	30.2	56.5	62.7	46.8
Crystallite size (nm)	3.21	2.82	2.01	2.92	3.04	0.32	0.97	1.83	1.12

6.2.2 Field Emission – Scanning Electron Microscopy

The SEM technique is used to thoroughly investigate the surface of the solid insulation materials. Unaged and aged samples of both materials are compared with the help of SEM magnified images in order to analyze the degree of degradation. Unaged samples of transformer pressboard were magnified at X250, whereas a slightly larger magnification of X350 and X400 were used to study the aged samples of solid insulation in finer details. Figure 6.7 shows the SEM images of unaged raw as well as aged pressboard samples. The average fiber width for each sample is shown in Table 6.2. The disruption of outer layers of cellulosic fibers in every aged pressboard sample can be seen. This disruption of outer surface of fibers leads to an overall reduction of fiber width which further indicates the level of degradation of material. In case of unaged pressboard, average fiber width was 20 µm which decreased for each pressboard sample after thermal stress treatment for 60 days. The average fiber width of P-OB60 is 14.3 µm which is least when compared to that of P-GNF60, P-TNF60 and P-ZNF60 samples which have fiber widths of 19.6 µm, 19.2 µm and 18.1 µm, respectively. This data again falls in line with the data obtained from XRD analysis, confirming that the NF impregnated pressboard samples showed lower structural damage as compared to the OB impregnated pressboard samples in which P-GNF is structurally better as compared to P-TNF and P-ZNF after an ageing period of 60 days.

Table 6.2 Average fiber widths of unaged and 60 days aged pressboard impregnated pressboard samples.

PRESSBOARD	*Unaged*	*P-OB60*	*P-GNF60*	*P-TNF60*	*P-ZNF60*
Fiber width (μm)	20	14.3	19.6	19.2	18.1

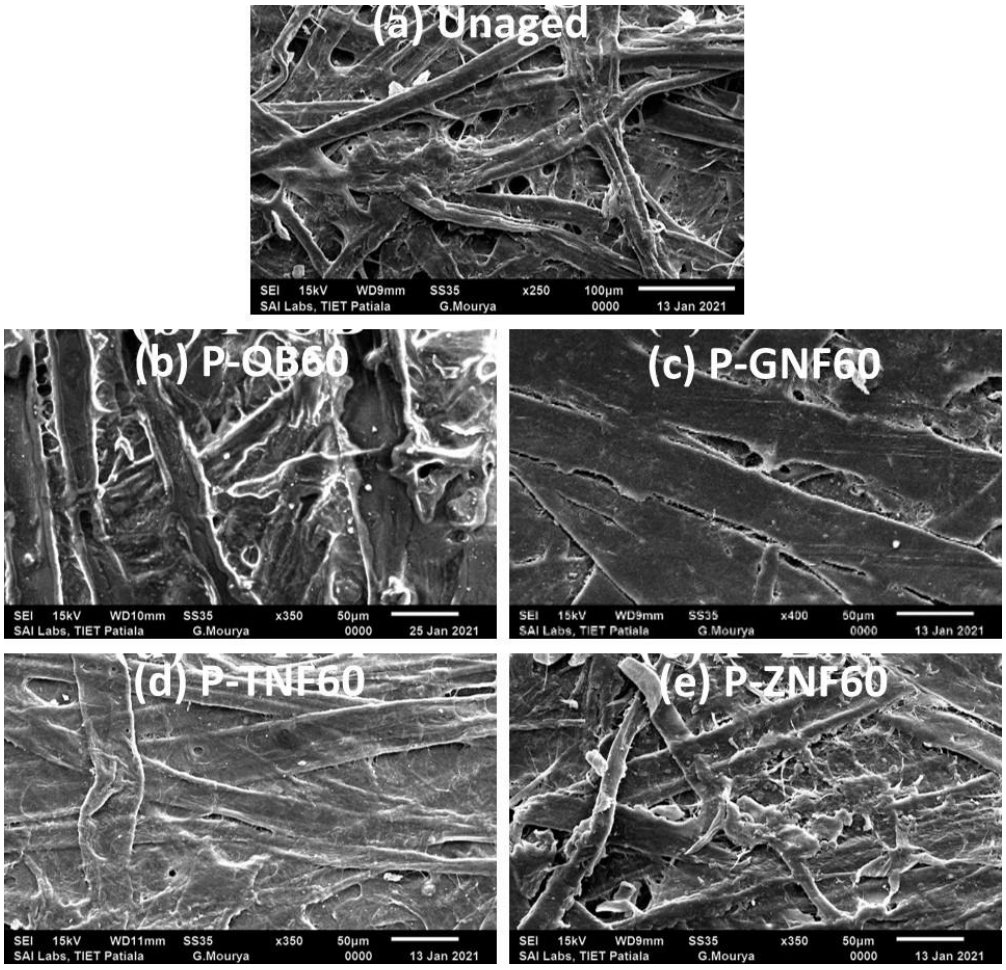

Figure 6.7 SEM images of unaged raw pressboard sample as well as OB and NF impregnated pressboard samples after 60 days of ageing.

6.2.3 Tensile Strength

The mechanical endurance of any solid insulation material is generally defined by its tensile strength. The tensile strength of unaged and aged P-OB and P-NF impregnated pressboard samples was measured using the constant rate of elongation method as per ASTM-D828 specifications

[127]. The tensile strength values of aged and unaged pressboard samples after undergoing different ageing stages have been plotted in Figure 6.8.

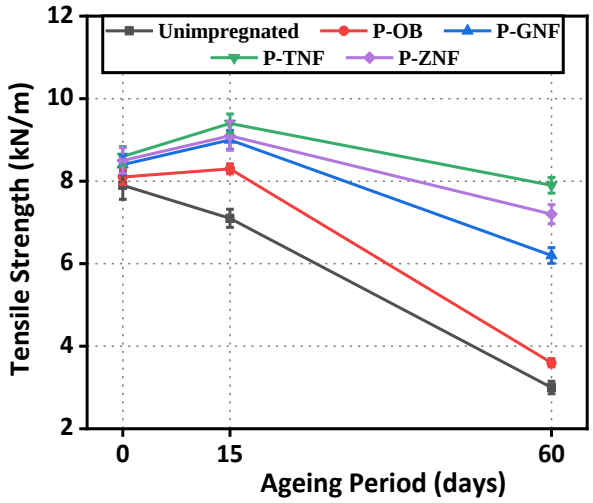

Figure 6.8 Tensile strength of unimpregnated raw pressboard as well as OB and NF impregnated pressboard samples after 15 days and 60 days of ageing.

The tensile strength of unimpregnated pressboard decreases sharply with the increasing ageing period. The unaged unimpregnated pressboard has a tensile strength of 7.9 kN/m and it decreases to 3 kN/m after being aged for 60 days. The cellulose fibers of unimpregnated pressboard act as brittle strands which are easily fractured thus destroying the surface microstructure of the cellulose molecules. However, OB impregnated pressboard as well as NF impregnated pressboard samples showed some increase in their respective tensile strengths after 15 days of ageing period. This slight increase in both types of impregnated pressboard samples may be due to the increase in density of cellulose fibers when subjected to the thermal stress. When pressboard samples are impregnated with the oil, a comparative increase in the values of tensile strength can be seen. This increase is due to the softening of wet cellulosic fibers which now act as elastic threads and thus increasing their density which enhances their mechanical endurance. When compared after aging period of 60 days, the tensile strength of P-GNF was 9 kN/m and 6.2 kN/m after 15 and 60 days of ageing as compared to that of P-OB sample which was 8.2 kN/m and 3.6 kN/m after 15 and 60 days of ageing. Tensile strength of P-TNF samples was 9.3 kN/m and 7.8 kN/m after 15 and 60 days of ageing, respectively, whereas the tensile strength of P-ZNF was 9.1 kN/m and 7.2 kN/m after 15 and 60 days of ageing respectively. Thus, the tensile strength of P-TNF was comparatively highest than that the P-GNF and P-ZNF samples after undergoing same ageing process. This

comparative lower decrease in the deterioration of tensile strength of NF impregnated pressboard is due to the adsorption of GO, TiO_2 and ZnO nanoparticles resulting in the formation of hydrogen bonds with the pressboard cellulose molecules under thermal stress conditions. This increases the interfacial adhesion which bears some part of the tension applied on the cellulose fibers thus increasing the tensile strength of NF impregnated pressboard when compared to the OB impregnated pressboard. This helps in bearing some fraction of the tension applied to the cellulosic fibers due to the increase in interfacial adhesion. Therefore, the decrease in tensile strength of NF impregnated pressboard is lower than that of the OB impregnated pressboard after the ageing period of 60 days.

6.3 DIELECTRIC PROPERTIES OF TRANSFORMER PRESSBOARD

The most important dielectric properties for any insulating material have been studied for both unaged as well as aged types of pressboard samples.

6.3.1 AC Breakdown Voltage

Figure 6.9 shows the ac BDV data of transformer pressboard after different ageing periods. Unaged unimpregnated pressboard showed lower BDV which increased once the pressboard was impregnated by the OB as well as the NF oils. Breakdown voltage of raw unimpregnated pressboard was 37.3 kV which decreased to 34.9 kV after 15 days of aging and further to 28.1 kV after an aging period of 60 days. Ac breakdown voltage of P-GNF was higher than that of the P-OB when measured under similar ageing conditions. Unaged P-GNF had breakdown voltage of 54.4 kV which is comparatively higher than measured value of 48.9 kV in case of unaged P-OB. After aging period of 60 days, P-GNF60 had breakdown voltage of 43.5 kV whereas P-OB60 had breakdown voltage at 40 kV. P-TNF and P-ZNF samples had BDV values of 59 kV and 56.2 kV before ageing, 56.3 kV and 53.2 kV after 15 days of ageing, and 46.1 kV and 48 kV after 60 days of ageing, respectively. These values were considerably higher than the BDV values of P-OB which were 49 kV before ageing, 44.7 kV after 15 days of ageing and 39.9 kV after 60 days of ageing period. This enhancement in the breakdown values of P-GNF is due to the hydrophilic nature of GO nanoparticles. These GO nanoparticles absorb the moisture from the insulation

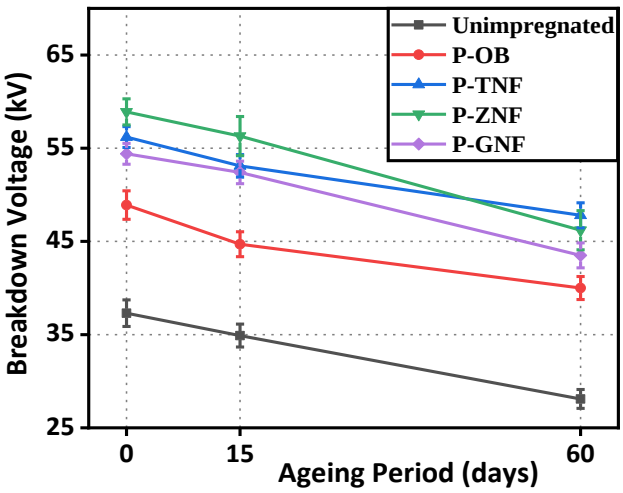

Figure 6.9 BDV of unimpregnated raw pressboard as well as OB and NF impregnated pressboard samples after 15 days and 60 days of ageing.

material and thus increasing its breakdown voltage. Another common factor responsible for the enhancement in the breakdown voltage of NF impregnated material is the increase in the density of cellulose fibers due to the adsorption of GO, TiO_2 and ZnO nanoparticles on their surface during the chain cross-linking under thermal stress. Cellulose fibers have small molecular gaps which are filled with oil in OB impregnated material and with nanoparticles in NF impregnated material. The nanoparticles improve the cellulose chain linking and thus modifying the external structure of the fibers. This leads to a decrease in trap levels and an increase in shallow traps resulting in the non-accumulation of charge. Under thermal stress conditions, the cellulose fibers of NF impregnated material become tightly linked which makes it difficult to destroy its internal structure. This results in the overall higher breakdown voltage in NF impregnated insulation material after going the thermal ageing process.

6.3.2 Relative Permittivity

Relative permittivity or dielectric constant of unimpregnated pressboard after undergoing different ageing periods have been measured at 50 Hz at a temperature of 25°C and plotted in Figure 6.10. Unaged unimpregnated pressboard had relative permittivity of 5.36 which decreased to 4.9 and 4 after 15 and 60 days of ageing respectively. Unaged OB impregnated pressboard showed relative permittivity of 5.78 which decreased to 5.2 and 4.06 after 15 and 60 days of ageing respectively. Unaged P-GNF showed relative permittivity of 6 which decreased to 5.7 and 5 after

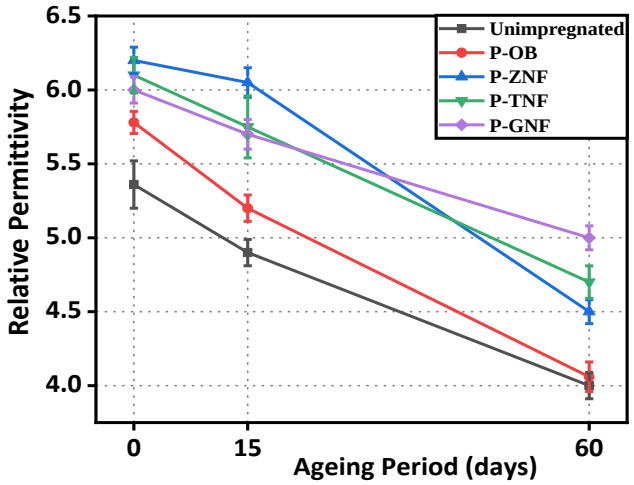

Figure 6.10 Relative permittivity of unimpregnated raw pressboard as well as OB and NF impregnated pressboard samples after 15 days and 60 days of ageing.

15 and 60 days of ageing respectively. P-TNF has relative permittivity of 6.1 before ageing, 5.7 after 15 days of ageing and 4.7 after 60 days of ageing, whereas P-ZNF has relative permittivity of 6.2 before ageing, 6.0 after 15 days of ageing and 4.5 after ageing period of 60 days. It is clear that the relative permittivity of the unimpregnated pressboard is lower than that of the both impregnated pressboard samples under all ageing conditions. However, the relative permittivity of NF impregnated pressboard is more that of the OB impregnated pressboard. This clearly indicates the better dielectric behavior of NF impregnated solid insulation.

6.3.3 Dissipation Factor

For any insulating material, dissipation factor, also called as loss tangent or tan delta, plays a very important role in governing the dielectric behavior of that material. The dissipation factor data plots of both unaged and aged pressboard samples have been plotted in Figure 6.11. Dissipation factor of NF impregnated pressboard is lower than all other samples indicating lowest leakage current through them which further means better dielectric behavior. A direct converse relation can be seen between the dissipation factor and dielectric constant of corresponding pressboard samples. Dissipation factor of P-OB was 0.13 before undergoing the ageing process, 0.17 after 15 days of ageing and 0.25 after undergoing ageing for 60 days. In case of NF impregnated pressboard, P-GNF samples had dissipation factor of 0.11 before ageing, 0.14 after 15 days of ageing and 0.17 after 60 days of ageing. P-TNF had dissipation factor values of 0.08

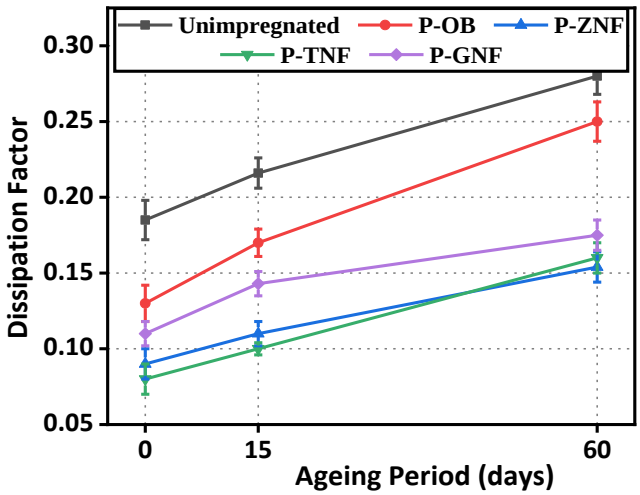

Figure 6.11 Dissipation factor of unimpregnated raw pressboard as well as OB and NF impregnated pressboard samples after 15 days and 60 days of ageing.

before the onset of ageing process, 0.1 after 15 days of ageing and 0.16 after the period of 60 days of ageing, whereas P-ZNF had dissipation factor values of 0.09 before ageing, 0.11 after 15 days of ageing and 0.15 after 60 days of ageing. It is evident, that the dissipation factor of pressboard decreases upon impregnating it with OB which decreases further upon impregnation with the NF.

6.4 MECHANISM OF IMPROVEMENT

Since the transformer pressboard is compositionally cellulosic in nature, the adsorption of nanoparticles like GO, TiO_2 and ZnO along the interface of nanofluid-pressboard insulation system results in the formation of hydrogen bonds with the cellulosic molecules of pressboard under the heating effect of thermal ageing process. This results in the increase in the adhesive forces along the interface which act as a support to the existing mechanical strength of the transformer pressboard. This adhesion is responsible for the absorption of some fraction of the tension faced by the cellulosic fibers of the pressboard. This factor is hugely responsible for the slower rate of deterioration in cellulosic fibers of nanofluid impregnates pressboard when compared the base oil impregnated pressboard after being subjected to ageing conditions as has been shown in the XRD analysis and FE-SEM images of these pressboard samples. This also increases the tensile strength

of nanofluid impregnated pressboard thus resulting in the enhancement of the overall mechanical strength of these pressboard samples [147-149].

One of the most important factors which is responsible for the enhancement of overall dielectric strength of nanofluid impregnated pressboard is the behavior of the Gouy-Chapman-Stern layer (GCS layer). This GCS layer is formed along the interface of the nanofluid and the nanoparticles and behaves like a pathway for the transfer of the charge. This GCS layer is formed due to the bounding of bi-product molecules to the nanoparticles-oil-pressboard interface. These bi-product molecules are produced over a period of time as a result of thermal ageing. The pathway formed by the GCS layer increases the interfacial conductive path resulting in an increased local conductivity. In dielectric nanofluids, this local conduction along the interface increases the shallow trap density within the solid-liquid insulation system. These shallow traps act as the store-houses for the charge carriers. With the increase in ageing period of nanofluids, these shallow traps in solid-liquid insulation increase as compared to the base oil-based insulation system., thus resulting in further enhancement in electron trapping phenomenon. This effectively plays a major in increasing the dielectric strength of nanofluid impregnated pressboard samples [148, 149].

6.4 CHAPTER SUMMARY

In this chapter, the effects of synthesized nanofluids on the transformer pressboard have been studied. The transformer pressboard samples have been impregnated with base oil blend as well as the synthesized nanofluids and two samples from each type of impregnated pressboard are thermally aged – one for a period of 15 days and another for a period of 60 days. The dielectric as well as mechanical properties of these different unaged as well as aged nanofluid impregnated pressboard samples are investigated and compared with the pressboard samples impregnated with the base oil blend. The XRD analysis of aged impregnated pressboard samples shows the decrease in their crystallinity. The crystallite size of each aged impregnated pressboard sample also decreases continuously with the increase in ageing period, thus, indicating the degradation of the crystalline structure of the pressboard. However, when compared with the aged oil blend impregnated pressboard (P-OB), all the nanofluid impregnated pressboard samples (P-OB80, P-GNF, P-TNF and P-ZNF) show considerably much lower levels of degradation in their structures.

After the completion of ageing process, P-TNF shows highest relative crystallinity of 62.7% with highest crystallite size of 1.83 nm followed by the P-GNF and P-ZNF samples. The decrease in fiber widths of the aged pressboard samples is also lowered down significantly by the impregnation by these nanofluids. P-GNF sample shows least deterioration of its fiber lengths followed closely by P-TNF and P-ZNF samples. The tensile test also shows the improved tensile strength of impregnated pressboard samples as compared to that of unimpregnated pressboard. However, P-TNF shows maximum tensile strength followed by P-ZNF and P-GNF after 60 days of thermal ageing.

In terms of dielectric properties, the BDV of impregnated pressboard samples is seen to be higher than the unimpregnated pressboard samples before as well as after ageing. Also, the nanofluid impregnated pressboard samples has better BDV values than the base oil blend impregnated pressboard. Before ageing, P-ZNF has the maximum BDV followed by P-TNF whereas P-GNF shows the lowest BDV. After ageing, this sequence changes to P-TNF having maximum BDV followed by P-ZNF and P-GNF samples. However, in case of relative permittivity, P-ZNF possesses maximum dielectric constant before ageing but lowest dielectric constant after 60 days of ageing. P-GNF sample has maximum dielectric constant after 60 days of ageing period.

CHAPTER 7

TRANSFORMER DESIGN CONSIDERATIONS

THE design of mineral oil filled distribution as well as power transformers has been studied in great details over the period of last century. More and more compact and cost-efficient models have been developed and put into application with time. However, the studies on the design considerations of vegetable oil filled transformers have been started recently.

7.1 CONSTRUCTIONAL DESIGN ANALYSIS

A lot of focus is being kept on developing the transformer models which are compatible with vegetable oil from the design perspective. Researchers have also started to focus on the design models which can be equally compatible with the both mineral as well as vegetable oil for a particular transformer. Since, the oil-blend used as base solvent in this research, i.e., OB80 has 80% ester oil content which is much greater than the content of the mineral oil in the blend, it can be safely assumed that the studies made till date on the design considerations of ester oil filled transformer can be related to the OB80 filled transformer as well. However, no such data is available when it comes to the design considerations of transformers filled with vegetable oil based nanofluids. This chapter focuses on analyzing the necessity of making required changes, if any, in the transformers due to the usage of synthesized ester oil based nanofluids in order to make them more compatible with the applications of the nanofluids.

The changes in the values of dielectric properties of natural ester oil based blend upon the dispersion of nanofluids can necessitate some modifications in the dielectric design of transformers. The various factors which have to be considered for analyzing the dielectric design considerations of any transformers are:

Stressed Oil Volume

Impulse Breakdown Voltage

Dielectric Stress Distribution

Hot-spot temperatures

The breakdown strength of any transformer oil is governed by a theory called as Stressed Oil Volume (SOV) theory. According to SOV theory, the breakdown strength of any liquid insulator is determined by the 'weak link' which defines the track having the maximum possible impurity present in the insulator. Thus, the portion under maximum stress and the volume of the oil in that portion collectively constitute the weak link which governs the dielectric breakdown strength of the transformer oil. This theory relates the breakdown strength as inversely proportional to the volume of oil under stress as can be explained by the Equation 7.1 [150].

$$E = \frac{17.9}{(SOV)^{0.137}} \frac{kV}{mm} \ (rms) \qquad 7.1$$

where the units for SOV are taken in cm^3. The higher BDV of NF samples at respective concentrations of nanoparticles thus indicates to the lower stressed oil volume. Therefore, at same conditions for lower acceptable BDV values, the insulation gap in the transformers can be reduced. Moreover, using the Equation 7.1, the design can be optimized by relating the calculated stress which can be kept slightly lower than the values of dielectric strength (E) for precautionary reasons.

In insulation designing of any oil-filled transformer, the critical areas that exist are solid insulation, liquid insulation and the stress distribution through the interface between the solid and liquid insulation. The insulation structure of a basic oil-filled transformer is shown in Figure 7.1. Due to the larger distance of HV winding from the core, it can be assumed that the entire winding/paper arrangement behaves as series connected parallel plate capacitors. The stress distributes capacitively having an inverse dependency on the permittivity of the insulating materials [151].

Stress in material 1, $E_1 = \frac{v}{Z * \varepsilon_1}$ 7.2

Stress in material 2. $E_2 = \frac{v}{Z * \varepsilon_2}$ 7.3

where, $Z = \left(\frac{d_1}{\varepsilon_1} + \frac{d_2}{\varepsilon_2}\right)$ 7.4

where v is the potential across HV winding with respect to the core, ϵ_1 and ϵ_2 are the permittivity values of HV and LV windings respectively whereas d_1 and d_2 are the thickness values of HV and LV windings respectively.

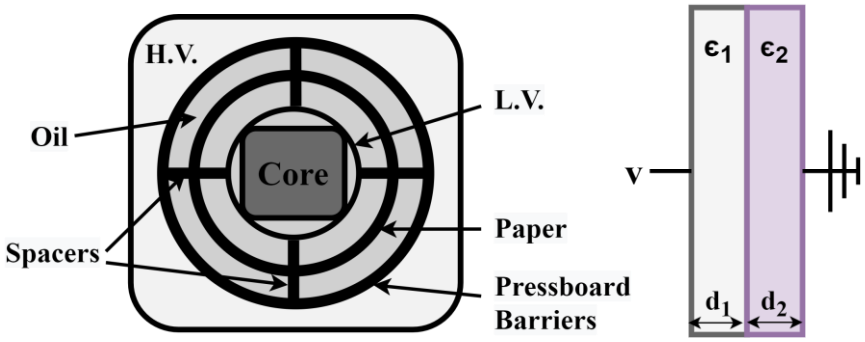

Figure 7.1 Basic insulation structure of a transformer.

An insulation structure is the most important factor governing the design of any transformer. The electric stress distribution along the interface of the solid/liquid insulation decides the design clearance of a transformer. This electric stress distribution can be analyzed by comparing the permittivity values of liquid and solid insulation materials [151]. If the permittivity values of liquid and solid insulation material lie closer to one another, the ratio of these values will be closer to unity. A ratio closer to unity means a more uniform dielectric stress across the entire insulation structure, thus giving the optimum solid/liquid insulation combination in terms of electric stress distribution. This reduces the chances of insulation failure as well as gives way to more design clearance in a transformer. The permittivity ratios of liquid to solid insulation materials have been calculated as shown in Table 7.1. The permittivity values of liquid and solid insulation structures have been calculated at the end of ageing period as discussed in chapters 5 and 6 in order to make calculations during that period when the insulation structure of a transformer faces maximum stress. The ratios are closer to unity in case of nanofluid based insulations when compared to base oil blend based insulation. However, the liquid/solid permittivity ratio in case of ZNF based insulation structure is closest to unity followed by the GNF and the TNF based insulation structures. Thus, ZNF/P-ZNF combination serves as best insulation structure in terms of increasing the temperature threshold and allowing better design compactness.

Table 7.1 Permittivity ratios of liquid to solid insulation material.

Relative permittivity of liquid oil samples		***Relative permittivity of solid pressboard samples***		***Ratio of respective liquid to solid insulations***	
ϵ_{OB80}	1.6	$\epsilon_{P\text{-}OB80}$	4.1	$\epsilon_{OB80} : \epsilon_{P\text{-}OB80}$	0.39
ϵ_{GNF}	2.6	$\epsilon_{P\text{-}GNF}$	5	$\epsilon_{GNF} : \epsilon_{P\text{-}GNF}$	0.52
ϵ_{TNF}	2.35	$\epsilon_{P\text{-}TNF}$	4.7	$\epsilon_{TNF} : \epsilon_{P\text{-}TNF}$	0.51
ϵ_{ZNF}	2.52	$\epsilon_{P\text{-}ZNF}$	4.5	$\epsilon_{ZNF} : \epsilon_{P\text{-}ZNF}$	0.56

For a typical core type transformer, the temperature difference between the center of the core and the outer surface at a distance of x from the center is given by [152],

$$\theta = \frac{q\rho x^2}{2} \text{ ℃} \qquad 7.5$$

Where q is the heat produced per unit volume in W/m^3 and ρ is the thermal resistivity of the core along the direction of heat flow in Ωm.

From Equation 7.5, we have,

$$x^2 = \frac{2\theta}{q\rho} \qquad 7.6$$

Taking q and ρ as constant values for a particular material based transformer core, Equation 7.6 can be written as,

$$x^2 = k\theta \qquad 7.7$$

where, $k = \frac{2}{q\rho}$

Above equation becomes,

$$x = k_1\sqrt{\theta} \qquad 7.8$$

where, $k_1 = \sqrt{k}$

Since, the temperature in a transformer is directly dependent on the dielectric stress and the dielectric stress reduces with the increase in the ratio of liquid to solid insulation permittivity values, the temperature also reduces with it [149]. Thus, θ can be replaced by the term $\frac{1}{\epsilon_{liquid} : \epsilon_{solid}}$ after introducing a new constant of proportionality k´. Thus, the Equation 7.8 becomes,

$$x = k' \sqrt{\frac{1}{\epsilon_{liquid} : \epsilon_{solid}}} \qquad 7.9$$

Putting the values of permittivity ratios of liquid to solid insulation for each oil sample separately in Equation 7.9, we get,

For base oil, OB80, $x_{OB80} = k' \sqrt{\frac{1}{\epsilon_{OB} : \epsilon_{P-OB}}} = k' \sqrt{(1/0.39)} = 1.60k'$ 7.10

For GNF sample, $x_{GNF} = k' \sqrt{\frac{1}{\epsilon_{GNF} : \epsilon_{P-GNF}}} = k' \sqrt{(1/0.52)} = 1.37k'$ 7.11

For TNF sample, $x_{TNF} = k' \sqrt{\frac{1}{\epsilon_{TNF} : \epsilon_{P-TNF}}} = k' \sqrt{(1/0.51)} = 1.40k'$ 7.12

For ZNF sample, $x_{ZNF} = k' \sqrt{\frac{1}{\epsilon_{ZNF} : \epsilon_{P-ZNF}}} = k' \sqrt{(1/0.56)} = 1.33k'$ 7.13

Thus, from the calculations, it can be analyzed that the distance from the center of the core can be reduced by 14.3% in case of GNF filled transformer, 12.5% in case of TNF filled transformer and 16.8% in case of ZNF filed transformer when compared to OB80 filled transformer for same temperature values.

Figure 7.2 shows the basic structure of assembled iron stampings of a core type transformer. As is the customary in high voltage transformers, the circular coils are preferred over the rectangular coils as well as the square cruciform sectioned core is preferred over the rectangular one due to the allowance of greater cross section area which means more iron within the coil.

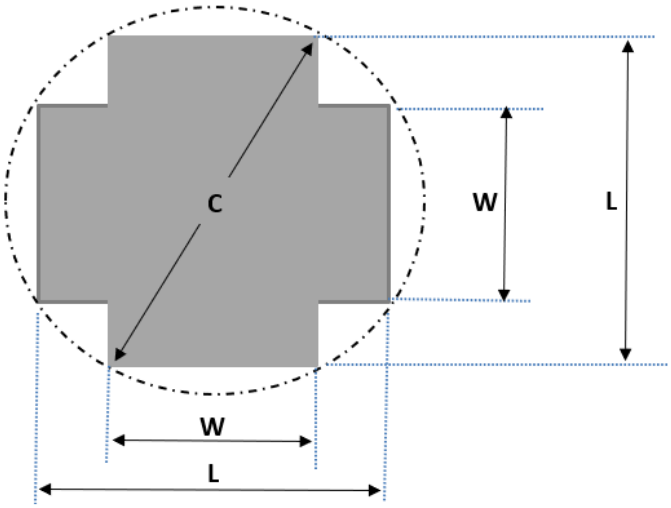

Figure 7.2. Iron stampings of a typical core type transformer.

The gross area of cross section is given by $2WL - W^2$ [153]. For constant diameter C, the largest core cross section can be obtained by differentiating it and equating the result to zero as,

$$\frac{d}{dW}(WL - W^2) = 0 \qquad 7.14$$

$$2\left(W\frac{dL}{dW} + L\right) - 2W = 0 \qquad 7.15$$

Also, due to Pythagorean rule, $W^2 + L^2 = C^2$ 7.16

Differentiating Equation 7.16, we get,

$$2WdW + 2LdL = 0 \qquad 7.17$$

$$2LdL = -2WdW \qquad 7.18$$

$$\frac{dL}{dW} = -\frac{W}{L} \qquad 7.19$$

Putting this in Equation 7.15, we get,

$$2\left[W\left(-\frac{W}{L}\right) + L\right] - 2W = 0 \qquad 7.20$$

$$-\frac{W^2}{L} + L - W = 0 \qquad 7.21$$

$$\frac{W^2}{L} - L + W = 0 \qquad 7.22$$

$$W^2 - L^2 + WL = 0 \qquad 7.23$$

Solving the Equation 7.23 in terms of L, we get,

$$W = 0.618L \qquad 7.24$$

Putting this in Equation 7.16 and solving for C in terms of L, we get,

$$(0.618L)^2 + L^2 = C^2 \qquad 7.25$$

$$1.382L^2 = C^2 \qquad 7.26$$

$$C = 1.176L \qquad 7.27$$

Putting this in Equation 7.16 and solving for C in terms of W, we get,

$$W^2 + (0.85C)^2 = C^2 \qquad 7.28$$

$$W^2 = 0.28C^2 \qquad 7.29$$

$$C = 1.92W \qquad 7.30$$

As already shown in Equations 7.10, 7.11, 7.12 and 7.13, the value of W and L from the center of the core can be reduced by 14.3%, 12.5% and 16.8% when immersed in GNF, TNF and ZNF nanofluids respectively as compared to the OB80 blend for same surface temperature values. Thus, the overall (end to end) decrease in the values of W and L will be twice these percentage values. It will, eventually, result in the decrease in net cruciform cross-section of the core in case of nanofluid immersed transformers, which can be calculated in terms of L and W parameters as below,

$$C' = 1.176L' \quad \text{and} \quad C' = 1.92W' \qquad 7.31$$

where (´) represents the new values in case of nanofluid filled transformers for which L´ and W´ with respect to OB80 filled transformer are:

(2*14.3=28.6%) shorter in case of GNF filled transformer,

(2*12.5=25%) shorter in case of TNF filled transformer,

(2*16.8=33.6%) shorter in case of ZNF filled transformer.

Considering two similar types of 3-phase transformers; one immersed with OB80 oil blend whereas another one immersed with the synthesized nanofluids. Considering the first case in which the second transformer is immersed with GNF oil. Since the linear dimensions of GNF filled transformer are 28.6% shorter than the OB80 filled transformer, thus in terms of proportions, the linear dimensions of OB80 and GNF filled transformers are in the ratio x: (1 – 0.286) x = x: 0.714x. Similarly, in second case where the second transformer is filled with TNF oil, its linear dimensions are 25% shorter, the ratio of linear dimensions of OB80 to TNF filled transformer will be x: (1 – 0.25) x = x: 0.75x. Whereas in the third case where the second transformer is filled with TNF, its linear dimensions are 33.6% shorter, thus giving the ratio of linear dimensions of OB80 to ZNF filled transformers as x: (1 – 0.336) x = x: 0.664x. Thus, we have the linear dimensions of these transformers in the ratio of OB80: GNF: TNF: ZNF as:

$$x: 0.714x: 0.75x: 0.664x$$

Since the window area (A_w) and the net iron area (A_c) of a transformer are directly proportional to the square of its linear dimensions [150], we have,

For OB80 filled transformer, $A_w \propto x^2$ and $A_c \propto x^2$

For GNF filled transformer, $A_w \propto (0.714x)^2 \propto 0.509x^2$. Similarly, $A_c \propto 0.509x^2$

For TNF filled transformer, $A_w \propto (0.75x)^2 \propto 0.562x^2$. Similarly, $A_c \propto 0.562x^2$

For ZNF filled transformer, $A_w \propto (0.664x)^2 \propto 0.440x^2$. Similarly, $A_c \propto 0.440x^2$

In terms of losses, total copper loss, Cu loss = Loss in primary + loss in secondary, i.e.,

$$Cu\ loss = I_p^2\left(\frac{T_p \rho L_{mtp}}{a_p}\right) + I_s^2 T_s\left(\frac{\rho L_{mts}}{a_s}\right) \qquad 7.32$$

Where I_p and I_s are the currents in the primary and secondary coils, respectively

T_p and T_s are the number of turns in the primary and secondary coils, respectively

ρ is the specific resistivity of the winding material

L_{mtp} and L_{mts} are the lengths of mean turn of primary and secondary coils, respectively

a_p and a_s are the areas of conductors of primary and secondary windings, respectively.

Also, we have $I_p = \delta a_p \quad and \quad I_s = \delta a_s\ ,\ \ where\ \delta\ is$ the current density in A/m^2

Putting these values in Equation 7.32, we have,

$$Cu\ loss = \delta^2 a_p T_p \rho L_{mtp} + \delta^2 a_s T_s \rho L_{mts} \qquad 7.40$$

$$Cu\ loss = \delta^2 \rho\left(a_p T_p L_{mtp} + a_s T_s L_{mts}\right) \qquad 7.41$$

$$Cu\ loss = \delta^2 \rho * volume\ of\ copper \qquad 7.42$$

Since, δ and ρ are constants, thus the total copper loss become,

$$Cu\ loss \propto \text{volume of copper} \qquad 7.43$$

Since for any typical transformer, the volume of copper windings is directionally proportional to the cube of its linear dimensions which leads to the direct dependency of the total copper losses on the cube of the transformer's linear dimensions [153], i.e.,

$$Cu\ loss \propto\ (linear\ dimensions)^3 \qquad 7.44$$

Also, the total iron loss = loss per unit volume * volume

And loss per unit volume is a constant term for same type of material, we have,

$$Iron\ loss \propto volume \qquad 7.45$$

$$Iron\ loss \propto\ (linear\ dimensions)^3 \qquad 7.46$$

Thus, from Equations 7.44 and 7.46, we have,

$$Total\ loss \propto (linear\ dimensions)^3 \qquad 7.47$$

For different oil filled transformers, we get,

For OB80 filled transformer, total losses $\propto x^3$

For GNF filled transformer, total losses $\propto (0.714x)^3 \propto 0.364x^3$

For TNF filled transformer, total losses $\propto (0.75x)^3 \propto 0.421x^3$

For ZNF filled transformer, total losses $\propto (0.664x)^3 \propto 0.292x^3$

Thus, the total losses in nanofluid immersed transformers show considerable decrease in their losses when compared to the OB80 filled transformer.

7.2 MATERIAL COMPATIBILITY

Another important factor when making the design considerations of any transformer with respect to a newly developed transformer oil is the material compatibility of the transformer components with that particular oil. While studying the material compatibility in a transformer, the main focus is kept on the non-metallic parts of the transformer body. It has been shown through vast research and studies that the metallic parts of the transformer, which mainly consist of iron and stainless steel, are, in general, compatible with every type of transformer oil developed till date – be it mineral oil, vegetable oil or silicone oil. However, non-metallic parts like rubber seals, gaskets, etc., show different behavior when exposed to different types of transformer oils. These compatibility tests include various testing techniques after which the results obtained in case of new oil are compared with the values of a particular reference oil as described in ABNT NBR 14274 [154]. If the obtained results fall within the accepted range or the permissible limits described by the reference oil, the constructional material is said to be compatible with the new oil. H. M. Wilhelm, et al. performed various material compatibility tests on transformer construction materials like transformer Kraft paper, transformer steel core, varnish and rubber gasket materials with respect to the conventional mineral oil as well as natural ester oils [155]. The

compatibility of two types of rubbers, nitrile rubber and fluorosilicone rubber were studied with conventional mineral oil and natural ester oil. These tests were performed as per the ASTM D3455 standards [156]. The testing standards used for various compatibility tests are shown in Table 7.2. It has been shown that the basic metallic parts like aluminum, copper, iron, etc. are generally compatible with the ester oils. However, the rubber parts may or may not be compatible and detailed research needs to be done to find out these results. The nitrile rubber based gaskets, as well as some applied rubber based mixtures, tend to become hard and brittle in ester oils whereas others show swelling in natural esters and thus becoming weak. The usage of flour polymer gaskets (VITON) can help in overcoming this problem.

Table 7.2 ASTM standards for material compatibility tests.

Compatibility test	ASTM standard
Shore A Hardness tests on rubber	ASTM D2240
Mechanical tests on new rubber	ASTM D412
Mechanical tests on aged rubber	ASTM D573
Chemical Resistance	ASTM D471

The results showed that after thermal ageing of the rubber materials in natural ester oil, the thermal stress at maximum load in case of aged nitrile rubber decreased by about 55% whereas the elongation at break was reported to decrease by about 77% when compared to the unaged nitrile rubber specimen. These values were found to be much greater than the values obtained for fluorosilicone rubber. In terms of chemical resistance, the variations in hardness and volume were found to be very little in both types of rubber. However, the changes in tensile strength were much higher in case of nitrile rubber as compared to fluorosilicone rubber. In other words, it can be summarized that the gaskets made up of nitrile rubber are prone to become inflexible when used in natural ester oils. This will result in increased risk of oil leakage especially in the case of On Load Tap Changers (OLTCs), thus making the nitrile rubber incompatible with the nautral ester oils. Therefore, these tests showed that the fluorosilicone rubbers possess greater compatibility

with natural ester oils. However, the design prospect of a transformer would require some more studies involving the behavior of fluorosilicone rubber in presence of nanofluids like, GNF, TNF and ZNF in this case.

7.3 CHAPTER SUMMARY

In this chapter, the design considerations for transformers filled with different oil samples have been studied. It has been shown that one of the most important governing factors responsible for the insulation design for any transformer, i.e., the ratio of relative permittivity values of liquid to solid insulation is closer to unity in nanofluid filled transformers when compared with the base oil-blend OB80 filled transformer. Thus, the dielectric stress in NF filled transformers is lower resulting in lower temperature values which can pave a way in the reduction of linear dimensions of NF transformers as compared to the OB80 filled transformer for same temperature values. Thus, linear dimensions of ZNF filled transformer have been calculated to show the maximum reduction of 33.6% followed by GNF filled transformer for which the linear dimensions get reduced by 28.6%. The linear dimensions of TNF filled transformer are calculated to show the reduction of 25%. Meanwhile the window area and the net iron area of NF filled transformer also decrease as square of their respective linear dimensions whereas the total losses of NF filled transformers decrease as cube of their respective linear dimensions when compared to the OB80 filled transformer. Material compatibility analysis from the literature also shows that the most of the metallic parts of the transformer are compatible with the base oil-blend. However, non-metallic parts like seals and gaskets made up of fluorosilicone rubber are more compatible that the ones made up of nitrile rubber in case of ester oil based transformer oils. But, the compatibility of these materials with the nanofluids needs to be studied further which would be included in the future scope of this research.

CHAPTER 8

CONCLUSIONS AND FUTURE SCOPE

8.1 CONCLUSIONS

In this work, the usage of vegetable based insulating nanofluids for power transformers has been studied. This research has been based on the theme of finding suitable alternative dielectric fluids which can be used to replace the conventional mineral oil in transformers. Considering the fact that mineral oil is highly toxic in nature and its spillage causes serious environmental threats, vegetable based soyabean extracted natural ester oil has been used as the primary oil in this research. In order to retain the better qualities of mineral oil like lower viscosity and better oxidation stability, the vegetable oil and mineral oil have been mixed in different proportions to form oil blend samples and one oil blend has been chosen as the base oil on the basis of its dielectric qualities and ester oil content when compared with other oil blends. The usage of vegetable based oil-blend has directly led to the elimination of toxicity and non-biodegradability related concerns raised by the mineral oil. However, this research has been carried out further to study the dielectric as well as physio-thermal properties of this oil blend by dispersing various nanomaterials in it. Three types of nanomaterials – non-conductive graphene oxide (GO), semi-conductive titanium di-oxide (TiO_2) and conductive zinc oxide (ZnO) have been used for this research, with main focus being on the application of non-conductive graphene oxide nanomaterial. The effects of thermal ageing on synthesized nanofluids have also been investigated whereas the effects of these nanofluids on solid insulation, i.e., transformer pressboard have also been studied in detail. The transformer design considerations necessitated by the usage of these nanofluids have been studied as well. All the experiments have been carried out using ASTM and IEC specified standards.

It has been shown that the addition of GO in natural ester-based oil blend first leads to a decrease in BDV and IBDV values at lower concentration values of 0.001 and 0.003 g/L. However, on increasing the concentration of GO to 0.005 g/L, the peak values of breakdown voltages are measured with about 15% increase in BDV and 11.7% increase in IBDV as compared to the base oil-blend. These peak values are greater than the respective breakdown voltages of the pure MO,

pure EO as well as the base oil-blend. This overall increase is be due to the hydrophilic nature of graphene oxide leading to the absorption of moisture from the oil by nanoparticles. Similarly, other electrical properties like relative permittivity and loss tangent have also improved significantly. The physio-thermal properties like interfacial tension and flash point of NF samples are also enhanced. However, no significant change in the viscosity of nanofluids with respect to the concentration of GO nanoparticles is noted. When compared with new TNF and ZNF samples, the results show that the breakdown voltage of TiO_2 dispersed nanofluid is reported to be about 30% greater than pure mineral oil, 24 % greater than pure ester oil, and 17% greater than the oil-blend. Likewise, the breakdown voltage of ZnO dispersed nanofluid is observed to be around 28% greater than pure mineral oil, 19% greater than pure ester oil, and 16% greater than the oil-blend. This is due to the higher shallow trapping leading to faster capability of electron trapping of conductive ZnO nanoparticles during the sudden increase in the voltage. Dispersing of TiO_2 slightly lowered down the viscosity of the nanofluid whereas, the addition of ZnO nanoparticles led to an overall increase in the viscosity of the oil thus deteriorating the cooling property of the ZNF nanofluid. Table 7.1 lists the synthesized NF samples which have shown the best and worst performances from each nanofluid category for respective parameters.

Table 8.1 Best performing NF sample within each NF category as well in overall category.

Parameter	***Best performing NF sample within each type of nanofluid***			***Best performing NF sample overall***
	GNF	***TNF***	***ZNF***	
Ac BDV	GNF5	TNF5	ZNF5	TNF5
IBDV	GNF5	TNF5	ZNF5	ZNF5
Relative permittivity	GNF3	TNF3	ZNF5	ZNF5
Dissipation factor	GNF3	TNF3	ZNF5	GNF3
Viscosity	GNF3	TNF5	ZNF1	TNF5
Interfacial tension	GNF3	TNF3	ZNF3	TNF3
Flash point	GNF5	TNF5	ZNF5	GNF5

When tested for their dielectric properties after being subjected to 60 days of thermal stress, all the three types of NF samples performed better than the base oil blend samples. The BDV values of GNF samples started to decrease right from the beginning of the ageing process, however, BDV values of ZNF and TNF samples increased slightly till the 15^{th} day of ageing and then reported a decrease at the end of 60^{th} day of ageing. Same trend was seen in the IBDV values of NF samples. Nevertheless, the peak values of all parameters before and after ageing were attained for same concentration levels of nanoparticles in the base oil blend. Results also showed that the effect of thermal ageing on the transformer solid insulation was less deteriorating when the solid insulation materials was impregnated with the NF samples as compared to when impregnated with the base oil-blend. The structural damage was investigated by calculating relative crystallinity and respective fiber widths and the results showed that P-GNF had a relative crystallinity of 56.5% with 0.97 nm crystallite size after 60 days of ageing. Relative crystallinity value for P-TNF after 60 days of ageing was 62.7% with crystallite size 1.83 nm whereas for P-ZNF, the relative crystallinity was 46.8% with 1.12 crystallite. When compared to the relative crystallinity of P-OB80 which was 31.6% with 0.62 crystallite size, the NF impregnated solid insulation showed better mechanical endurance even after 60 days of ageing. it can also be confirmed by the fiber widths which were calculated to be 19.6 µm, 19.2 µm and 18.1 µm for P-GNF, P-TNF and P-ZNF samples after 60 days of ageing when compared to the P-OB80 which was much lower at 14.3 µm. Similarly, after 60 days of ageing, the dielectric properties of solid insulation material impregnated with NF samples were also enhanced when compared to those of the solid material impregnated with base oil blend.

In terms of transformer design considerations, the insulation structure based on NF samples and NF impregnates pressboard was found to be better than the insulation structure based on the base oil blend. The relative permittivity values of liquid and solid insulation were closer to one another in NF based insulation when compared to OB80 based insulation, thus, forming a more uniform dielectric stress distribution which governs the insulation design of any transformer. ZNF based insulation structure had the most uniform stress distribution whereas the GNF based insulation structure had the least, nevertheless, better than the stress distribution in base oil based insulation structure. Also, from the calculations, it can be analyzed that the distance from the center of the core can be reduced by 14.3% in case of GNF filled transformer, 12.5% in case of TNF filled transformer and 16.8% in case of ZNF filed transformer when compared to OB80 filled

transformer for same hotspot temperature values, thus giving a more compact design in NF immersed transformers as compared to the base oil immersed transformer.

8.2 FUTURE SCOPE OF THIS RESEARCH

The present work has a good aspect for future research which is appended below:

1. In future, all these research outcomes can be verified for actual power transformer models. The applications of these NFs can be verified in prototypes having accelerated thermal ageing mechanism as well as after real-time ageing.

2. The dielectric performance of any insulating fluid also depends upon the moisture level in the fluid. This dependency will be studied in future research.

3. The application of these NFs can also be extended to On-Line Tap-Changers (OLTCs) after performing the related experiments.

4. The optimization of oil-blend can be varied as per the requirements and the desired properties can be achieved by changing the contents of the mineral oil and ester oil in the blend.

5. Low synthesis cost and large-scale production will enable graphene oxide dispersed ester oil based nanofluid to be effectively used as insulating oils in transformers.

REFERENCES

[1] I. A. Metwally, “Failures, Monitoring and New Trends of Power Transformers,” IEEE Potentials, vol. 30, no. 3, pp. 36-43, 2011.

[2] L. E. Lundgaard, W. Hansen, D. Linhjell and T. J. Painter, "Aging of oil-impregnated paper in power transformers," IEEE Transactions on Power Delivery, vol. 19, no. 1, pp. 230-239, Jan. 2004.

[3] M. Khanajli, A. H. Soloot, H. K. Hoidalen and S. Jayaram, “Study on locating transformer internal faults using sweep frequency response analysis,” Electric Power System Research, vol. 145, pp. 55-62, 2017.

[4] D. Peterchuck and A. Pahwa, “Sensitivity of transformer's hottest-spot and equivalent aging to selected parameters”, IEEE Transactions on Power Delivery, vol. 17, no. 4, pp. 996–1001, 2002.

[5] M. Rafiq, M. Shafique, A. Azam and M. Ateeq, “The impacts of nanotechnology on the improvement of liquid insulation of transformers: Emerging trends and challenges”, Journal of Molecular Liquids, vol. 302, 112482, 2020.

[6] EPRI Portfolio 2007—Transmission reliability and performance: 37.002, transformer life extension, http://www.epri.com/portfolio/

[7] D. Vrsaljko, V. Haramija and A. Skerlev, “Determination of phenol, m-cresol and o-cresol in transformer oil by HPLC method”, Electrical Power System Research. vol. 93, pp. 24-31, 2012.

[8] M. Rajňák, J. Kurimský, R. Cimbala, Z. Čonka, P. Bartko, M. Šuga, K. Paulovičová, J. Tóthová, M. Karpets, P. Kopčanský and M. Timko, “Statistical analysis of AC dielectric breakdown in transformer oil-based magnetic nanofluids,” Journal of Molecular Liquids, vol. 309, no. 113243, 2020.

[9] S. Maneerot, K. Jariyanurat, P. Nimsanong, C. Bunlaksananusor, A. Kunakorn and N. Pattanadech, "Studies of Electrical and Thermal Characteristics of Natural Ester Immersed Transformer Compared with Mineral Oil Immersed and Palm Oil Immersed Transformer," *2018 Condition Monitoring and Diagnosis (CMD)*, 2018, pp. 1-4.

[10] Y. Xu, S. Qian, Q. Liu and Z. D. Wang, “Oxidation stability assessment of a vegetable transformer oil under thermal aging”, IEEE Transactions on Dielectrics and Electrical Insulations, vol. 21, no. 2, pp. 683-692, 2014.

[11] M. Rafiq, Y. Z. Lv, Y. Zhou, K.B. Ma, W. Wang, C. R. Li, and Q. Wang, “Use of vegetable oils as transformer oil – a review”, Renewable and sustainable Energy Reviews, vol. 52, pp. 308-324, 2015.

[12] R. Liao, J. Hao, G. Chen, Z. Ma and L. Yang, “A comparative study of physicochemical, dielectric and thermal properties of pressboard insulation impregnated with natural ester and mineral oil”, IEEE Transactions on Dielectrics and Electrical Insulations, vol. 18, issue 5, pp. 1626-1637, 2011.

[13] L. Yang, R. Liao, C. Sun, J. Yin and M. Zhu, "Influence of vegetable oil on the thermal aging rate of kraft paper and its mechanism," *2010 International Conference on High Voltage Engineering and Application*, 2010, pp. 381-384.

[14] M. H. Abderrazzaq and F. Hijazi, “Impact of multi-filtration process on the properties of olive oil as a liquid dielectric”, IEEE Transactions on Dielectrics and Electrical Insulations, vol. 5, issue 19, pp. 1673-1680, 2012.

[15] J. Rouabeh, L. M’barki, A. Hammami, I. Jallouli and A. Driss, “Studies of different types of insulating oils and their mixture as an alternate to mineral oil for cooling power transformers”, Heliyon, vol. 5, issue 3, 2019.

[16] T. Kano, T. Suzuki, R. Oba, A. Kanetani and H. Koide, "Study on the oxidative stability of palm fatty acid ester (PFAE) as an insulating oil for transformers," in *2012 IEEE International Symposium on Electrical Insulation*, 2012, pp. 22-25.

[17] S. S. Kumar, M. W. Iruthayarajan and M. Bakrutheen, “Analysis of vegetable liquid insulating medium for applications in high voltage transformers”, in *International Conference on Science Engineering and Management Research (ICSEMR)*, India, 2014, pp. 1-5.

[18] R. V. Radhika, M. W. Iruthayarajan, “Investigation of critical parameters of mixed insulating fluids”, in *International Conference on Circuits, Power and Computing Technologies (ICCPCT),* India, 2014, pp. 357-362.

[19] J. E. Contreras, J. Rodriguez-Diaz, E. A. Rodriguez, “Environmentally Friendly Fluids for High-Voltage Applications”, *Handbook of Ecomaterials*, pp. 1-26, 2017.

[20] W. Yu and H. Xie, “A review on nanofluids: Preparation, stability mechanisms, and applications," Journal of Nanomaterials, vol. 2012, Art. no. 435873. 2012.

[21] S. Aberoumand and A. Jafarimoghaddam, “Tungsten (III) oxide (WO_3) Silver/transformer oil hybrid nanofluid: Preparation, stability, thermal conductivity and dielectric strength," Alexandria Engineering Journal, vol. 57, pp. 169-174, Mar. 2018.

[22] P. Kopcanský, L. Tomco, K. Marton, M. Koneracká, M. Timko, and I. Potocová, “The DC dielectric breakdown strength of magnetic fluids based on transformer oil," Journal of Magnetism and Magnetic Materials, vol. 289, pp. 415-418, Mar. 2005.

[23] Y. Zhong, Y. Lv, C. Li, Y. Du, M. Chen, S. Zhang, Y. Zhou, and L. Chen, “Insulating properties and charge characteristics of natural ester fluid modified by TiO_2 semiconductive nanoparticles," IEEE Transactions on Dielectrics and Electrical Insulation, vol. 20, no. 1, pp. 135-140, Feb. 2013.

[24] C. Choi, H. S. Yoo, and J. M. Oh, “Preparation and heat transfer properties of nanoparticle-in-transformer oil dispersions as advanced energy efficient coolants," Current Appl. Phys., vol. 8, no. 6, pp. 710-712, 2008.

[25] C. P. Y. Alicia, W. Rashmi, M. Khalid, A. K. Rasheed, and T. Gupta, “Synthesis and thermo-physical characterization of graphene based transformer oil," Journal of Engineering Science and Technology, vol. 11, no. 5, pp. 140-152, Feb. 2016.

[26] Z. Liu, “Global Energy Development: The Reality and Challenges” *Global Energy Interconnection,* 2015

[27] B. Stoffel, “The Role of Pumps for Energy Consumption and Energy Saving” *Assessing the Energy Efficiency of Pumps and Pump Units,* 2015.

[28] M. Humayun, M. Z. Degefa, A. Safdarian and M. Lehtonen, "Utilization Improvement of Transformers Using Demand Response," *IEEE Transactions on Power Delivery*, vol. 30, no. 1, pp. 202-210, Feb. 2015.

[29] M. Whelan, J. Cunningham and S. Rockwell, "The History of Alternating Current: AC Power History and Timeline' *Edison Tech Center*. https://edisontechcenter.org/AC-PowerHistory.html

[30] F. Devaux and R. Bardsley, "A short history of power transformers through the age", *The transformation of transformers*, 2019. https://www.think-grid.org/transformation-transformers

[31] E. Casserly, "Naphthenic mineral electrical insulating oils", Transformers, vol. 2, no. 3, 2015.

[32] X. Wang, C. Tang, B. Huang, J. Hao and G. Chen, "Review of Research Progress on the Electrical Properties and Modification of Mineral Insulating Oils Used in Power Transformers" Energies, vol. 11, no. 3, pp. 487, 2018.

[33] R. Jilani, M. Lotfi, A. Hammami, I. Jallouli and A. Driss, "Studies of different types of insulating oils and their mixtures as an alternative to mineral oil for cooling power transformers," Heliyon, vol. 5, no. 3, 2019.

[34] C.W. Bamforth, "BEERS | Chemistry of Brewing" in *Encyclopedia of Food Sciences and Nutrition (Second Edition), 2003*.

[35] I. Dhimitruka and J. S. Lucia, Jr., "Investigation of the Yamaguchi Esterification Mechanism. Synthesis of a Lux-S Enzyme Inhibitor Using an Improved Esterification Method" Organic Letters. vol. 8, no. 1, pp. 47-50, 2018.

[36] E. W. Hammond, "Vegetable oils-Types and Properties" *Encyclopedia of Food Sciences and Nutrition (Second Edition)*, 2003.

[37] B. Freedman, E. H. Pryde and T. L. Mounts, "Variables affecting the yields of fatty esters from trans-esterified vegetable oils" Journal of the American Oil Chemists Society, vol. 61, no. 10, pp 1638–1643, 1984.

[38] K. M. Phillips 1, D. M. Ruggio, J. I. Toivo, M. A. Swank and A. H. Simpkins, “Free and Esterified Sterol Composition of Edible Oils and Fats”, Journal of Food Composition and Analysis, vol. 15, no. 2, pp 123-142, 2002.

[39] A. Kumar, A. Sharma and K.C. Upadhyaya, “Vegetable Oil: Nutritional and Industrial Perspective” Current Genomics, vol. 17, no. 3, pp. 230–240, 2016.

[40] S. Ravulapalli, R. Kunta and M. Ramamoorty, “Preparation, characterization and feasibility analysis of methyl ester of Sesbania seeds oil (MESSO) as alternate liquid dielectrics in distribution transformers” Royal society of chemistry, vol. 9, pp. 3311-3319, 2019.

[41] T. K. Sindhu, P. Preetha and J. Joyce, “A Review on Natural Ester and Nanofluid as Alternative to Transformer Mineral Oil” IET Nanodielectrics, vol. 3, no. 6, 2020.

[42] A. Čejková, P. Trnka and V. Mentlík, "Natural ester — Moisture and acidity issue," *2016 Conference on Diagnostics in Electrical Engineering (Diagnostika)*, 2016, pp. 1-4.

[43] D. M. Mehta, P. Kundu, A. Chowdhury, V. K. Lakhiani and A. S. Jhala, "A review on critical evaluation of natural ester vis-a-vis mineral oil insulating liquid for use in transformers: Part 1," *IEEE Transactions on Dielectrics and Electrical Insulation,* vol. 23, no. 2, pp. 873-880, April 2016.

[44] M. Jaroszewski and K. Rakowiecki, "Partial discharge inception voltage in transformer natural ester liquid — Effect of the measurement method in the presence of moisture," *IEEE Transactions on Dielectrics and Electrical Insulation,* vol. 24, no. 4, pp. 2477-2482, 2017.

[45] D. M. Mehta, P. Kundu, A. Chowdhury, V. K. Lakhiani and A. S. Jhala, "A review of critical evaluation of natural ester vis-a-vis mineral oil insulating liquid for use in transformers: Part II," I*EEE Transactions on Dielectrics and Electrical Insulation,* vol. 23, no. 3, pp. 1705-1712, June 2016.

[46] M. Bakrutheen, M. W. Iruthayarajan and A. Narayani, "Statistical failure reliability analysis on edible and non edible natural esters based liquid insulation for the applications in high voltage transformers," *IEEE Transactions on Dielectrics and Electrical Insulation*, vol. 25, no. 5, pp. 1579-1586, Oct. 2018.

[47] M. Lyutikova, S. Korobeynikov and A. Konovalov, "Evaluation of the Properties of Mixtures of Aromatic Mineral Oil and Synthetic Ester for High-Voltage Equipment," *IEEE Transactions on Dielectrics and Electrical Insulation,* vol. 28, no. 4, pp. 1282-1290, August 2021.

[48] P. Thomas, N. E. Hudedmani, R. T. A. R. Prasath, N. K. Roy and S. N. Mahato, "Synthetic ester oil based high permittivity $CaCu_3Ti_4O_{12}$ (CCTO) nanofluids an alternative insulating medium for power transformer," *IEEE Transactions on Dielectrics and Electrical Insulation,* vol. 26, no. 1, pp. 314-321, Feb. 2019.

[49] A. Reffas, A. Beroual and H. Moulai, "Comparison of breakdown voltage of vegetable olive with mineral oil, natural and synthetic ester liquids under DC voltage," *IEEE Transactions on Dielectrics and Electrical Insulation,* vol. 27, no. 5, pp. 1691-1697, Oct. 2020.

[50] Z. W. Yan, T. Kihampa, S. Y. Matharage, Q. Liu and Z. D. Wang, "Measuring Low Molecular Weight Acids in Mineral and Ester Transformer Liquids," in *2020 8th International Conference on Condition Monitoring and Diagnosis (CMD)*, 2020, pp. 354-357.

[51] M. R. Hussain, Q. Khan, A. A. Khan, S. S. Refaat and H. Abu-Rub, "Dielectric Performance of Magneto-Nanofluids for Advancing Oil-Immersed Power Transformer," *IEEE Access*, vol. 8, pp. 163316-163328, 2020.

[52] S. -Y. Xia, Z. Huang, F. Wang, L. Tao, J. LI, T. Jiang and Z. Lou, "Anti-aging and Dielectric Performance of Synthetic Tri-ester Blended with Natural Ester," *IEEE Transactions on Dielectrics and Electrical Insulation,* vol. 28, no. 3, pp. 1005-1011, June 2021.

[53] D. K. Mahanta, "A Study of Biodegradable Oil as Transformer Insulating Material," *2018 IEEE 7th International Conference on Power and Energy (PECon)*, Kuala Lumpur, Malaysia, 2018, pp. 263-266.

[54] J. Xiang, Q. Liu and Z. D. Wang, "Streamer characteristic and breakdown in a mineral oil and a synthetic ester liquid under DC voltage," IEEE Transactions on Dielectrics and Electrical Insulation, vol. 25, no. 5, pp. 1636-1643, Oct. 2018.

[55] H. M. Wilhelm, M. B. C. Stocco, L. Tulio, W. Uhren and S. G. Batista, "Edible natural ester oils as potential insulating fluids," *IEEE Transactions on Dielectrics and Electrical Insulation*, vol. 20, no. 4, pp. 1395-1401, August 2013.

[56] G. Dombek and J. Gielniak, "Fire safety and electrical properties of mixtures of synthetic ester/mineral oil and synthetic ester/natural ester," *IEEE Transactions on Dielectrics and Electrical Insulation*, vol. 25, no. 5, pp. 1846-1852, Oct. 2018.

[57] K. Bandara, C. Ekanayake and T. K. Saha, "Compare the performance of natural ester with synthetic ester as transformer insulating oil," *2015 IEEE 11th International Conference on the Properties and Applications of Dielectric Materials (ICPADM)*, 2015, pp. 975-978, doi: 10.1109/ICPADM.2015.7295437.

[58] M. Z. Villaverde and D. U. Cuadros, "Evaluation of Physical-Chemical Characteristics of Mineral Oils Mixed with Synthetic Esters," *2019 6th International Advanced Research Workshop on Transformers (ARWtr)*, 2019, pp. 78-82.

[59] M. Meira, C. Verucchi, R. Álvarez and L. Catalano, "Dissolved Gas Analysis in Mineral Oil and Natural Ester Liquids from Thermal Faults," *IEEE Transactions on Dielectrics and Electrical Insulation*, vol. 28, no. 4, pp. 1317-1325, August 2021.

[60] S. S. Kumar, M. W. Iruthayarajan, M. Bakrutheen and S. G. Kannan, "Effect of antioxidants on critical properties of natural esters for liquid insulations," *IEEE Transactions on Dielectrics and Electrical Insulation*, vol. 23, no. 4, pp. 2068-2078, August 2016.

[61] A. Reffas, H. Moulai and A. Beroual, "Comparison of dielectric properties of olive oil, mineral oil, and other natural and synthetic ester liquids under AC and lightning impulse stresses," *IEEE Transactions on Dielectrics and Electrical Insulation*, vol. 25, no. 5, pp. 1822-1830, Oct. 2018.

[62] S. -Y. Xia *et al.*, "Anti-aging and Dielectric Performance of Synthetic Tri-ester Blended with Natural Ester," *IEEE Transactions on Dielectrics and Electrical Insulation*, vol. 28, no. 3, pp. 1005-1011, June 2021.

[63] U. M. Rao, H. Pulluri and N. G. Kumar, "Performance analysis of transformer oil/paper insulation with ester and mixed dielectric fluids," *IEEE Transactions on Dielectrics and Electrical Insulation*, vol. 25, no. 5, pp. 1853-1862, Oct. 2018.

[64] Z. B. Siddique, S. Mehta and P. Basak, "Prediction of Insulating Oil for Transformers Through Fuzzy Logic Approach," *2020 IEEE 9th Power India International Conference (PIICON)*, 2020, pp. 1-6.

[65] N. Baruah, R. Sangineni, M. Chakraborty and S. K. Nayak, "Statistical Analysis of Natural Ester based Insulating Liquid using Hypothesis Testing," in *2020 International Symposium on Electrical Insulating Materials (ISEIM)*, 2020, pp. 347-350.

[66] C. Perrier, M. Marugan and A. Beroual, "DGA comparison between ester and mineral oils," *IEEE Transactions on Dielectrics and Electrical Insulation*, vol. 19, no. 5, pp. 1609-1614, October 2012.

[67] S. P. Moore, W. Wangard, K. J. Rapp, D. L. Woods and R. M. Del Vecchio, "Cold Start of a 240-MVA Generator Step-Up Transformer Filled With Natural Ester Fluid," *IEEE Transactions on Power Delivery*, vol. 30, no. 1, pp. 256-263, Feb. 2015.

[68] M. Talhi, I. Fofana and S. Flazi, "Comparative study of the electrostatic charging tendency between synthetic ester and mineral oil," *IEEE Transactions on Dielectrics and Electrical Insulation*, vol. 20, no. 5, pp. 1598-1606, Oct. 2013.

[69] A. Rajab, M. Tsuchie, M. Kozako, M. Hikita and T. Suzuki, "Low thermal fault gases of various natural monoesters and comparison with mineral oil," *IEEE Transactions on Dielectrics and Electrical Insulation*, vol. 23, no. 6, pp. 3421-3428, Dec. 2016, doi: 10.1109/TDEI.2016.006068.

[70] K. Yasuda, S. Arazoe, T. Igarashi, S. Yanabu, G. Ueta and S. Okabe, "Comparison of the insulation characteristics of environmentally-friendly oils," *IEEE Transactions on Dielectrics and Electrical Insulation*, vol. 17, no. 3, pp. 791-798, June 2010.

[71] K. Yasuda, S. Arazoe, T. Igarashi, S. Yanabu, G. Ueta and S. Okabe, "Comparison of the insulation characteristics of environmentally-friendly oils," *IEEE Transactions on Dielectrics and Electrical Insulation*, vol. 17, no. 3, pp. 791-798, June 2010.

[72] ISO/TS 80004-1:2015, "Nanotechnologies - Vocabulary - Part 1: Core terms". http://www.iso.org/iso/home/standards_development/resources-for-technical-work/foreword.html

[73] S. Bhatia, "Nanoparticles types, classification, characterization, fabrication methods and drug delivery applications", *Natural Polymer Drug Delivery Systems*, pp. 33-93, Springer, Cham, 2016.

[74] M. D. L. F. Jesus and V. Grazu, "Nanobiotechnology: inorganic nanoparticles vs organic nanoparticles", *Frontiers of Nanoscience*, pp.2-252, Elsevier, 2012.

[75] Moreno-Vega, Aura-Ileana, T. Gomez-Quintero, Rosa-Elvira Nunez-Anita, Laura-Susana Acosta-Torres, and V. Castaño. "Polymeric and ceramic nanoparticles in biomedical applications." Journal of Nanotechnology, vol. 2012, no. 936041, 2012.

[76] V. D. Szabo and D. Vollath. "Nanocomposites from coated nanoparticles." Advanced Materials, vol. 11, no. 15, pp. 1313-1316, 1999.

[77] M.Z. H. Makmud, H. A. Illias, C. Y. Chee, and M. S. Sarjadi. "Influence of conductive and semi-conductive nanoparticles on the dielectric response of natural ester-based nanofluid Insulation." Energies 11, no. 2, pp. 333, 2018.

[78] Nayak, Satish and L. Andrew Lyon. "Soft nanotechnology with soft nanoparticles." in *Angewandte Chemie International Edition 44*, no. 47, pp. 7686-7708, 2005.

[79] C. Sauter, M. A. Emin, H. P. Schuchmann, and S. Tavman. "Influence of hydrostatic pressure and sound amplitude on the ultrasound induced dispersion and de-agglomeration of nanoparticles." Ultrasonics sonochemistry, vol. 15, no. 4, pp. 517-523, 2008.

[80] Y. Zare, "Study of nanoparticles aggregation/agglomeration in polymer particulate nanocomposites by mechanical properties." Composites Part A: Applied Science and Manufacturing, vol. 84, pp. 158-164, 2016.

[81] Y. Zare, K. Y. Rhee, and D. Hui, "Influences of nanoparticles aggregation/agglomeration on the interfacial/interphase and tensile properties of nanocomposites." Composites Part B: Engineering, vol. 122, pp. 41-46, 2017.

[82] Z. Jha, N. Behar, S. N. Sharma, G. Chandel, D. K. Sharma, and M. P. Pandey, "Nanotechnology: prospects of agricultural advancement." Nano Vision, vol. 1, no. 2, pp. 88-100, 2011.

[83] D. Jasinski, F. Haque, D. W. Binzel, and P. Guo, "Advancement of the emerging field of RNA nanotechnology." ACS Nano, vol. 11, no. 2, pp. 1142-1164, 2017.

[84] A. Verma, S. P. Gautam, K. K. Bansal, N. Prabhakar, and J. M. Rosenholm. "Green nanotechnology: advancement in phytoformulation research." Medicines, vol. 6, no. 1, pp. 39, 2019.

[85] D. Pradhan, P. Biswasroy, A. Goyal, G. Ghosh, and G. Rath, "Recent Advancement in Nanotechnology-Based Drug Delivery System Against Viral Infections." Aaps Pharmscitech, vol. 22, no. 1, pp. 1-19, 2021.

[86] A. S. Bale, K. P. Raksha, R. Alagawadi, N. Nisha, and R. Deeksha, "Advancement of Nanotechnology in Batteries." International Journal of Energetic Materials, vol. 6, no. 2, 18-24, 2020.

[87] K. N. Koutras, I. A. Naxakis, E. C. Pyrgioti, V. P. Charalampakos, I. F. Gonos, A. E. Antonelou and S. N. Yannopoulos, “The influence of nanoparticles’ conducting and charging on dielectric properties of ester oil based nanofluids,” Energies, vol. 13, no. 24, pp. 6540, 2020.

[88] A. Sharma, S. Basu and N. Gupta, "Detection of Charge around a Nanoparticle in a Nanodielectric," in *2019 IEEE 4th International Conference on Condition Assessment Techniques in Electrical Systems (CATCON)*, 2019, pp. 1-3.

[89] M. Rajnak, Z. Wu, B. Dolnik, K. Paulovicova, J. Tothova, R. Cimbala, J. Kurimsky, P. Kopcansky, B. Sunden, L. Wadso and M. Timko, “Magnetic field effect on thermal, dielectric and viscous properties of a transformer oil based magnetic nanofluid,” Energies, vol. 12, no. 23, pp. 4532, 2019.

[90] A. Sharma, S. Basu and N. Gupta, "Modeling of Interface Dielectric Constant in Nanodielectrics," in *2021 IEEE Electrical Insulation Conference (EIC)*, 2021, pp. 309-312.

[91] S. S. Dey, S. Rohith, N. Baruah and S. K. Nayak, "Study of Heat Transfer Property of the Transformer Oils on Addition of CuO Nanoparticles," *2021 IEEE International Conference on the Properties and Applications of Dielectric Materials (ICPADM)*, 2021, pp. 218-221.

[92] J. Rouabeh, L. M'barki, A. Hammami, I. Jallouli, and A. Driss, "Studies of different types of insulating oils and their mixtures as an alternative to mineral oil for cooling power transformers." Heliyon, vol. 5, no. 3, e01159, 2019.

[93] M. H. Jabal, F. N. Ani, and S. Syahrullail, "The tribological characteristic of the blends of Rbd palm olein with mineral oil using four-ball tribotester." Jurnal Teknologi, vol. 69, no. 6 2014.

[94] U. M. Rao, Y. N. Kumar and R. K. Jarial, “Understanding the ageing behavior of transformer oil-paper insulation with ester and mixed dielectric fluids,” IET, vol. 10, no. 7, pp. 851-857, 2018.

[95] M. A. Usman, O. O. Olanipekun, and U. T. Hensha,. "A comparative study of soya bean oil and palm kernel oil as alternatives to transformer oil." Journal of Emerging Trends in Engineering and Applied Sciences 3, no. 1, pp. 33-37, 2017.

[96] S. Senthilkumar, A. Karthick, R. Madavan, A. A. M. Moshi, S. Sundara Bharathi, S. Saroja, and C. S. Dhanalakshmi, "Optimization of transformer oil blended with natural ester oils using Taguchi-based grey relational analysis." Fuel vol. 288, no. 119629, 2021.

[97] I. Fernandez, R. Valiente, F. Ortiz, C. J. Renado, and A. O. Ortiz, “Effect of TiO_2 and ZnO nanoparticles on the performance of dielectric nanofluid based on vegetable esters during their ageing,” Nanomaterials, vol. 10, no. 4, pp. 692, 2020.

[98] N. Yadav, R. K. Jarial and U. M. Rao, “Characterization of mineral oil based Fe_3O_4 nanofluid for application in oil filled transformers,” International Journal on the Engineering and Informatics, vol. 10, no. 2, 2018.

[99] X. Zhou, P. Werle, E. Gockenbach, H. Shi and M. Kuhnke, "Study of Oil/Pressboard Creeping Discharges under Divergent AC Voltage—Part 1: Fundamental Phenomena and Influencing

Factors," IEEE Transactions on Dielectrics and Electrical Insulation, vol. 28, no. 2, pp. 355-363, April 2021.

[100] B. Charaborty, K. Y. Raj, A. K. Pradhan, B. Chatterjee, S. Chakravorti and S. Dalai, “Investigation of dielectric properties of TiO_2 and $Al2O_3$ nanofluids by frequency domain spectroscopy at different temperatures,” Journal of Molecular Liquids, vol. 330, no. 115642, 2021.

[101] R. Karthik and A. Raymon, "Effect of silicone oxide nanoparticles on dielectric characteristics of natural ester," *2016 IEEE International Conference on High Voltage Engineering and Application (ICHVE)*, Chengdu, 2016, pp. 1-3.

[102] B. X. Du, X. L. Li, J. Li and X. Y. Tao, "Effects of BN nanoparticles on thermal conductivity and breakdown strength of vegetable oil," *2015 IEEE 11th International Conference on the Properties and Applications of Dielectric Materials (ICPADM)*, Sydney, NSW, 2015, pp. 476-479.

[103] W. Saenkhumwong and A. Suksri, "Investigation on Voltage Breakdown of Natural Ester Oils Based-On Zno Nanofluids", Advanced Materials Research, vol. 1119, pp. 175-178, 2015

[104] A. Mohamad, N. Azis, J. Jasni, Z. kadir, R. Yunus and Z. Yaakub, “Impact of Fe_3O_4, CuO and Al_2O_3 on the AC Breakdown Voltage of Palm Oil and Coconut Oil in the Presence of CTAB,” Energies, vol. 12, no. 9, pp. 1605, 2019.

[105] V. P. Charalampakos and A. Bakandritsos, “A comparative study of natural ester based nanofluids with Fe_2O_3 and SiO_2 Nanoparticles,” in *19th IEEE International Conference on Dielectric Liquids (ICDL), Manchester, United Kingdom*, 2017, pp. 25-29.

[106] N. S. Suhaimi, M. F. M. Din, M. T. Ishak, A. R. A. Rahman, M. M. Ariffin, N. Hashim and J. Wang, “Systematical study of multi-walled carbon nanotube nanofluids based disposed transformer oil” Nature, vol. 10, no. 20984, 2020.

[107] S. Potivejkul, N. Pattanadech, K. Jariyanurat and W. Wattakapaiboon, "Electrical characteristics of natural ester based nanofluid," 2017 International Electrical Engineering Congress (iEECON), Pattaya, 2017, pp. 1-3.

[108] U. Khaled and A. Beroual, "AC dielectric strength of synthetic ester-based Fe_3O4, Al_2O_3 and SiO_2 nanofluids — conformity with normal and Weibull distributions," IEEE Transactions on Dielectrics and Electrical Insulation, vol. 26, no. 2, pp. 625-633, April 2019.

[109] V. P. Charalampakos, E. Chatzikalymnios, E. Pyrgioti, G. D. Peppas, A. Bakandritsos, A. Polykrati and I. F. Gonos, "AC Breakdown Strength of Natural Ester Oil based Nanofluid with Graphene Nanosheets," *2018 IEEE International Conference on High Voltage Engineering and Application (ICHVE),* 2018, pp. 1-4.

[110] P. Dhar, A Katiya, L. S. Magarti, A. Pattanatta and S. K. Das, "Superior dielectric breakdown strength of Graphene Oxide and CarbonNano Tubes based nanofluids", IEEE Transaction on dielectric and Electrical Insulation, vol. 23, No.2, April 2016.

[111] R. T. Prasath, S. N. Mahato, N. K. Roy and P. Thomas, "Dielectric and Thermal Conductivity Studies on Synthetic Ester Oil based TiO_2 Nanofluids", in *3rd International Conference on Condition Assessment Techniques in Electrical Systems (CATCON),* 2017.

[112] Q. Khan, R. Hussain and A. A. Khan, "Dielectric Characterization of Fe_2P Nanoparticles based Ester Oil", IET Journal, August 2018.

[113] M. Taro, D. Shill, A. K. Das and S. Chatterjee, "Experimental investigation of transformer oil based nanofluids for applications in distribution transformers," in *2017 3rd International Conference on Condition Assessment Techniques in Electrical Systems (CATCON),* 2017, pp. 367-370.

[114] J. Jacob, N. R. Uppu, A. Jha, C. D. Sai, S. Katta and P. Prabhu, "Compatibility Study of Paper and Epoxy with Natural Ester- A substitute for Transformer Mineral Oil," in *TENCON 2019 - 2019 IEEE Region 10 Conference (TENCON),* 2019, pp. 1514-1517.

[115] J. Jacob and P. Preetha and S. Thiruthi Krishnan, "Review on natural ester and nanofluids as an environmental friendly alternative to transformer mineral oil," IET Nanodielectrics, 2020.

[116] Y. Zhao, Z. Wu, S. Guo, Z. Zhou, Z. Miao, S. Xie, R. Huang and Laifeng Li, "Hyperbranched graphene oxide structure-based epoxy nanocomposite with simultaneous enhanced mechanical

properties, thermal conductivity, and superior electrical insulation," Composites Science and Technology, vol. 217, no. 109082, 2022.

[117] H. Liu, P. Wang, W. Yuan and H. Li, "Study on the thermal insulation performance of the core shell skeleton graphene oxide/carbon composite aerogel", Journal of Polymer Engineering, 2021.

[118] Y. Lei, Z. Hu, B. Cao, X. Chen and H. Song, "Enhancements of thermal insulation and mechanical property of silica aerogel monoliths by mixing graphene oxide, "Materials Chemistry and Physics, vol. 187, pp. 183-190, 2017.

[119] S. N. Alam, N. Sharma, and L. Kumar. "Synthesis of graphene oxide (GO) by modified hummers method and its thermal reduction to obtain reduced graphene oxide (rGO)." Graphene, vol. 6, no. 1, pp. 1-18, 2017.

[120] N. I. Zaaba, K. L. Foo, U. Hashim, S. J. Tan, Wei-Wen Liu, and C. H. Voon. "Synthesis of graphene oxide using modified hummers method: solvent influence." Procedia Engineering, vol. 184, pp. 469-477, 2017.

[121] J. N. Hasnidawani, H. N. Azlina, H. Norita, N. N. Bonnia, S. Ratim, and E. S. Ali. "Synthesis of ZnO nanostructures using sol-gel method." Procedia Chemistry, vol. 19, pp. 211-216, 2016.

[122] R. M. Alwan, Q. A. Kadhim, K. M. Sahan, R. A. Ali, R. J. Mahdi, N. A. Kassim, and A. N. Jassim. "Synthesis of zinc oxide nanoparticles via sol–gel route and their characterization." Nanoscience and Nanotechnology 5, no. 1, pp. 1-6, 2015.

[123] X. Ma, Y. Zare, and K. Y. Rhee. "A two-step methodology to study the influence of aggregation/agglomeration of nanoparticles on Young's modulus of polymer nanocomposites." Nanoscale Research Letters, vol. 12, no. 1, pp. 1-7, 2017.

[124] H. Machrafi, G. Lebon, and C. S. Iorio. "Effect of volume-fraction dependent agglomeration of nanoparticles on the thermal conductivity of nanocomposites: Applications to epoxy resins, filled by SiO_2, AlN and MgO nanoparticles." Composites Science and Technology, vol. 130, pp. 78-87, 2016.

[125] C. Bantz, O. Koshkina, T. Lang, H. J. Galla, C. J. Kirkpatrick, R. H. Stauber, and M. Maskos. "The surface properties of nanoparticles determine the agglomeration state and the size of the particles under physiological conditions." Beilstein Journal of Nanotechnology, vol. 5, no. 1, pp. 1774-1786, 2014.

[126] S. Mishra, N. G. Shimpi, and A. D. Mali. "Influence of stearic acid treated nano-$CaCO_3$ on the properties of silicone nanocomposites." Journal of Polymer Research, vol. 18, no. 6, pp. 1715-1724, 2011.

[127] S. H. Ahn, S. H. Kim, and S. G. Lee. "Surface-modified silica nanoparticle–reinforced poly (ethylene 2, 6-naphthalate)." Journal of Applied Polymer Science, vol. 94, no. 2, pp. 812-818, 2004.

[128] F. Wang, C. Yin, X. Wei, Q. Wang, L. Cui, Y. Wang, T. Li, and J. Li. "Synthesis and characterization of superparamagnetic Fe_3O_4 nanoparticles modified with oleic acid." Integrated Ferroelectrics, vol. 153, no. 1, pp. 92-101, 2014.

[129] M. Brahmayya, S. A. Dai, and S. Suen, “Sulfonated reduced graphene oxide catalyzed cyclization of hydrazides and carbon dioxide to 1,3,4-oxadiazoles under sonication,” Scientific reports, vol. 7, no. 1, pp. 1-13, 2017.

[130] L. Wenjun, R. Liang, A. Hu, Z. Huanga and Y. N. Zhou, “Generation of oxygen vacancies in visible light activated one-dimensional iodine TiO_2 photocatalysts,” RSC Advances, vol 70, 2014.

[131] P. Basnet, et al., “Assessment of synthesis approaches for tuning the photocatalytic property of ZnO nanoparticles,” SN Applied Sciences, vol. 1, no. 633, 2019.

[132] S. Niu, Y. Zhou, H. Yu, C. Lu, and K. Han. "Investigation on thermal degradation properties of oleic acid and its methyl and ethyl esters through TG-FTIR." Energy conversion and management, vol. 149, pp. 495-504, 2017.

[133] A. Viinikanoja, J. Kauppila, P. Damlin, M. Suominen, and C. Kvarnström. "In-situ FTIR and Raman spectroelectrochemical characterization of graphene oxide upon electrochemical

reduction in organic solvents." Physical Chemistry Chemical Physics, vol. 17, no. 18, pp. 12115-12123, 2015.

[134] P. M. Kumar, S. Badrinarayanan, and M. Sastry. "Nanocrystalline TiO_2 studied by optical, FTIR and X-ray photoelectron spectroscopy: correlation to presence of surface states." Thin Solid Films, vol. 358, no. 1-2, pp. 122-130, 2000.

[135] G. Xiong, U. Pal, J. G. Serrano, K. B. Ucer, and R. T. Williams. "Photoluminesence and FTIR study of ZnO nanoparticles: the impurity and defect perspective." Physica Status Solidi-C, vol. 3, no. 10, pp. 3577-3581, 2006.

[136] IEC 60156:2018: Insulating liquids - Determination of the breakdown voltage at power frequency - Test method. https://webstore.iec.ch/publication/28297

[137] IEC 60897:1987: Methods for the determination of the lightning breakdown voltage of insulating liquids. https://webstore.iec.ch/publication/3852

[138] IEC 61620:1998: Insulating liquids - Determination of the dielectric dissipation factor by measurement of the conductance and capacitance - Test method. https://webstore.iec.ch/publication/5671

[139] ASTM D445-21: Standard Test Method for Kinematic Viscosity of Transparent and Opaque Liquids (and Calculation of Dynamic Viscosity). https://www.astm.org/d0445-21.html

[140] ASTM D971-20: Standard Test Method for Interfacial Tension of Insulating Liquids Against Water by the Ring Method. https://www.astm.org/d0971-20.html

[141] ASTM D93: Standard test methods for Flash Point by Pensky-Martens Closed Cup Tester. https://www.astm.org/Standards/D93.html

[142] M. Rafiq, L. Chengrong and Y. Lv, “Effect of Al_2O_3 nanorods on dielectric strength of aged transformer oil/paper insulation system, Journal of Molecular Liquids, vol. 284, pp. 700–708, 2019.

[143] E. Husain, M. M. Mohsin, A. Masood, M. U. Zuberi and M. S. Alam, "Dielectric behavior of insulating materials under liquid nitrogen," IEEE Transactions on Dielectrics and Electrical Insulation, vol. 9, no. 6, pp. 932-938, Dec. 2002.

[144] ASTM D828: Standard Test Method for Tensile Properties of Paper and Paperboard Using Constant-Rate-of-Elongation Apparatus. https://www.astm.org/d0828-16e01.html

[145] IEC 60243-1:2013: Electric strength of insulating materials - Test methods - Part 1: Tests at power frequencies. https://webstore.iec.ch/publication/1101

[146] D150-18: Standard Test Methods for AC Loss Characteristics and Permittivity (Dielectric Constant) of Solid Electrical Insulation. https://www.astm.org/Standards/D150

[147] Zhou Y, et. al, "Effect of nanoparticles on electrical characteristics of transformer oil-based nanofluids impregnated pressboard," 2012. IEEE International Symposium on Electrical Insulation 2012:650-653.

[148] El-Refaie E, et. al, "Enhancing flashover strength along oil/pressboard interface using nanofluids", Alexandria Engineering Journal, vol. 59, no. 1, pp. 475-483.

[149] Shan B, et al, "Effect of TiO_2 nanoparticles on DC breakdown performance of transformer oil-impregnated pressboard", IEEE Transactions on Dielectrics and Electrical Insulation, vol. 26, no. 9, pp. 1998-2004, 2019.

[150] J. K. Nelson, "An assessment of the physical basis for the application of design criteria for dielectric structures," IEEE Transactions on Electrical Insulation, vol. 24, no. 5, pp. 835-847, 1989.

[151] Prevost, "Dielectric Properties of Natural Esters and their Influence on Transformer Insulation System Design and Performance," *2005/2006 IEEE/PES Transmission and Distribution Conference and Exhibition*, 2006, pp. 30-34.

[152] S. V. Kulkarni and S. A. Khaparde, "Transformer Engineering - Design and Practice", *Marcel Dekker,* 2004.

[153] A. K. Sawhney, "A course in Electrical Machine Design", *Dhanpat Rai and Co.*, 2003.

[154] ABNT NBR 14274, Mineral insulating oil – Determination of compatibility of materials used in electrical equipment, ABNT NBR Standard, BR, 2013, http://www.abnt.org.br

[155] H. M. Wilhelm, V. Franch, L. Tulio and A. F. Franch, "Compatibility of transformer construction materials with natural ester-based insulating fluids," IEEE Transactions on Dielectrics and Electrical Insulation, vol. 22, no. 5, pp. 2703-2708, October 2015.

[156] ASTM D3455, Standard test methods for compatibility of construction material with electrical insulating oil of petroleum origin, ASTM International, West Conshohocken, PA, 2011, https://www.astm.org/d3455-11r19.html

LIST OF PUBLICATIONS FROM THIS RESEARCH

Science Citation Indexed (SCI) Papers Published/Accepted:

[1] Zaid Bin Siddique, Soumen Basu and Prasenjit Basak, "Development of graphene oxide dispersed natural ester based insulating oil for transformers," *IEEE Transactions on Dielectrics and Electrical Insulation,* vol. 28, no. 4, pp. 1326-1333, August 2021. (Impact Factor: 2.93). DOI: https://doi.org/10.1109/TDEI.2021.009445

[2] Zaid Bin Siddique, Soumen Basu and Prasenjit Basak, "Dielectric behavior of natural ester based mineral oil blend dispersed with TiO_2 and ZnO nanoparticles as insulating fluid for transformers," *Journal of Molecular Liquids*, vol. 339, no. 116825, October 2021. (Impact Factor: 6.16). DOI: https://doi.org/10.1016/j.molliq.2021.116825

[3] Zaid Bin Siddique, Soumen Basu and Prasenjit Basak, "Effect of graphene oxide dispersed natural ester based insulating oil on transformer solid insulation," *IEEE Transactions on Dielectrics and Electrical Insulation*, vol. 29, no. 2, pp. 378-385, April 2022. (Impact Factor: 2.93). DOI: https://doi.org/10.1109/TDEI.2022.3157926

[4] Zaid Bin Siddique, Soumen Basu and Prasenjit Basak, "Ageing of transformer pressboard impregnated with conductive and semi-conductive nanoparticles dispersed soyabean oil-blend" *IEEE Transactions on Dielectrics and Electrical Insulation.* (accepted) (Impact Factor: 2.93).

Science Citation Indexed (SCI) Papers Under Review:

[1] Zaid Bin Siddique, S. Basu and P. Basak, "Ageing of vegetable-based transformer oil dispersed with graphene oxide nanoparticles" *IEEE Transactions on Dielectrics and Electrical Insulation.* Paper number:10154

[2] Zaid Bin Siddique, Soumen Basu and Prasenjit Basak, "Effect of thermal stress on TiO_2 and ZnO dispersed ester oil as transformer liquid insulation," *Journal of Molecular Liquids.* MOLLIQ-D-22-0035

International/National Conferences Published

[1] Z. B. Siddique, S. Mehta and P. Basak, "Prediction of insulating oil for transformers through fuzzy logic approach," *2020 IEEE 9th Power India International Conference (PIICON), Haryana, India,* 2020, pp. 1-6, DOI: https://doi.org/10.1109/PIICON49524.2020.9112968

[2] A. Garg, Z. B. Siddique and P. Basak, "Significance of material compatibility for ester oil and nanofluids as an alternative liquid insulation for transformer applications," *Michael Faraday IET International Summit 2020 (MFIIS 2020), Kolkata, India,* 2020, pp. 41-45. DOI: https://doi.org/10.1049/icp.2021.1184

Somewhere something incredible is waiting to be known.

Carl Sagan